Studies on the Effects of Cold Terrestrial Biogenic Emissions of Organics on the Cloud Forming Potential of Atmospheric Aerosols

（寒冷陸域植生から放出される有機物が大気エアロゾルの雲生成ポテンシャルに及ぼす影響に関する研究）

DISSERTATION

Astrid Müller

15 February 2018

GRADUATE SCHOOL OF ENVIRONMENTAL SCIENCE
HOKKAIDO UNIVERSITY

Acknowledgements

This thesis is the result of the three years' work at the Institute of Low Temperature Science in the Atmospheric Chemistry Group, and the former Atmospheric and Organic Geochemistry Group. During this time, I had the opportunity to work with many inspiring people who contributed directly or indirectly to this work. I want to thank everyone for their expert advice, support, and encouragement throughout the experimental and theoretical work of this project.

I would particularly like to express my deepest gratitude to my supervisor **Asst. Prof. Yuzo Miyazaki** for his guidance, many discussions and advices, and his indefatigable eagerness in correcting my numerous mistakes. Without the manifold support he gave me, I would have not been able to complete this thesis. I would also like to offer my special thanks to **Prof. Kimitaka Kawamura** for giving me the opportunity to start my work on hygroscopicity in the Atmospheric and Organic Geochemisty Group, his supervision and support during the first half of my Ph.D. course. I owe a very important debt to **Dr. Suresh Kumar Reddy Boreddy** for teaching me the operation of the HTDMA, for the insightful discussions, assistance with different measurements, and his constructive comments and suggestions. Special thanks also to **Dr. Kaori Kawana** for her expert advice and particularly for her great technical assistance in the operation of the CCN and HTDMA.

I would like to show my greatest appreciation to **Assoc. Prof. Michihiro Mochida** for giving me the opportunity to visit his laboratory, and would especially like to thank **Ms. Yange Deng** for teaching me the handling of the CCN counter and the initial data analysis. I like to express my deep gratitude to **Ms. Eri Tachibana** for the chemical analyses, her expertise, help and guidance. Special thanks are also given to **Prof. Kazuma Aoki** from the University of Toyama for providing me the Sky-radiometer data, the permission to use them for this thesis, and his expert advices and comments. I greatly appreciate the assistance and manifold help

with questions in the laboratory offered by **Dr. Tomoki Mochizuki, Dr. Divyavani Gowda**, and **Dr. Chunmao Zhu**.

Special thanks go to **Dr. Sam Atwood** from Colorado State University for his expertise in solving various problems in the operation of the CCN counter. I would also like to express my gratitude to **Dr. Jeffrey S. Reid** from the Naval Research Laboratory for providing me the contact.

I want to thank all **members of the Atmospheric Chemistry Group** and the **former Atmospheric and Organic Geochemistry Group** for their suggestions and discussions. Especially, I owe my deepest gratitude to the **committee members of the Graduate School of Environmental Science** for their understanding and support, who enabled me to pass my pre-defense and defense in spite of difficult circumstances. Therefore, I would like to offer my special thanks to **Prof. Tsutomu Watanabe**, Chief of the committee, the Institute of Low Temperature Science (ILTS), **Prof. Fumio Hasabe** (the Graduate School of Environmental Science), and **Prof. Yoshito Chikaraishi** (ILTS). Special thanks also go to **Assoc. Prof. Jun Hirokawa** (the Graduate School of Environmental Science), and **Assoc. Prof. Naoto Murao** (the Graduate School of Engineering). I would like to thank the **Graduate School of Environmental Science of the Hokkaido University** for providing me the scholarship "Special Grant Program for International Students", the **Ministry of Education, Culture, Sports, Science and Technology (MEXT)**, Japan for the Grants-in-Aid for Scientific Research and Scientific Research and the **Sumitomo Foundation** in Japan. Without their financial support, this thesis would be impossible.

I want to thank everyone who had a part in this work and whom I did not mention here by name. I humbly ask for their indulgence.

Thanks are also given to my **friends** who accompanied me during the past years of this thesis, and my **family** for the encouragements. Particularly, I like to express my deepest gratitude to my **mother** for her continuous support and for her trust in me and my abilities to achieve my goals.

And finally, I especially thank my partner **Mr. Ryoma Miura** for his love and support, and his patience during the past years. I'm grateful for our baby **Kenzo** who gave me the motivation and energy to complete the final steps of this thesis.

Abstract

Terrestrial biogenic emissions of organics can affect the cloud condensation nuclei (CCN) activity and optical properties of atmospheric aerosols, and subsequently impact climate change. Large uncertainties exist in how different types of biogenic emissions and changes in the emission strength affect the formation of organic aerosol and its subsequent CCN activity. In order to investigate the effects of biogenic organic compounds on the CCN properties, two field experiments were made at suburban (Sapporo) and cool-temperate forest (Tomakomai) sites to measure the chemical composition, particle hygroscopicity, and CCN properties of submicron aerosols.

The time-resolved online measurements of submicron aerosols at the suburban site in summer showed that temporal variation in the CCN activity, described by the hygroscopicity parameter κ, was closely related to changes in the chemical composition and mixing state of aerosols. The temporal variation of water-soluble organic matter (WSOM)-to-sulfate ratio was closely linked to that of κ, where WSOM was likely dominated by the influence of biogenic sources. From a two year-long measurement of water-soluble aerosols at the forest site, κ derived from CCN measurements (κ_{CCN}) exhibited a distinct seasonal trend with a minimum in autumn. The results also showed that κ_{CCN} depends on the WSOM/sulfate ratio, where the significant reduction in the κ_{CCN} values in autumn was linked to the increase of WSOM. Positive matrix factorization analysis indicates that α-pinene derived secondary organic aerosols (SOA) substantially contributed to the WSOM mass (~75%) in autumn, the majority of which was attributable to emissions from litter/soil near the forest floor. These findings suggest that WSOM, most likely originated from the forest floor, can significantly suppress the CCN activity of aerosols in cool-temperate forests. The reduction of the CCN activity can be explained by α-pinene derived SOA coating pre-existing hygroscopic particles, which was estimated to reduce the number of activated CCN particles by ~32% in autumn. Considering

the atmospheric lifetime of α-pinene derived SOA, emissions of α-pinene from the forest floor can affect the activation of CCN within the spatial scale of ~800 km (τ = ~3 days).

Comparison of the filter-based aerosol measurements with aerosol optical properties retrieved from a Sky Radiometer at the forest site showed that the increased aerosol mass in the forest canopy corresponded to increase in the aerosol optical depth of fine mode particles (diameter < 1 μm) in autumn. In summer, the increased mass fraction of sulfate was linked to the enhanced properties of aerosol scattering. In contrast, the increase in the mass fraction of WSOM in autumn was found to be mainly associated with more absorbing characteristics of aerosols. This suggests that the biogenic organic aerosols at the forest site can modify the aerosol optical properties on a regional scale. The overall results demonstrate that changes in types and amounts of biogenic organic emissions in cool-temperate forests can control the cloud forming potential and can affect the aerosol optical properties. This study has important implications for predicting regional climate effects by changes in biogenic emissions of organics in the future.

Table of Contents

Chapter 4. Impact of Biogenic Organic Aerosols on Aerosol Optical Properties

List of publications

Müller, A., Y. Miyazaki, S. G. Aggarwal, Y. Kitamori, S. K. R. Boreddy, and K. Kawamura (2017a), Effects of chemical composition and mixing state on size-resolved hygroscopicity and cloud condensation nuclei activity of submicron aerosols at a suburban site in northern Japan in summer, *Journal of Geophysical Research Atmospheres*, 122(17), 9301–9318, doi:10.1002/2017JD027286.

Müller, A., Y. Miyazaki, E. Tachibana, K. Kawamura, and T. Hiura (2017b), Evidence of a reduction in cloud condensation nuclei activity of water-soluble aerosols caused by biogenic emissions in a cool-temperate forest, *Scientific Reports*, 7(1), 8452, doi:10.1038/s41598-017-08112-9.

Abbreviations

AE	Ångström exponent
AIE	aerosol indirect radiative effect
AOD	aerosol optical depth
AS	ammonium sulfate
BC	black carbon
BrC	brown carbon
BSOA	biogenic secondary organic aerosol
BVOC	biogenic volatile organic compound
CCN	cloud condensation nuclei
CCNC	cloud condensation nuclei counter
CPC	condensation particle counter
DMA	differential mobility analyser
DRE	direct radiative effect
EC	elemental carbon
GF	growth factor
HTDMA	hygroscopicity tandem differential mobility analyser
IC	ion chromatograph
NPF	new particle formation
NO_x	nitrogen oxides
OA	organic aerosol
OC	organic carbon
OH	hydroxyl
OM	organic matter

OPC	optical particle counter
PBAP	primary biological aerosol particle
PILS	particle-into-liquid sampler
PM	particulate matter
PMF	positive matrix factorization
POA	primary organic aerosols
RH	relative humidity
SMCA	scanning mobility CCN analysis
SMPS	scanning mobility particle sizer
SOA	secondary organic aerosol
SS	supersaturation
SSA	single scattering albedo
TOC	total organic carbon
TOT	thermal-optical-transmittance
TSM	total soluble mass
VOC	volatile organic compounds
WIOC	water-insoluble organic carbon
WIOM	water-insoluble organic matter
WSOC	water-soluble organic carbon
WSOM	water-soluble organic matter

Nomenclature

α_ω	water activity, unitless
α	Ångström exponent, unitless
D_{act}	activation diameter, nm
D_{dry}	dry particle diameter, nm
ε_{AS}	volume fraction of ammonium sulfate, unitless
ε_{org}	volume fraction of organics, unitless
I	irradiance, W m^{-2}
κ	hygroscopicity parameter kappa, unitless
m (ξ)	optical air mass, unitless
M_w	molar mass of water, kg mol^{-1}
N_{CN}	total number concentration of condensation nuclei, cm^{-3}
N_{CCN}	number concentration of CCN, cm^{-3}
R	universal gas constant, J K^{-1} mol^{-1}
ρ_W	density of pure water, kg m^{-3}
SS_c	critical supersaturation, %
σ_{abs}	absorption cross section, m^2
σ_{sca}	scattering cross section, m^2
$\sigma_{s/a}$	surface tension of the pure water–air interface, J m^{-2}
T	absolute temperature, K
τ	optical depth, unitless
ω	single scattering albedo, unitless

1. General Introduction

1.1 Biogenic aerosols and their effects on climate

Atmospheric aerosols are suspended solid or liquid particles in the atmosphere, which have the size range from a few nanometers to tens of micrometers in diameter [*Seinfeld and Pandis*, 2006]. Aerosol particles with sizes between 10 nm to 1 μm in diameter have typical residence times from days to weeks in the atmosphere [*Seinfeld and Pandis*, 2006], and play a key role in the climate system as they control the atmospheric radiative forcing. They can affect the radiative forcing directly by absorbing and scattering radiation [*Ångström*, 1964], and indirectly by acting as cloud condensation nuclei (CCN) to form cloud particles, which leads to changes in the albedo (and thus ambient temperature) and precipitation [*Twomey*, 1974; *Albrecht*, 1989].

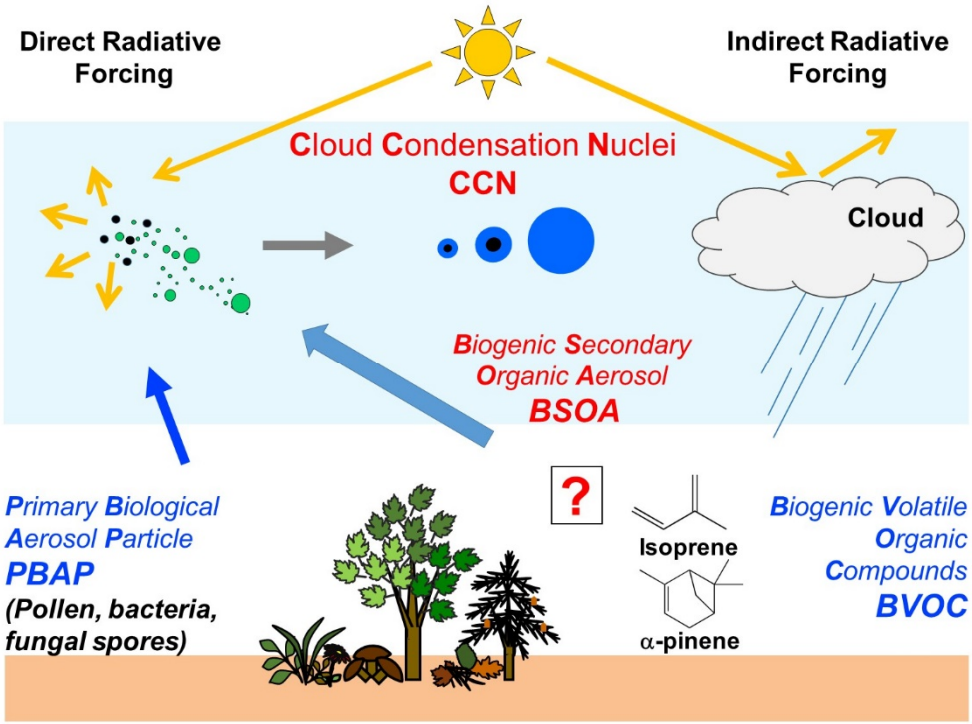

Figure 1.1 Schematic of mechanisms for the possible impact of biogenic emissions of organics on the climate.

Aerosols are emitted directly into the atmosphere in particle phase (primary aerosols) or formed by gas-to-particle conversion processes (secondary aerosol). Both primary and secondary aerosols have anthropogenic sources such as traffic and industrial emissions, and natural sources such as terrestrial vegetation, microbial activities in terrestrial and marine environments. Organic material contribute significantly to the submicron aerosol mass up to ~90%, especially in regions influenced by biogenic sources [*Kanakidou et al.*, 2005]. **Figure 1.1** illustrates the general mechanism of how biogenic emissions impact the climate. Primary biological aerosol particle (PBAP) include pollen, bacteria, fungal spores and their fragments. The emission of biogenic volatile organic compounds (BVOCs) can lead to the subsequent formation of biogenic secondary organic aerosol (BSOA). Globally, the dominant components of BVOCs are isoprene (C_5H_8, 750 TgC yr^{-1}) and monoterpenes ($C_{10}H_{16}$, 250 TgC yr^{-1}), both of which are the major precursors of BSOA [*Guenther et al.*, 1995; *Wiedinmyer et al.*, 2004]. Within the atmospheric boundary layer, photooxidation in the gas-phase of isoprene and α-pinene with hydroxyl radicals (OH), ozone (O_3), or nitrate radicals (NO_3) leads to the formation of low volatile oxidation products that condense to form BSOA [*Claeys*, 2004; *Ng et al.*, 2008; *Zhang et al.*, 2015]. Additional yield of BSOA can result from the oxidation in the aqueous-phase such as cloud droplets [*Carlton et al.*, 2009; *Aljawhary et al.*, 2015]. *Andreae and Crutzen* [1997] estimated the global production of BSOA of 30 Tg yr^{-1} to 270 Tg yr^{-1}. This amount is comparable to that of sulfate aerosols (90 Tg yr^{-1} to 140 Tg yr^{-1}). In particular, boreal and cool-temperate forests can serve as important sources of monoterpene [*Guenther et al.*, 1995; *Rinne et al.*, 2009]. These forest region covers 14 million km^2 on the global surface, which is the second largest forest region in the world [*FAO*, 2001].

Figure 1.2 presents the estimated ranges of the aerosol indirect radiative effect (AIE) induced by biogenic aerosols, together with the intermediate values of AIE, for global and the boreal forest region in summer. In general, the direct and indirect radiative effects of biogenic

organic aerosols is expected to induce atmospheric cooling [e.g., *Lihavainen et al.*, 2009; *Scott et al.*, 2014]. However, large uncertainties exist in the estimate of the radiative forcing, especially for the indirect radiative effect, because of the uncertainties in the aerosol–cloud interaction [*Intergovernmental Panel on Climate Change (IPCC)*, 2014]. Recent studies pointed out that large uncertainties of the AIE are attributable to uncertainties in the emissions and characteristics of biogenic aerosols, as well as in the feedback of aerosols on the biogeochemical cycles [*Mahowald*, 2011; *Carslaw et al.*, 2013]. Moreover, the major uncertainties also include the hygroscopic properties of organic aerosols [*Liu and Wang*, 2010]. As shown in **Figure 1.2**, the AIE due to biogenic aerosols ranges from atmospheric cooling (-0.77 W m^{-2}) to warming ($+0.23$ W m^{-2}) [e.g., *O'Donnell et al.*, 2011; *Rap et al.*, 2013; *Scott et al.*, 2014]. On the other hand, uncertainties in biogenic emissions dominated by monoterpene

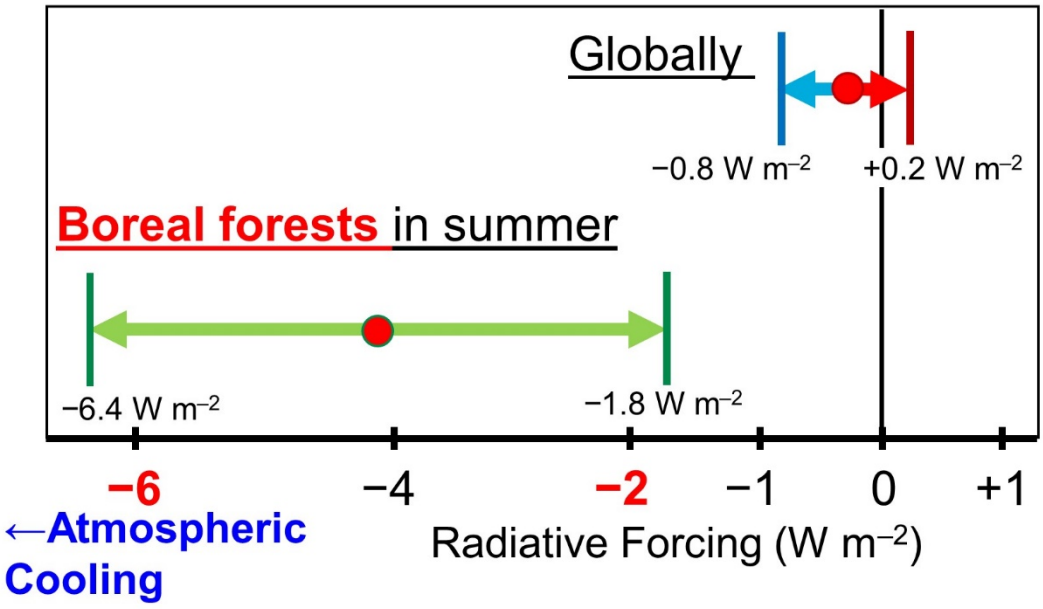

Figure 1.2 Estimated ranges of the aerosol indirect radiative effect (AIE) induced by biogenic aerosols. The intermediate values of AIE are -0.3 ± 0.5 W m^{-2} and -4.1 ± 2.3 W m^{-2} for the global estimate [e.g., *O'Donnell et al.*, 2011; *Rap et al.*, 2013; *Scott et al.*, 2014] and for the boreal forests in summer [*Spracklen et al.*, 2008; *Lihavainen et al.*, 2009], respectively.

in boreal forests in summer lead to the negative feedback on the regional climate with a wide range of −1.8 W m^{-2} to −6.4 W m^{-2} [*Spracklen et al.*, 2008; *Lihavainen et al.*, 2009] (**Figure 1.2**). These large variations emphasize the necessity to comprehensively understand the effects of terrestrial biogenic emissions of organics on the cloud forming potential of atmospheric aerosols to minimize these large uncertainties, particularly in cold regions.

1.2 Hygroscopicity and Cloud Condensation Nuclei (CCN) activity of biogenic aerosols

Biogenic aerosols can affect the cloud formation and the properties of clouds by acting as and/or altering cloud condensation nuclei (CCN). The cloud forming potential of aerosols depends on chemical composition, sizes, and the mixing state of particles, which determine the aerosol hygroscopicity and the CCN activity [e.g., *McFiggans et al.*, 2006; *Farmer et al.*, 2015]. *Dusek et al.* [2006] suggested that CCN activity primarily depends on particle sizes, whereas *Burkart et al.* [2011] showed that the complexity in externally and internally mixed aerosols prevents us from accurately predicting CCN activation from the size distributions alone. Among the chemical and physical properties of particles, the major factors controlling the activation of CCN include particle solubility and hygroscopicity, which are functions of the chemical composition of aerosol [*McFiggans et al.*, 2006; *Lee et al.*, 2010].

Figure 1.3 shows the relative humidity and supersaturation (SS) around a droplet as a function of the droplet diameter for different chemical components. The Köhler theory [*Wex et al.*, 2008] represents the competition between the following two effects: the Kelvin effect and the Raoult effect. The former effect represents the surface tension and accounts for enhanced vapor pressure due to the curvature of the droplet. This is reflected by an increase of the SS around the droplet, which suppresses its activation to form a cloud droplet. The Raoult effect represents the solute mass which depresses the vapor pressure due to dissolved mass. This is reflected by a decrease of the SS, which facilitates the cloud droplet formation [*McFiggans et*

al., 2006] (**Figure 1.3**). The critical value for the activation is the maximum SS around the droplet as represented by the peaks of the curves in **Figure 1.3**. Specifically, the competition of Kelvin effect and Raoult effect determines this level of SS, which is defined as critical supersaturation (SS_c) at the corresponding droplet diameter. SS_c depends on the chemical composition of the solute. If the ambient air has a value of SS larger than the SS_c threshold of the droplet, then it leads to the growth to a cloud droplet with sizes of several tens of µm [*Seinfeld and Pandis*, 2006]. For single inorganic compounds like ammonium sulfate, the activation characteristic is well understood. In contrast, SS_c for organics is highly uncertain, especially when organics are mixed with inorganics in ambient aerosols.

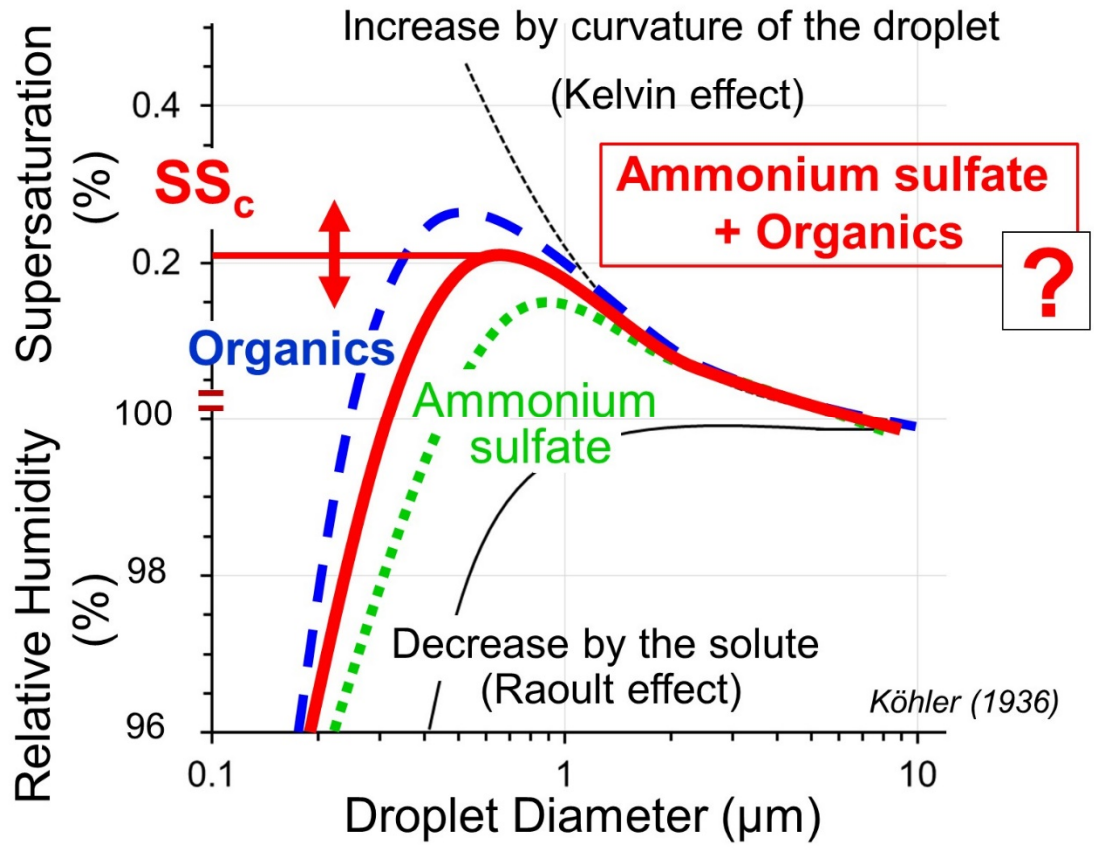

Figure 1.3 Critical supersaturation for activation (SS_c). The figure is based on *McFiggans et al.* [2006] and *Frosch et al.* [2011]. The variation of the relative humidity and supersaturation adjacent to a solution droplet containing organics (blue broken line), ammonium sulfate + organics (red line), and ammonium sulfate (green dotted line). All of the colored lines are called Köhler curves.

The single hygroscopicity parameter κ, parameterized by the κ-Köhler theory, describes the influence of the chemical composition on the CCN activity of aerosol particles of a specific diameter [*Petters and Kreidenweis*, 2007]. κ is calculated as follows:

$$\kappa(SS, D_{dry}) \approx \frac{4\,A^3}{27\,D_{dry}^3\,\ln^2 SS_c} \quad \textbf{(1.1)}$$

$$A = \frac{4\,\sigma_{s/a}\,M_w}{R\,T\,\rho_w} \quad \textbf{(1.2)}$$

where SS_c represents the critical supersaturation for activation, D_{dry} is the particle dry diameter, ρ_W is the density of water, M_W is the molar mass of water, $\sigma_{s/a}$ is the surface tension of the pure water–air interface ($\sigma_{s/a} = 0.072$ J m^{-2}), R is the universal gas constant, and T is the absolute temperature (T = 298 K). κ represents a scaled volume fraction of soluble material in particles and provides a theoretical framework to derive bulk hygroscopicity for particles with internal mixtures.

Figure 1.4 illustrates the dependence of the CCN activation on the SS and the D_{dry}. κ can be determined by obtaining the activation diameter (D_{act}) of the particle at the corresponding SS followed by using **equation 1.1**. D_{act} of CCN is the D_{dry} at which 50% of the number of the total particles (N_{CN}) are activated as CCN (N_{CCN}). Highly hygroscopic particles can be activated at low SS with small particle diameter, which is represented by large κ values. κ~1.4 is recognized as an upper limit for the most hygroscopic particles typically found in the atmosphere [*Petters and Kreidenweis*, 2007]. On the other hand, κ = 0 represents non-hygroscopic particles.

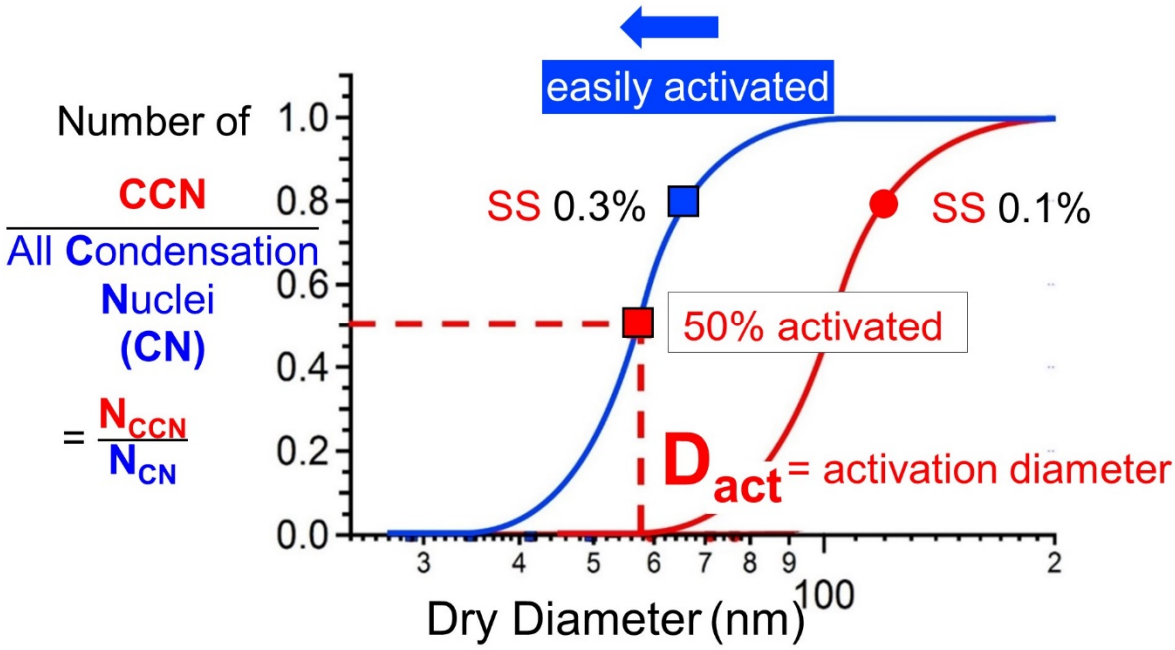

Figure 1.4 Dependence of the CCN activation on the supersaturation (SS) and the particle dry diameter, which is described by the hygroscopicity parameter kappa (κ) [*Petters and Kreidenweis*, 2007; *Parmonov et al.*, 2013; *Whitehead et al.*, 2016].

Sulfate aerosol is one of the most effective component to activate particles as CCN [*Seinfeld and Pandis*, 2006] with κ values of greater than 0.6. On the other hand, primary organic aerosols (POA) generally have lower κ values between 0 and 0.1 [*Sun and Ariya*, 2006; *Petters and Kreidenweis*, 2007; *Duplissy et al.*, 2011]. Atmospheric aging and the formation of secondary organic aerosols (SOA) can change the CCN activity. This is typically attributable to changes in the surface composition of particles by heterogeneous oxidation and the resulting changes in the particle's ability to uptake water.

Previous studies reported that the value of κ for bulk SOA ranges between 0 and ~0.4 [*Engelhart et al.*, 2008]; these values likely represent the volume-weighted average of a broader range of κ values for each constituent [*Suda et al.*, 2012]. For example, the oxidation products of 3-methylfuran with OH in the presence of NO_x have κ = 0.06 [*Suda et al.*, 2012], whereas κ values reported for SOA derived from monoterpene and isoprene are 0.10−0.15 [*Prenni et al.*,

2007; *Engelhart et al.*, 2008] and 0.10−0.12 [*King et al.*, 2010; *Engelhart et al.*, 2011], respectively. In forested environments, BSOA show κ values of typically below 0.3 obtained in intensive field studies [e.g., *Levin et al.*, 2014; *Whitehead et al.*, 2016], while studies of long-term measurements showed lower κ values in summer, which was attributed to increased emissions of BVOCs in that season. However, those previous studies had limited chemical measurements available to confirm that interpretation [e.g., *Fors et al.*, 2011; *Paramonov et al.*, 2013]. Furthermore, a change in the CCN activity can be the result of the mixing of chemical species with different hygroscopic properties. Therefore, the formation and abundance of water-soluble biogenic organic aerosol relative to sulfate can modify the CCN activity when organics are mixed with sulfate in a particle. The mixing state can change the surface composition and water affinity of the particle.

The complexity of the chemical composition and mixing state of aerosol particles, particularly for the organic fraction, prevents atmospheric models from accurately reproducing and predicting the aerosol–cloud interaction. The formation and abundance of biogenic organic aerosol relative to hygroscopic components are expected to modify the CCN activity of particles, and thus can change the cloud properties. Therefore, comprehensive field measurements of chemical composition and mixing state of biogenic aerosols together with their effect on the CCN activity is needed to accurately predict the global distribution of CCN and their impact on climate change.

1.3 Objectives of this thesis

The objective of this thesis is to elucidate the effects of terrestrial biogenic emissions of organics on the CCN properties and optical properties of atmospheric aerosols. This study investigates how different types of biogenic emissions and changes in the emission strength of biogenic sources can affect the formation of organic aerosol (OA) and its subsequent impact on the CCN properties. In particular, it is still controversial how biogenic aerosols affect the radiative forcing when they are mixed with anthropogenic aerosols. Two field experiments were made at a suburban site in Sapporo (Chapter 2) and a cool-temperate forest in Tomakomai (Chapter 3), whose locations are shown in **Figure 1.5**, to measure the chemical composition, particle hygroscopicity, and CCN properties of submicron aerosols. Additionally, filter-based measurements were compared with aerosol optical properties obtained at the same forest site to investigate how the biogenic emissions of organics are linked to the radiative effect (Chapter 4).

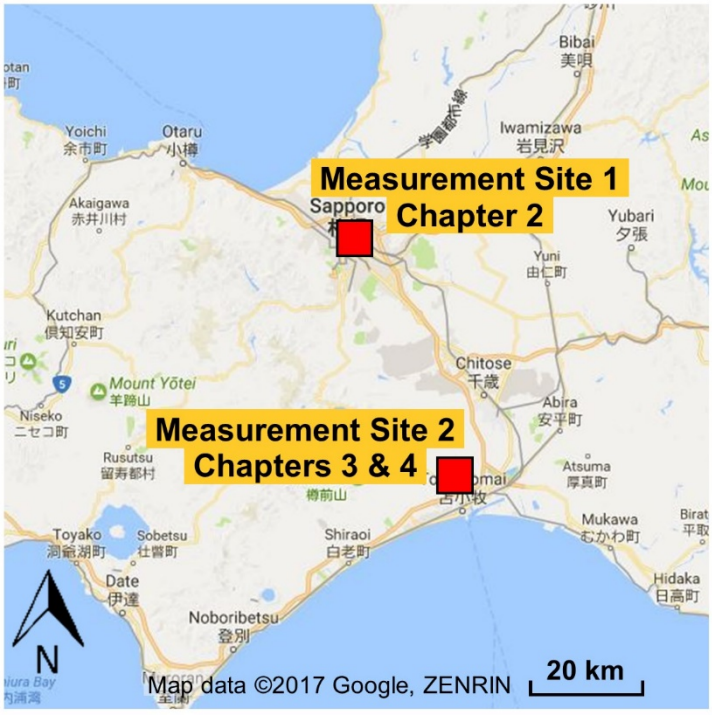

Figure 1.5 Locations of the two study sides in suburban Sapporo and the cool-temperate forest in Tomakomai.

References

Albrecht, B. a. (1989), Aerosols, Cloud Microphysics, and Fractional Cloudiness, Science, 245(4923), 1227–1230, doi:10.1126/science.245.4923.1227.

Aljawhary, D., R. Zhao, A. K. Y. Lee, C. Wang, and J. P. D. Abbatt (2015), Kinetics, Mechanism, and Secondary Organic Aerosol Yield of Aqueous Phase Photo-oxidation of α-Pinene Oxidation Products, J. Phys. Chem. A, doi:10.1021/acs.jpca.5b06237.

Andreae, M. O. (1997), Atmospheric Aerosols: Biogeochemical Sources and Role in Atmospheric Chemistry, Science, 276(5315), 1052–1058, doi:10.1126/science.276.5315.1052.

Ångström, A. (1964), The parameters of atmospheric turbidity, Tellus, 16(1), 64–75, doi:10.1111/j.2153-3490.1964.tb00144.x.

Burkart, J., G. Steiner, G. Reischl, and R. Hitzenberger (2011), Long-term study of cloud condensation nuclei (CCN) activation of the atmospheric aerosol in Vienna, Atmos. Environ., 45(32), 5751–5759, doi:10.1016/j.atmosenv.2011.07.022.

Carlton, A. G., C. Wiedinmyer, and J. H. Kroll (2009), A review of Secondary Organic Aerosol (SOA) formation from isoprene, Atmos. Chem. Phys., 9(14), 4987–5005, doi:10.5194/acp-9-4987-2009.

Carslaw, K. S. et al. (2013), Large contribution of natural aerosols to uncertainty in indirect forcing, Nature, 503(7474), 67–71, doi:10.1038/nature12674.

Claeys, M. (2004), Formation of Secondary Organic Aerosols Through Photooxidation of Isoprene, Science (80-.)., 303(5661), 1173–1176, doi:10.1126/science.1092805.

Duplissy, J. et al. (2011), Relating hygroscopicity and composition of organic aerosol particulate matter, Atmos. Chem. Phys., 11(3), 1155–1165, doi:10.5194/acp-11-1155-2011.

Dusek, U. et al. (2006), Size Matters More Than Chemistry for Cloud-Nucleating Ability of Aerosol Particles, Science (80-.)., 312(5778), 1375–1378, doi:10.1126/science.1125261.

Engelhart, G. J., A. Asa-Awuku, A. Nenes, and S. N. Pandis (2008), CCN activity and droplet growth kinetics of fresh and aged monoterpene secondary organic aerosol, Atmos. Chem. Phys., 8(14), 3937–3949, doi:10.5194/acp-8-3937-2008.

Engelhart, G. J., R. H. Moore, A. Nenes, and S. N. Pandis (2011), Cloud condensation nuclei activity of isoprene secondary organic aerosol, J. Geophys. Res., 116(D2), 1–11, doi:10.1029/2010JD014706.

FAO (2001), Global Forest Resources Assessment 2000 Main Report, Rome.

Farmer, D. K., C. D. Cappa, and S. M. Kreidenweis (2015), Atmospheric Processes and Their

Controlling Influence on Cloud Condensation Nuclei Activity, Chem. Rev., 115(10), 4199–4217, doi:10.1021/cr5006292.

Fors, E. O., E. Swietlicki, B. Svenningsson, A. Kristensson, G. P. Frank, and M. Sporre (2011), Hygroscopic properties of the ambient aerosol in southern Sweden – a two year study, Atmos. Chem. Phys., 11(16), 8343–8361, doi:10.5194/acp-11-8343-2011.

Guenther, A. et al. (1995), A global model of natural volatile organic compound emissions, J. Geophys. Res., 100(D5), 8873, doi:10.1029/94JD02950.

Intergovernmental Panel on Climate Change (IPCC) (2014), Climate Change 2013 - The Physical Science Basis, edited by Intergovernmental Panel on Climate Change, Cambridge University Press, Cambridge.

Kanakidou, M. et al. (2005), Organic aerosol and global climate modelling: a review, Atmos. Chem. Phys., 5, 1053–1123, doi:10.5194/acp-5-1053-2005.

King, S. M., T. Rosenoern, J. E. Shilling, Q. Chen, Z. Wang, G. Biskos, K. a. McKinney, U. Pöschl, and S. T. Martin (2010), Cloud droplet activation of mixed organic-sulfate particles produced by the photooxidation of isoprene, Atmos. Chem. Phys., 10(8), 3953–3964, doi:10.5194/acp-10-3953-2010.

Lee, S., Y. S. Ghim, S. W. Kim, and S. C. Yoon (2010), Effect of biomass burning and regional background aerosols on CCN activity derived from airborne in-situ measurements, Atmos. Environ., 44(39), 5227–5236, doi:10.1016/j.atmosenv.2010.08.044.

Levin, E. J. T., a. J. Prenni, B. B. Palm, D. a. Day, P. Campuzano-Jost, P. M. Winkler, S. M. Kreidenweis, P. J. DeMott, J. L. Jimenez, and J. N. Smith (2014), Size-resolved aerosol composition and its link to hygroscopicity at a forested site in Colorado, Atmos. Chem. Phys., 14(5), 2657–2667, doi:10.5194/acp-14-2657-2014.

Lihavainen, H., V.-M. Kerminen, P. Tunved, V. Aaltonen, A. Arola, J. Hatakka, A. Hyvärinen, and Y. Viisanen (2009), Observational signature of the direct radiative effect by natural boreal forest aerosols and its relation to the corresponding first indirect effect, J. Geophys. Res., 114(D20), D20206, doi:10.1029/2009JD012078.

Liu, X., and J. Wang (2010), How important is organic aerosol hygroscopicity to aerosol indirect forcing?, Environ. Res. Lett., 5(4), 44010, doi:10.1088/1748-9326/5/4/044010.

Mahowald, N. (2011), Aerosol Indirect Effect on Biogeochemical Cycles and Climate, Science (80-.)., 334(6057), 794–796, doi:10.1126/science.1207374.

McFiggans, G. et al. (2006), The effect of physical and chemical aerosol properties on warm cloud droplet activation, Atmos. Chem. Phys., 6(9), 2593–2649, doi:10.5194/acp-6-2593-2006.

Ng, N. L. et al. (2008), Secondary organic aerosol (SOA) formation from reaction of isoprene with nitrate radicals (NO_3), Atmos. Chem. Phys., 8(14), 4117–4140, doi:10.5194/acp-8-4117-2008.

O'Donnell, D., K. Tsigaridis, and J. Feichter (2011), Estimating the direct and indirect effects of secondary organic aerosols using ECHAM5-HAM, Atmos. Chem. Phys., 11(16), 8635–8659, doi:10.5194/acp-11-8635-2011.

Paramonov, M., P. P. Aalto, a. Asmi, N. Prisle, V. M. Kerminen, M. Kulmala, and T. Petäjä (2013), The analysis of size-segregated cloud condensation nuclei counter (CCNC) data and its implications for cloud droplet activation, Atmos. Chem. Phys., 13(20), 10285–10301, doi:10.5194/acp-13-10285-2013.

Petters, M. D., and S. M. Kreidenweis (2007), A single parameter representation of hygroscopic growth and cloud condensation nucleus activity, Atmos. Chem. Phys., 7(8), 1961–1971, doi:10.5194/acp-7-1961-2007.

Prenni, A. J., M. D. Petters, S. M. Kreidenweis, P. J. DeMott, and P. J. Ziemann (2007), Cloud droplet activation of secondary organic aerosol, J. Geophys. Res., 112(D10), D10223, doi:10.1029/2006JD007963.

Rap, A., C. E. Scott, D. V. Spracklen, N. Bellouin, P. M. Forster, K. S. Carslaw, A. Schmidt, and G. Mann (2013), Natural aerosol direct and indirect radiative effects, Geophys. Res. Lett., 40(12), 3297–3301, doi:10.1002/grl.50441.

Rinne, J., J. Bäck, and H. Hakola (2009), Biogenic volatile organic compound emissions from the Eurasian taiga: Current knowledge and future directions, Boreal Environ. Res., 14(4), 807–826.

Scott, C. E. et al. (2014), The direct and indirect radiative effects of biogenic secondary organic aerosol, Atmos. Chem. Phys., 14(1), 447–470, doi:10.5194/acp-14-447-2014.

Seinfeld, J. H., and S. N. Pandis (2006), Atmospheric chemistry and physics: from air pollution to climate change, 2nd ed., Wiley, Inc., New York, USA.

Spracklen, D. V, B. Bonn, and K. S. Carslaw (2008), Boreal forests, aerosols and the impacts on clouds and climate, Philos. Trans. R. Soc. A Math. Phys. Eng. Sci., 366(1885), 4613–4626, doi:10.1098/rsta.2008.0201.

Suda, S. R., M. D. Petters, A. Matsunaga, R. C. Sullivan, P. J. Ziemann, and S. M. Kreidenweis (2012), Hygroscopicity frequency distributions of secondary organic aerosols, J. Geophys. Res. Atmos., 117(D4), doi:10.1029/2011JD016823.

Sun, J., and P. Ariya (2006), Atmospheric organic and bio-aerosols as cloud condensation nuclei (CCN): A review, Atmos. Environ., 40(5), 795–820,

doi:10.1016/j.atmosenv.2005.05.052.

Twomey, S. (1974), Pollution and the planetary albedo, Atmos. Environ., 8(12), 1251–1256, doi:10.1016/0004-6981(74)90004-3.

Wex, H., F. Stratmann, D. Topping, and G. McFiggans (2008), The Kelvin versus the Raoult Term in the Köhler Equation, J. Atmos. Sci., 65(12), 4004–4016, doi:10.1175/2008JAS2720.1.

Whitehead, J. D. et al. (2016), Biogenic cloud nuclei in the central Amazon during the transition from wet to dry season, Atmos. Chem. Phys., 16(15), 9727–9743, doi:10.5194/acp-16-9727-2016.

Wiedinmyer, C., A. Guenther, P. Harley, N. Hewitt, C. Geron, P. Artaxo, R. Steinbrecher, and R. Rasmussen (2004), Global Organic Emissions from Vegetation, in Emissions of Atmospheric Trace Compounds, pp. 115–170.

Zhang, X., R. C. McVay, D. D. Huang, N. F. Dalleska, B. Aumont, R. C. Flagan, and J. H. Seinfeld (2015), Formation and evolution of molecular products in α-pinene secondary organic aerosol, Proc. Natl. Acad. Sci., 112(46), 14168–14173, doi:10.1073/pnas.1517742112.

Chapter 2. Effects of Chemical Composition and Mixing State on Size-Resolved Hygroscopicity and Cloud Condensation Nuclei Activity of Submicron Aerosols at a Suburban Site in Summer

2.1 Introduction

Among the chemical and physical properties of particles, solubility and hygroscopicity play important roles in the complex aerosol–cloud interaction beside the number concentration, sizes, and mixing state of chemical species in aerosol particles [*McFiggans et al.*, 2006; *Lee et al.*, 2010]. The dependence of the hygroscopicity and cloud condensation nuclei (CCN) activity on the chemical composition and mixing state can be determined by the single hygroscopicity parameter κ (Chapter 1.2). The hygroscopic properties of single compounds, such as hygroscopic sulfate (κ = 0.6) or hydrophobic elemental carbon (EC, κ = 0), are well understood [*Seinfeld and Pandis*, 2006]. However, κ for aersols with complex chemical mixtures is still uncertain, which can change associated with photochemical oxidation in the atmosphere.

Specifically, the atmospheric processing of particles and the subsequent formation of secondary organic aerosol (SOA) can affect the hygroscopicity and CCN activity of the aerosols. The processing of aerosols depends on various chemical and physical reactions in the atmosphere as well as differences in their origin and transport processes. Understanding how such processes lead to changes in the particle size and particle chemical composition, and how they are interrelated is important to accurately reproduce the global distributions of CCN and their impacts on climate change. Due to the complexity of the atmospheric processing, time-resolved field measurements relating CCN activity to hygroscopicity and chemical composition have been extensively conducted in previous studies [*Fors et al.*, 2011; *Jurányi et*

al., 2011; *Sihto et al.*, 2011; *Silvergren et al.*, 2014; *Kawana et al.*, 2016]. In spite of the importance of the size dependence of aerosol hygroscopicity and CCN properties, field studies are limited on size-resolved hygroscopicity and cloud forming potential of atmospheric particles affected by both anthropogenic and biogenic sources.

The objective of this chapter is to understand the impact of aerosol composition on both subsaturated and supersaturated particle hygroscopicity in anthropogenic and biogenic aerosols. Simultaneous measurements of size-resolved CCN concentrations, hygroscopic growth, particle size distributions, and chemical composition in submicron aerosols were made at a suburban site in northern Japan in the summer of 2008. In spite of the suburban environment, the observational site has been suggested to be largerly influenced by biogenic sources in addition to anthropogenic sources, especially in summer [*Pavuluri et al.*, 2013]. Therefore, the study site provides unique opportunities to investigate the effects of inhomogeneity of sources and aerosol aging on CCN activity. This chapter discusses the relevance of the aerosol mixing state, chemical composition, and different possible sources.

2.2 Experiments

2.2.1 Measurement site

Figure 2.1 shows the location of the measurement site and the surrounding area. The site is located at the campus of Hokkaido University (43º3’56’’ N and 141º21’27’’ E) at the north of the downtown area of Sapporo, northern Japan. The study site, which belongs to the cool temperate zone, is surrounded by vegetation and residential areas. Urban industrial areas are located south to east, whereas vegetation and residential areas are located in west to northwest of the sampling site.

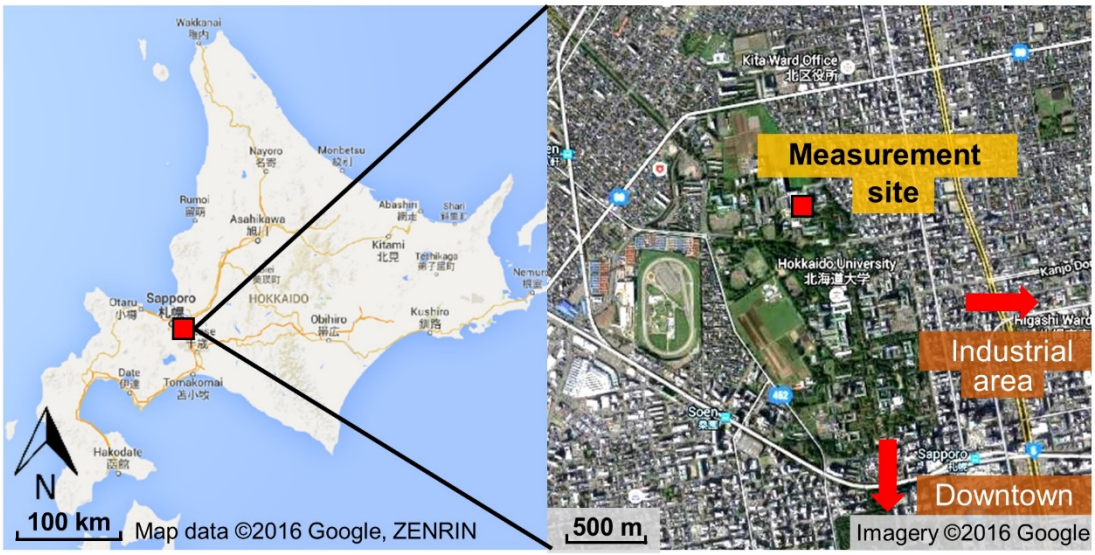

Figure 2.1 Location of the measurement site at north campus of Hokkaido University, Sapporo, northern Japan (43˚3'56'' N and 141˚21'27'' E). Map data ©2016 Google, ZENRIN; Imagery ©2016 Google, DigitalGlobe, (https://maps.google.com/). Maps are modified with Microsoft PowerPoint 2013.

Ambient aerosol measurements were carried out during the period of July 1 to 17, 2008. Previous field studies suggested that, in summer, both isoprene- and α-pinene-derived SOA similarly contribute to the production of the water-soluble organic carbon (WSOC) mass in aerosols at the same site and at a nearby forest site [*Miyazaki et al.*, 2012; *Pavuluri et al.*, 2013]. Consequently, similar contributions of isoprene and α-pinene emissions are expected to affect ambient aerosols at this site in summer. During the study period, the average temperature was 21.0°C ± 2.7°C, while precipitation was only observed on July 11. The ambient aerosols were sampled through a $PM_{1.0}$ cyclone inlet. The sampled aerosols were then introduced to each on-line instrument as explained below.

2.2.2 CCN and particle number size distribution

Figure 2.2 shows the instrument setup for the measurements of the CCN, hygroscopic growth factors (GF), and particle size distributions. Ambient aerosol particles ($PM_{1.0}$) were dried at relative humidity (RH) < 5% with two diffusion dryers filled with silica gel and a

molecular sieve. Number concentrations of CCN (N_{CCN}) were measured as a function of dry diameter (D_{dry}, RH < 5%) and supersaturation using a continuous-flow thermal-gradient Cloud Condensation Nuclei counter (CCNC-100: Droplet Measurement Technologies) [*Roberts and Nenes*, 2005]. The CCN counter was operated in parallel with a condensation nuclei (CN) counter (CPC 1; TSI, Model 3010) downstream of a differential mobility analyzer (DMA 1: TSI Model 3081) (**Figure 2.2**) to obtain the total particle number concentration (N_{CN}).

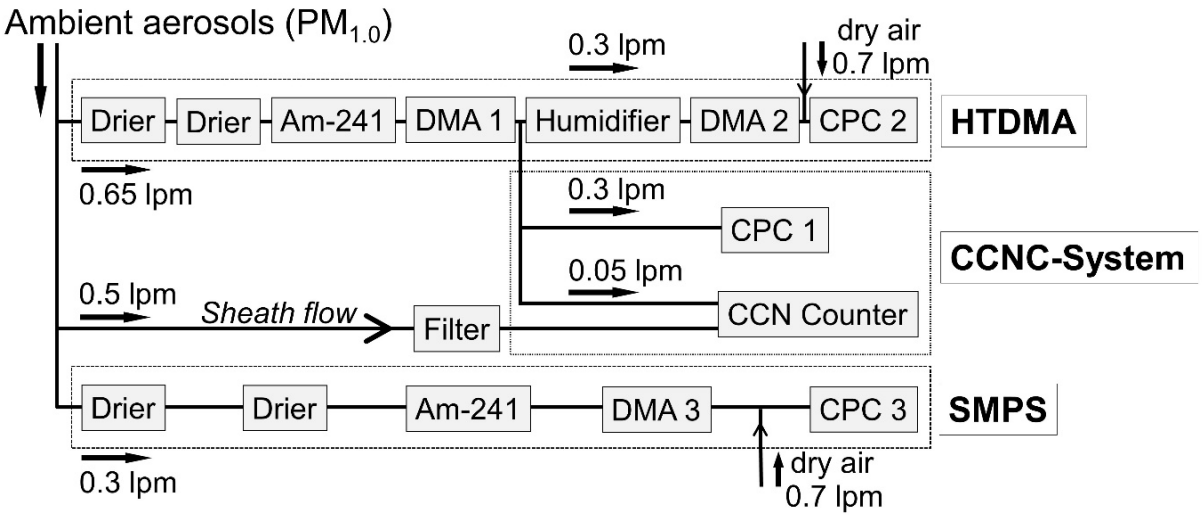

Figure 2.2 Schematic of the experimental setup for the HTDMA, CCNC, and SMPS.

The total flow rate of air into the CCN counter was 0.5 L min^{-1} with the ratio of sheath to sample flows of ~10. The CCN counter was stepped through four different column temperature gradients, which were calibrated to supersaturations (SS) of 0.10%, 0.30%, 0.50%, and 0.80%. The concentration of CCN was measured for particles with D_{dry} ranging from 20.2 to 429 nm for 1.5 h at each SS. The residence time of the particles in the column was ~10 s, which is sufficient for the particles to grow to droplets with diameters between 0.75 µm and 1 µm [*Paramonov et al.*, 2013]. Calibration of the CCN counter was performed using ammonium sulfate (AS). Each SS was measured three times for laboratory-generated AS, and the presented data are the averages of these measurements.

For the calibration using particles with identical size and chemical composition, the activation diameter of CCN is generally defined as D_{dry} at which N_{CCN} reaches 50% of the total particle number concentration (N_{CN}) at a certain supersaturation (SS) [e.g., *Rose et al., 2008*]. Here, the activation diameter of CCN for ambient particles is defined as D_{act}. The overall uncertainty of the N_{CCN}/N_{CN} ratio controlled by the counting efficiencies of the CPC and the optical particle counter (OPC) in the CCN counter was estimated to be less than 10%. The estimation of the uncertainty is based on the variation of the maximum ratios of the N_{CCN}/N_{CN} for the AS aerosols during the calibration. Once D_{act} at a certain SS is determined, the hygroscopicity parameter, κ_{CCN}, can be calculated for particles corresponding to that D_{dry} [*Petters and Kreidenweis*, 2007].

$$\kappa(SS, D_{dry}) \approx \frac{4\,A^3}{27\,D_{dry}^3 \ln^2\left(1 + \frac{SS}{100\%}\right)} \qquad \textbf{(2.1)}$$

$$A = \frac{4\,\sigma_{s/a}\,M_w}{R\,T\,\rho_w} \qquad \textbf{(2.2)}$$

where ρ_W is the density of water, M_W is the molar mass of water, $\sigma_{s/a}$ is the surface tension of the solution–air interface of pure water ($\sigma_{s/a}$ = 0.072 J m^{-2}), R is the universal gas constant, T is the absolute temperature (T = 298.15 K).

Particle size distributions were measured using a Scanning Mobility Particle Sizer (SMPS). After drying and single charging via an aerosol bipolar charger (AM-241), the particles were measured with DMA 3 and CPC 3 (TSI, Model 3022). The particle number dN/dlogd in the 64 channel per decade resolution was normalized by the total number (dN/dlogd/N_{TOTAL} (particle cm^{-3})).

2.2.3 Hygroscopic growth factor

The hygroscopic GF at 85% RH were measured with a hygroscopicity tandem differential mobility analyzer (HTDMA) as a function of D_{dry} ranging from 24.1 to 359 nm. The hygroscopic GF is defined as the particle diameter at a given RH (D(RH)) divided by its D_{dry}:

$$GF(RH) = \frac{D(RH)}{D_{dry}} \quad \textbf{(2.3)}$$

The ambient aerosol particles ($PM_{1.0}$) were dried to RH < 5% via two diffusion dryers as described in the previous subsection (**Figure 2.2**). The aerosols were then passed through the AM-241 to achieve single charged particles and classified by a differential mobility analyzer (DMA 1: TSI Model 3081). The particles were selected at sixteen specific mobility diameters between 24.1 and 359 nm. Humidification of the particles at 85% ± 1% RH was performed using a humidity conditioner consisting of a Nafion tube. The RH was regulated by controlling the dried and humidified airflows into the tubing. The residence time of the particles between the inlet of the humidity conditioner and the DMA 2 was approximately 10 s [*Boreddy et al.*, 2014], which is considered to be sufficient for the particles to reach their equilibrium [*Chan and Chan*, 2005; *Duplissy et al.*, 2009]. The resulting number size distribution after humidification was measured using the second DMA (DMA 2) and the condensation particle counter (CPC 2). Calibration of the HTDMA system was made with AS. The measurement uncertainty for GF at 85% RH was ± 1%, which is similar to that reported in previous studies using the same measurement system [*Aggarwal et al.*, 2007; *Jung et al.*, 2011; *Boreddy et al.*, 2014]. More details about the principle are described in previous studies [e.g., *Mochida et al.*, 2006].

Like the supersaturated hygroscopicity parameter (κ_{CCN}), κ values were also calculated using the GF data (κ_{GF}) [*Petters and Kreidenweis*, 2007], which relates the water activity to the dry particle volumes.

$$\kappa = \frac{(GF(RH)^3 - 1)(1 - a_\omega)}{a_\omega} \quad \textbf{(2.4)}$$

$$a_\omega = RH \left(\exp\left(\frac{4\,\sigma_{s/a} / M_W}{R\,T\,\rho_W\,GF(RH)\,D_{dry}} \right) \right)^{-1} \quad \textbf{(2.5)}$$

where α_ω is the water activity, ρ_W is the density of water, M_W is the molar mass of water, $\sigma_{s/\alpha}$ is the surface tension of the solution–air interface of pure water ($\sigma_{s/a}$ = 0.072 J m^{-2}), R is the universal gas constant, T is the absolute temperature, and D_{dry} the particle dry diameter. The comparison between κ_{GF} and κ_{CCN} values is discussed in Section 2.3.2.

To calculate the fraction of the particle number concentration of the GF distributions, the k-means cluster analytical tool of the Igor Pro software (ver. 6.3.7.2) was used. The tool uses an iterative algorithm to classify the clustering of data into groups; hence, each data point belongs to a group of the closest mean value. It then calculates peaks of the number fractions of particles of the GF distributions, which is discussed in Section 2.3.3.

2.2.4 Measurements of aerosol chemical composition

Semi-continuous measurement of WSOC in $PM_{1.0}$ was made using a particle-into-liquid sampler (PILS) coupled to a total organic carbon (TOC) analyzer (Model 810; Sievers, Boulder, CO) [*Miyazaki et al.*, 2006, 2012] in parallel with the measurements of GF and CCN. The details of the instrument are given elsewhere [*Miyazaki et al.*, 2006]. The inlet for the PILS was identical to that for the CCN and hygroscopicity measurements.

The mass concentrations of organic carbon (OC) and EC were measured using a semi-

continuous EC/OC analyzer (Sunset Laboratory Inc., Tigard, OR). The measurement procedure of the EC/OC analyzer used in this study is given in *Miyazaki et al.* [2006]. The NO_x mixing ratios were measured using a NO_x analyzer (Thermo Scientific, Waltham, MA). The instrument collected ambient $PM_{1.0}$ particles on a quartz-fiber filter for 45 min at a flow rate of 8 L min^{-1}. The collected particles were then analyzed using the thermal-optical-transmittance (TOT) method for 15 min. Using the measured mass concentrations of OC and WSOC, water-insoluble OC (WIOC) is defined as WIOC = OC − WSOC. In the present study, the mass concentrations of WSOC and WIOC were converted to water-soluble organic matter (WSOM) and water-insoluble organic matter (WIOM). A factor of 1.8 was used for the conversion of WSOC to WSOM [*Yttri et al.*, 2007; *Finessi et al.*, 2012], and a factor of 1.2 was used to convert the mass of WIOC to that of WIOM [*Wang et al.*, 2005].

The inorganic bulk composition of aerosols was also obtained using another PILS coupled to two ion chromatographs (IC) (761 Compact IC, Metrohm Switzerland) [*Orsini et al.*, 2003] with another inlet including a $PM_{1.0}$ cyclone. The mass concentrations of sulfate (SO_4^{2-}) and other inorganic components were obtained every 15 min. The mass contributions of inorganics other than sulfate to the submicron particle mass were insignificant: the avarage mass concentrations of nitrate and ammonium were less than 15% of that of sulfate. Consequently, the fractions of those inorganic components are not shown in this study. PILS-IC data were obtained during a limited period (9:00−23:00 LT on July 7; 0:00−14:00 LT on July 12; 10:00 LT on July 13 to 22:00 LT on July 15) due to a problem with the instrument. The inorganic compositions were also measured with a filter-based off-line method as described below.

A high-volume Andersen sampler was used to collect $PM_{1.0}$ samples on quartz filters at a flow rate of 670 L min^{-1}. The sampling duration was ~3 h during the day and ~6 h at night. Only during the period from July 5 to July 8, the filter sample was obtained every 12 h. Inorganic ions were measured using the same type of IC as used for the PILS measurement

during the period of July 4 to 12. Briefly, inorganic ions were extracted from the filter samples (20 mm diameter punch) with 10 ml of ultrapure water under ultrasonication. The extracts were penetrated through a syringe filter (Millex-GV, 0.22 μm, Millipore), before being injected into the IC [*Miyazaki et al.*, 2009]. Concentrations of sulfate measured with PILS-IC ($sulfate_{PILS}$) agreed with those of the filter measurement ($sulfate_{filter}$) to within 10% for the data obtained on July 7. Although the data used for the comparison was limited, it indicates that $sulfate_{PILS}$ was almost identical to $sulfate_{filter}$ in the current study.

2.3 Results and Discussion

2.3.1 Temporal variation

Figures 2.3a–2.3d show the temporal variations of the local wind speed and directions and the chemical composition of the observed aerosols. Three distinct periods were observed in terms of different characteristics of the observed air masses. The predominant local wind directions during July 4–8 were east and southeast with typical local wind speeds > 1.5 m s^{-1} (av. 2.2 ± 0.7 m s^{-1}; **Figure 2.3a**). Consequently, the air sampled during this period was frequently influenced by emissions from urban areas (**Figure 2.1**). During the period from July 8 to July 11, the local wind speed was generally low (< 1.5 m s^{-1} with an average of 1.5 ± 0.8 m s^{-1}), indicating that the observed air masses stagnated and were influenced by local emissions from the surrounding area. On the other hand, the local wind direction from July 11 to July 17 was northwesterly with the average wind speed of 1.3 ± 0.8 m s^{-1}. Based on these differences in the local wind speeds and wind direction, the three periods were defined as P1, P2, and P3, respectively. GF measurements for P3 are not available.

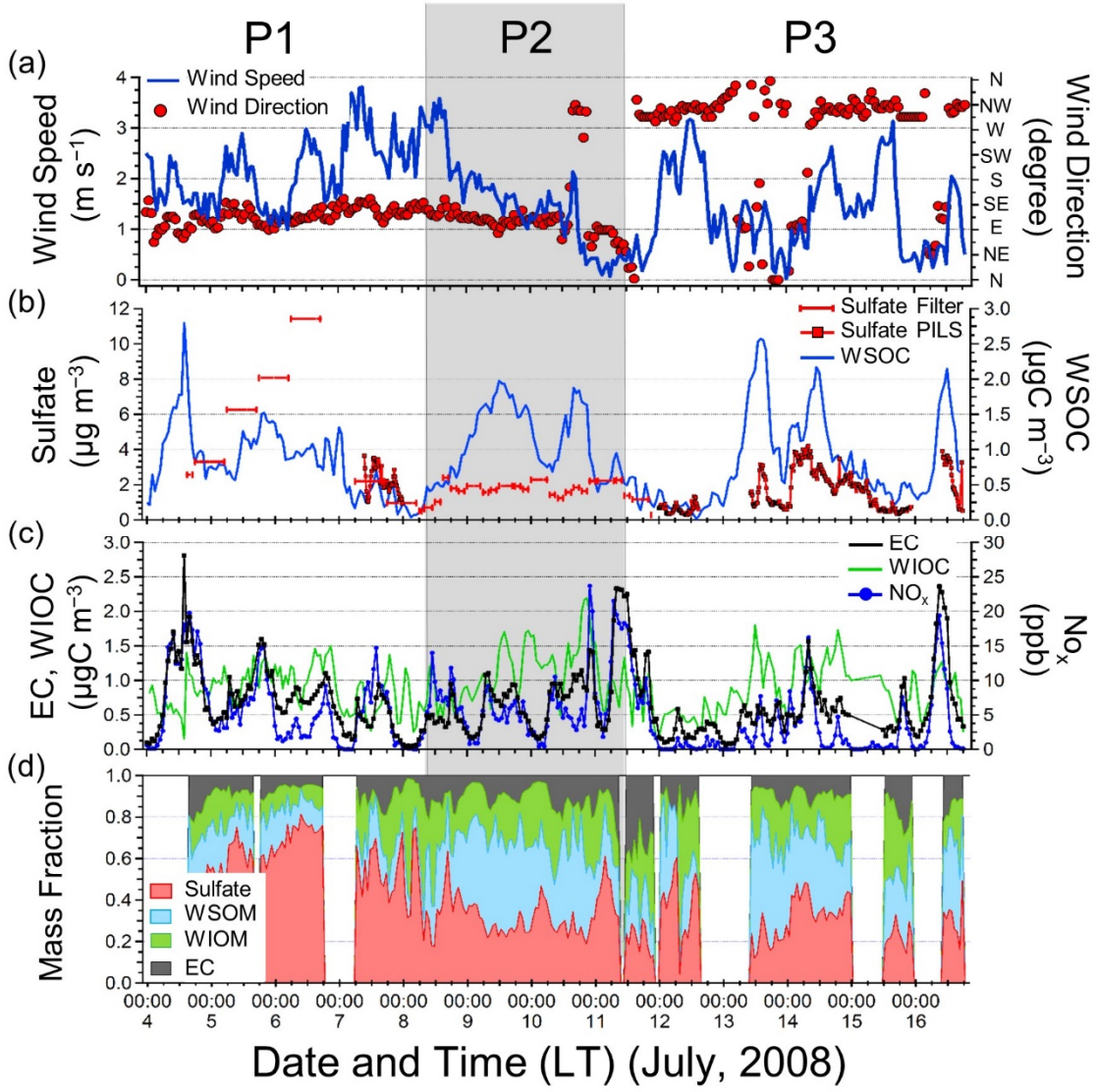

Figure 2.3 Time series of (a) local wind speeds and direction, (b) the concentrations of sulfate and WSOC, (c) EC, WIOC, and NO_x mixing ratios, and (d) the mass fraction of the measured component of submicron aerosols during the periods of 4 July–16 July 2008. Shaded area divides three periods (P1, P2, and P3).

2.3.1.1 Aerosol chemical composition

Table 2.1 summarizes the average mass concentrations of the major chemical components for each period. During P1, sulfate (5.20 ± 3.65 µg m^{-3}) was the most abundant accounting for 62.0% of the submicron particle mass measured during that period. On July 6 (P1), the sulfate concentration showed a substantial increase with a maximum of 11.42 µg m^{-3} (**Figure 2.3b**).

Table 2.1. Mass concentrations of EC, WIOM, WSOM, and SO_4^{2-}, together with the N_{CCN}/N_{CN} ratios of particles at 146 nm for SS of 0.1% to 0.8%. Average values are given for day (6:00–18:00 LT), night (18:00–6:00 LT), and the whole periods of P1, P2 and P3.

	P1 (July 4–8)			P2 (July 8–11)			P3 (July 11–17)		
	Day	Night	All	Day	Night	All	Day	Night	All
EC ($\mu gC\ m^{-3}$)	0.86 ± 0.47	0.52 ± 0.41	0.70 ± 0.48	0.75 ± 0.23	0.48 ± 0.34	0.62 ± 0.32	0.83 ± 0.67	0.42 ± 0.29	0.66 ± 0.58
WIOM ($\mu g\ m^{-3}$)	1.02 ± 0.54	1.05 ± 0.56	1.03 ± 0.55	1.29 ± 0.60	1.37 ± 0.72	1.33 ± 0.66	1.10 ± 0.62	0.97 ± 0.63	1.04 ± 0.62
WSOM ($\mu g\ m^{-3}$)	1.59 ± 0.94	1.31 ± 0.78	1.46 ± 0.88	2.24 ± 0.98	1.91 ± 0.73	2.08 ± 0.89	1.75 ± 1.34	1.04 ± 0.58	1.45 ± 1.13
SO_4^{2-} [a] ($\mu g\ m^{-3}$)	5.65 ± 3.89	4.24 ± 2.84	5.20 ± 3.65	1.68 ± 0.41	1.98 ± 0.25	1.83 ± 0.37	1.58 ± 1.02	1.44 ± 0.99	1.53 ± 1.01
N_{CCN}/N_{CN}	0.77 ± 0.10	0.91 ± 0.10	0.83 ± 0.12	0.46 ± 0.16	0.74 ± 0.16	0.58 ± 0.21	0.42 ± 0.19	0.65 ± 0.18	0.52 ± 0.2

[a] Concentrations are averaged from on- and offline measurements.

Conversely, the mass concentrations and fractions of organics during P2 and P3 were much larger than those during P1 as shown in **Figures 2.3b–2.3d**. The result clearly shows the change in the chemical compositions from sulfate-rich aerosols during P1 to organic-rich aerosols during P2/P3. The difference in the chemical compositions in the observed aerosol during each period can be explained by the difference in the local wind speeds and wind direction. As described above, the average local wind speed during P1 ($2.2 \pm 0.7\ m\ s^{-1}$) was higher than that during P2 ($1.5 \pm 0.8\ m\ s^{-1}$) and P3 ($1.3 \pm 0.8\ m\ s^{-1}$; **Figure 2.3a**). During P1, the predominant local winds were east to southeasterly, suggesting that most of the observed air masses were transported from the urban industrial areas, as described in Section 2.2.1. This explains the observed sulfate-rich aerosols, most of which were likely of anthropogenic origin. Although the predominant wind direction during P2 was similar to that during P1, the lower local wind speeds and the lower levels of sulfate during P2 suggest a difference in the dominant source of the air masses compared with P1. The predominant wind direction during P3 was northwest, which indicates the influence of emissions from vegetation and residential areas, as described

in Section 2.2.1. The chemical characteristics of the aerosols with the dominance of organics during P3 were rather similar to that observed during P2.

In order to investigate possible sources of organics, **Figure 2.4** presents the WSOC and WIOC concentrations as a function of EC for each period. The average concentrations of EC were similar in each period (0.62–0.70 μgC m^{-3}; **Table 2.1**) and the temporal variations in the EC concentrations generally agreed well with those in the NO_x mixing ratios during the entire period (R^2 = 0.71, **Figure 2.3c**). In urban areas, traffic emissions have been found to be the dominant source for NO_x, whereas EC is emitted by motor vehicles with burning diesel [e.g., *Seinfeld and Pandis*, 2006]. Indeed, *Gu et al.* [2011] reported that large concentrations of EC correlate well with those of NO_x in an urban environment and they attributed the dominant source of EC to traffic emission. Therefore, the current result indicates that the majority of the observed EC originated from combustion-derived sources, most likely traffic emissions. During P1 only, the WSOC showed a positive correlation with EC (**Figure 2.4a**), whereas the correlations were insignificant during P2 and P3 (**Figures 2.4b** and **2.4c**). This result and the possible source of EC as discussed above suggest that combustion-derived anthropogenic sources were the dominant sources of WSOC during P1. The result of the correlation and the larger concentrations of sulfate indicate the presence of more anthropogenically influenced aerosols during P1.

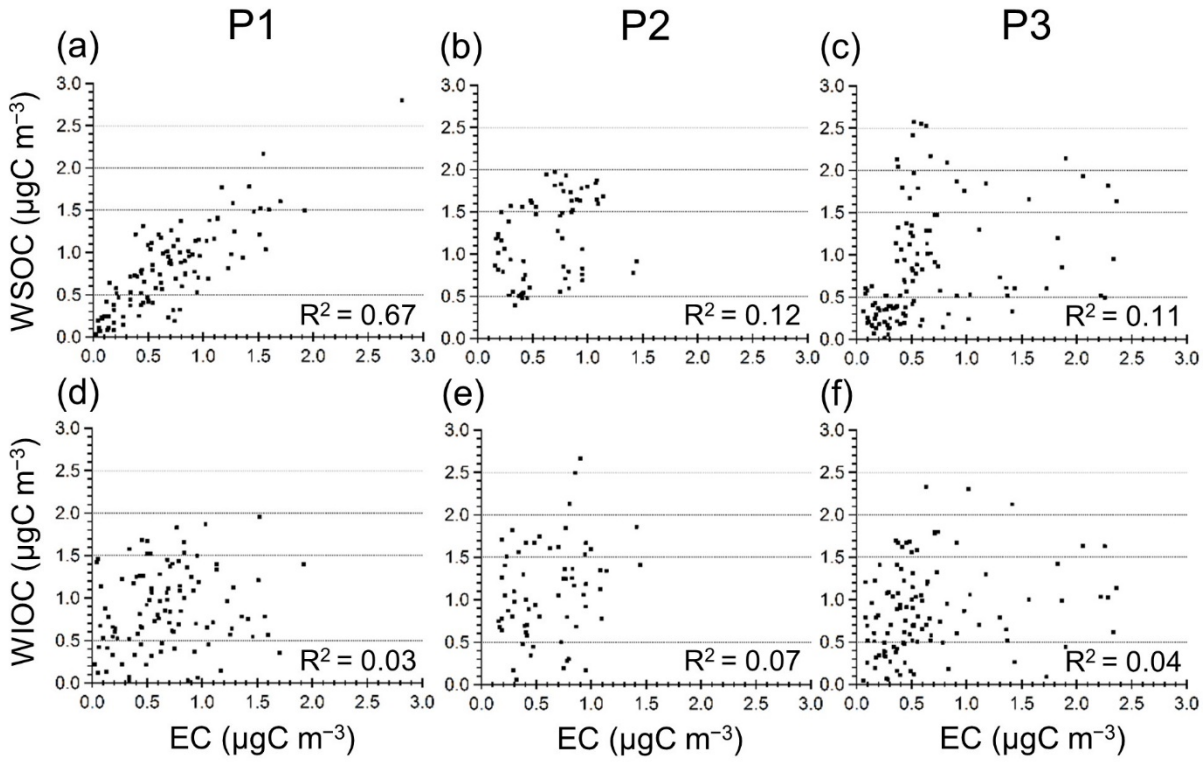

Figure 2.4 Scatterplots of (a–c) water-soluble organic carbon (WSOC) and (d–f) water-insoluble organic carbon (WIOC) versus elemental carbon (EC) for the periods P1, P2, and P3.

In contrast, the WSOC and WIOC concentrations showed insignificant correlations with EC, with a substantial decrease in the sulfate concentrations both during P2 and P3 (**Figures 2.4b, 2.4c, 2.4e,** and **2.4f**). This indicates that the majority of observed WSOC and WIOC during these periods did not originate from combustion-derived anthropogenic sources. Moreover, the diurnal profiles of the WSOC concentrations showed peaks during the daytime of these two periods, as shown in **Figure 2.3b**. These results suggest that the effects of local biogenic sources surrounding the study site (**Figure 2.1**) and the subsequent formation of OA on the temporal variations in WSOC were significant compared with variations due to the regional transport of air masses. In fact, *Pavuluri et al.* [2013] measured radiocarbon (^{14}C) of WSOC observed at the same sampling site in summer, which allows the quantitative apportionment between fossil fuel (dead carbon) and biogenic (modern carbon) sources. Based on this method, they found that 88% of WSOC consists of biogenic carbon, which supports the

present result.

2.3.1.2 Number concentrations and CCN activity

Figures 2.5a–2.5b show a time series of the size distribution of particle number concentrations and the N_{CN} during the study period. The N_{CN} at D_{dry} = 20.2–429 nm ranged from 230 cm^{-3} to 5,440 cm^{-3}, with an average of 1,560 cm^{-3}. This range is similar to that reported in previous field studies conducted at the same sampling site [*Jung et al.,* 2013]. The N_{CN} reached a maximum at the dominant size range in the Aitken mode (D_{dry} = 30–100 nm). The maximum of N_{CN} in the nucleation and Aitken modes was also reported by previous field measurements at the same sampling site [*Jung et al.,* 2013]. The measured N_{CN} in this study generally ranges from 1,000 to 10,000 cm^{-3}, which is typical of rural sites [e.g., *Hussein et al.,* 2004] in northern latitudes.

In this study, a D_{dry} of 146 nm was chosen as typical size for CCN at which even less hygroscopic particles in the ambient atmosphere can be activated at a SS of 0.1% [*Dusek et al.*, 2006; *Petters and Kreidenweis*, 2007; *Mochida et al.*, 2010]. The N_{CCN}/N_{CN} ratio showed a wide range between 0.04 and 1.02 with an uncertainty of 10% at a SS of 0.1% (**Figure 2.5c**).

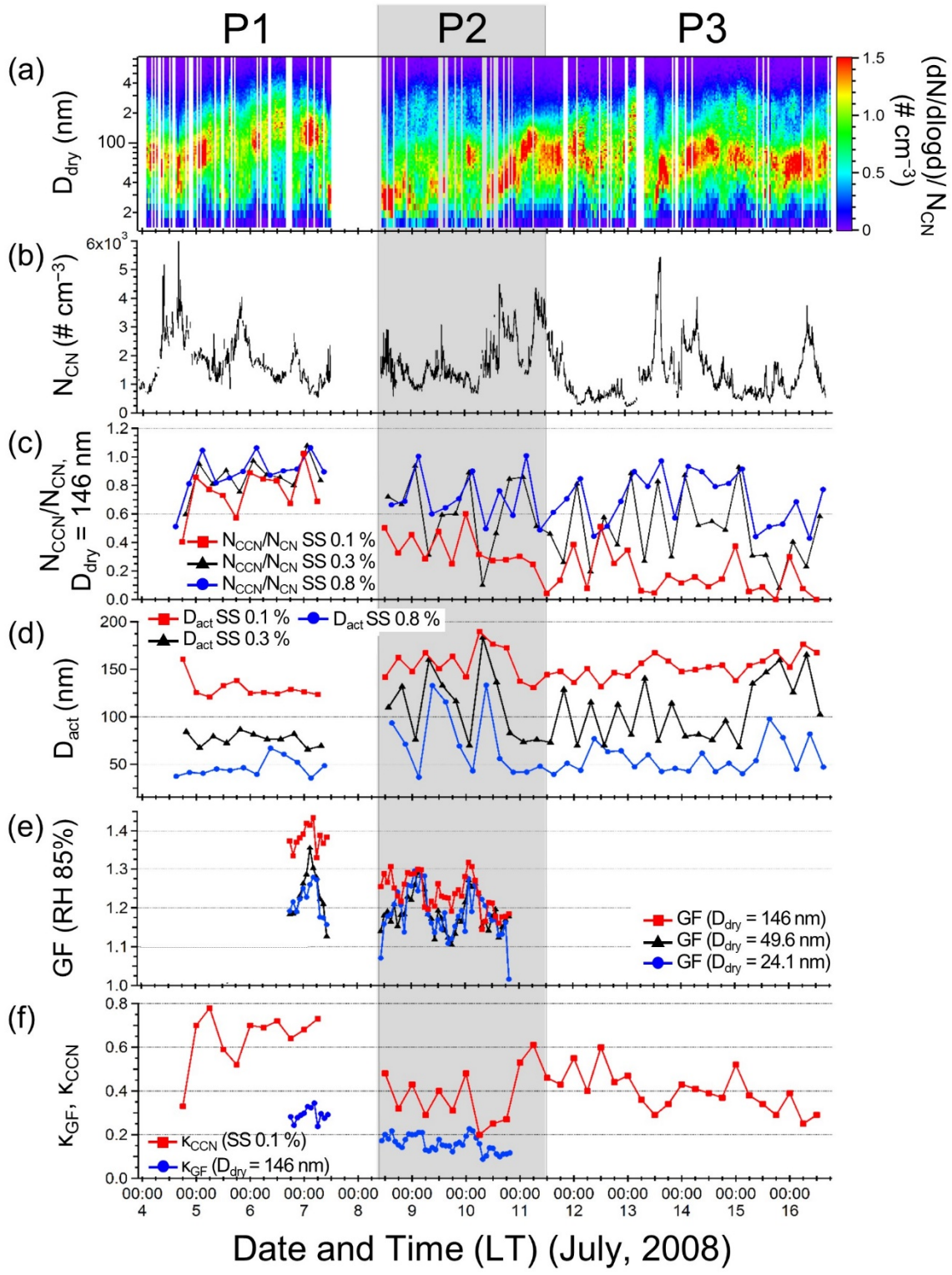

Figure 2.5 Time series of (a) the particle number size distribution, (b) the total particle number concentration (N_{CN}), (c) N_{CCN}/N_{CN} ratios (D_{dry} = 146 nm) at supersaturations (SS) of 0.1%, 0.3% and 0.8%, (d) activation diameter D_{act}, (e) hygroscopic growth factors (GF) for dry mobility sizes 146 nm, 49.6 nm and 24.1 nm under RH of 85%, and (f) hygroscopicity parameter kappa (κ) values each obtained by the GF (D_{dry} = 146 nm) and CCN (SS = 0.1%) measurements.

The wide range of the ratio indicates the presence of particles with different CCN activation properties. The N_{CCN}/N_{CN} ratios and their temporal variations were rather similar at each SS during P1, whereas the ratios at SS = 0.1% were much smaller than those at SS = 0.3% and 0.8% during P2 and P3 (**Figure 2.5c**). The similarity in the N_{CCN}/N_{CN} ratios with larger values during P1 suggests that the particles were highly CCN active, which did not significantly depend on SS, indicating internally mixed particles with highly hygroscopic chemical composition. This is supported by the dominance of sulfate during P1 (**Figure 2.3d**). On the other hand, the larger difference in the N_{CCN}/N_{CN} ratio at a different SS suggests that the majority of the observed particles during P2 and P3, even if they were in the same aerosol population, was externally mixed with different CCN characteristics. Similar results were obtained by *Silvergren et al.* [2014] who found that the N_{CCN}/N_{CN} ratio was less sensitive to SS for highly hygroscopic, internally mixed particles, whereas the sensitivity was high for less hygroscopic, externally mixed particles influenced by anthropogenic emissions. In summary, the difference in the N_{CCN}/N_{CN} ratios among the different SS values in this study indicates that the reduction of the CCN activity depends on the chemical composition and mixing state of the observed aerosols.

Figure 2.5d presents temporal variations of activation diameter D_{act}, the average values of which during each period are shown in **Table 2.2**. The average D_{act} values at 0.1% SS during P2 and P3 were 156.8 ± 17.1 nm and 152.4 ± 11.0 nm, respectively, which are substantially larger than that during P1 (130.1 ± 10.7 nm). These D_{act} values correspond to the average κ_{CCN} values of 0.64 ± 0.12, 0.38 ± 0.12, and 0.40 ± 0.09 for P1, P2, and P3, respectively. The differences in D_{act} and κ_{CCN} during each period suggest that the CCN were less active during P2 and P3 than during P1.

Table 2.2. Average values (± SD) of activation diameter (D_{act}) at each supersaturation (SS) and κ_{CCN} during P1, P2, and P3.

SS (%)	P1 (July 4–8)		P2 (July 8–11)		P3 (July 11–17)	
	D_{act} (nm)	κ_{CCN}	D_{act} (nm)	κ_{CCN}	D_{act} (nm)	κ_{CCN}
0.1	130.1 ± 10.7	0.64 ± 0.12	156.8 ± 17.1	0.38 ± 0.12	152.4 ± 11.0	0.40 ± 0.09
0.3	76.5 ± 6.7	0.36 ± 0.10	115.7 ± 35.8	0.15 ± 0.13	104.1 ± 30.9	0.21 ± 0.15
0.8	46.5 ± 9.0	0.26 ± 0.12	75.9 ± 35.5	0.15 ± 0.15	55.6 ± 15.5	0.17 ± 0.10

New particle formation (NPF) for particles with D_{dry} < 30 nm and subsequent growth of the particles were observed on July 9–11 during P2 (**Figure 2.5a**). Several NPF events in summer were also reported for the same site in previous studies [e.g., *Jung et al.*, 2013]. An increase in the number concentrations of the particles with D_{dry} = 146 nm resulted in a decrease of the N_{CCN}/N_{CN} ratios at a SS of 0.1%. Note that a significant decrease was observed during P2/P3 rather than during P1, in spite of the similarity in the number size distribution (**Figure 2.5a**). The suppression of the CCN activity during P2 and P3 can therefore be related to the change in the chemical composition and mixing state of the particles.

2.3.1.3 Hygroscopic growth factor

Figure 2.5e shows the temporal variation of the GF for particles at each measured diameters, whereas the average values during each period are summarized in **Table 2.3**.

Although the hygroscopic GF data were obtained during the limited period of P1 and P2, a significant difference in the GF values was observed between these two periods. The average GF at D_{dry} = 146 nm during P1 (1.37 ± 0.04) was larger than those during P2 (1.24 ± 0.05). The observed GF values in the current study generally agree with those (1.19–1.27) at D_{dry} of 120 nm, obtained at the same site in summer 2011 [*Jung and Kawamura*, 2014]. Other studies reported GF values of 1.20–1.50 at similar values of D_{dry} at a suburban site in Paris

[*Jurányi et al.*, 2013; *Laborde et al.*, 2013]. The larger GF values were associated with aged air masses in those previous studies, similar to those observed during P1 in this study.

Table 2.3. Average values (± SD) of hygroscopic growth factor (GF) at each size, and their averages (bulk) during the periods of P1 and P2.

	P1 (July 4 – 8)	P2 (July 8 – 11)
D_{dry} = 146 nm	1.37 ± 0.04	1.24 ± 0.05
D_{dry} = 49.6 nm	1.23 ± 0.06	1.19 ± 0.05
D_{dry} = 24.1 nm	1.21 ± 0.05	1.19 ± 0.06
bulk	1.28 ± 0.09	1.21 ± 0.05

Table 2.4 lists typical GF values for different types of aerosols reported in previous studies. The observed GF of 1.37 at D_{dry} of 146 nm, obtained during P1, is close to the lower end of GF for AS (1.50–1.70). This is consistent with the aerosol chemical measurements, which showed the dominant contribution of sulfate to the submicron particle mass as discussed above. In contrast, the GF for the smaller particles (D_{dry} < 50 nm) in P2 (1.19; **Table 2.3**) is rather similar to typical values for secondary organic aerosols (SOA; 1.03–1.16) [*Virkkula et al.*, 1999; *Saathoff et al.*, 2003; *Varutbangkul et al.*, 2006; *Duplissy et al.*, 2011] and EC (< 1.05) [*Weingartner et al.*, 1997] (**Table 2.4**). The enrichment of sulfate in the accumulation mode, and the largest fraction of organic mass being found in the Aitken size mode, has also been found in other environments [*Pöschl et al.*, 2010; *Whitehead et al.*, 2016]. The present data suggest that the GF depends on the particle size, which is attributable to the size-dependent chemical composition. This point is further discussed in Section 2.3.3.

In order to discuss the link between hygroscopicity at each particle size and chemical composition, **Figures 2.6a–2.6c** show temporal variations in the particle number concentrations as a function of the GF at D_{dry} of 146 nm, 49.6 nm, and 24.1 nm. The GF and particle number

Table 2.4. Typical values of hygroscopic growth factor (GF) for various aerosol components reported in previous studies.

Aerosol type	Growth factor	RH	Author
BC, mineral dust	Almost hydrophobic, GF < 1.05	94%, 95%	Weingartner et al. (1997); Vlasenko et al. (2005)
Biomass burning	Wide range, up to 1.65, GF is lower at the source, increases after mixing with secondary inorganic ions	89%, 90%	Cocker et al. (2001); Swietlicki et al. (2008)
Ammonium sulfate $(NH_4)_2SO_4$, ammonium nitrate NH_4NO_3	GF 1.5–1.7 Associated inorganic ions: NO_3^-, SO_4^{2-}, NH_4^+	85%, 90%	Gysel et al. (2002); Wise (2003); Swietlicki et al., (2008)
Secondary organic aerosol (SOA)	1.01–1.16 Aged SOA in simulation chamber: up to 1.65	84%, 85%, 90%, 95%	Virkkula et al. (1999); Saathoff et al. (2003); Varutbangkul et al. (2006); Duplissy et al. (2011)
Organic compounds	1.0–1.7	80%, 85%, 90%, 95%	Peng et al. (2001); Chan and Chan (2003); Prenni et al. (2003); Wise (2003); Huff Hartz et al. (2006); Koehler et al. (2006)
Secondary organic aerosols from terpenes, α–pinene, β–pinene	1.03–1.18	85%, 90%	Saathoff et al. (2003); Varutbangkul et al. (2006); Prenni et al. (2007)
Sea–salt, sulfuric acid	> 2.0	90%, 95%	Gysel et al. (2002); Koehler et al. (2006)

distributions indicate a large dependence of the GF on the particle size. The GF at D_{dry} = 146 nm during P1 showed a unimodal distribution with a peak as high as 1.40, which is more significant than those at smaller particle sizes (49.6 and 24.1 nm as seen in **Figures 2.6b** and **2.6c**, respectively). This result supports the idea that most of the particles were internally mixed during P1, with the dominance of sulfate mostly residing in the accumulation size mode, as

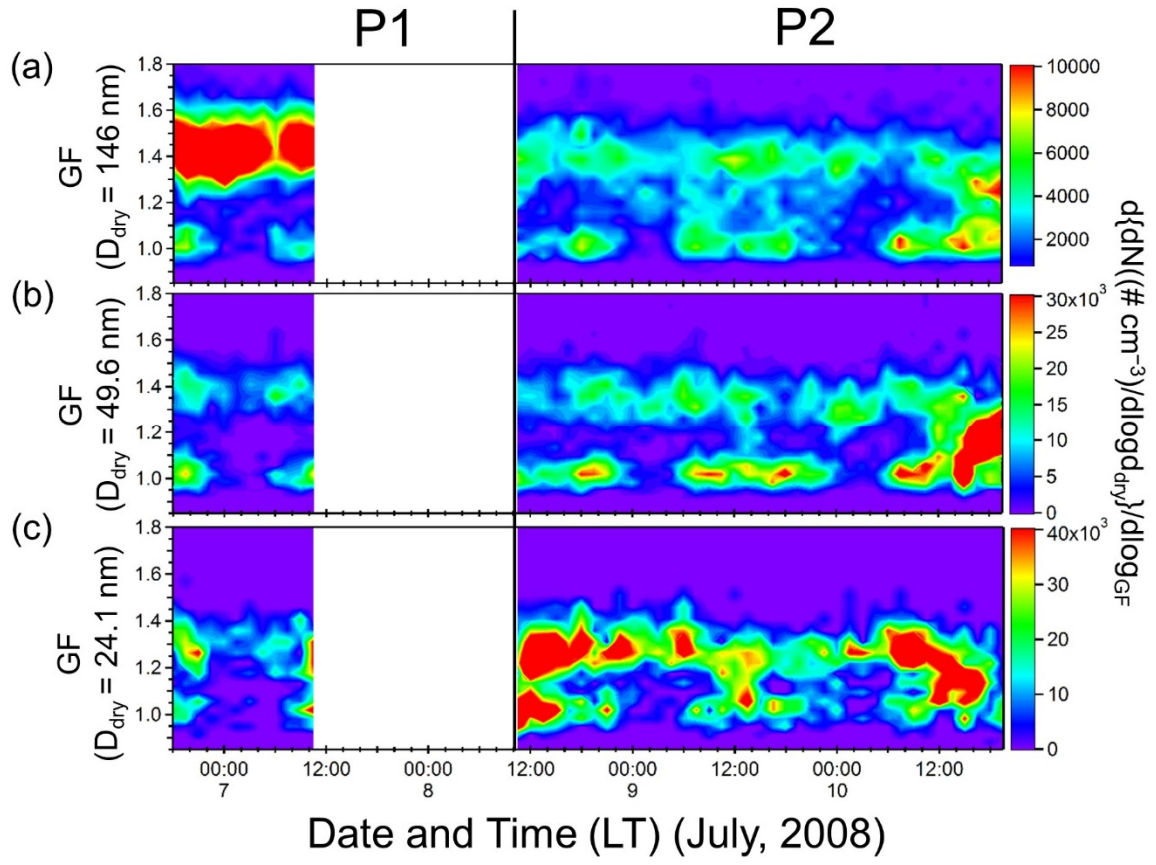

Figure 2.6 Temporal variations in the particle number concentrations as a function of the growth factor (GF) at D_{dry} of (a) 146 nm, (b) 49.6 nm, and (c) 24.1 nm.

discussed above. For the smaller particles (D_{dry} = 24.1 and 49.6 nm), bimodal GF distributions became more pronounced during P2, which supports the idea that the majority of the particles were externally mixed during this period. The contributions of the particle number to the high GF values were more significant at these smaller sizes (**Figures 2.6b** and **2.6c**). This is attributable to the increase in the particle number concentrations in the Aitken mode (**Figures 2.5a** and **2.5b**) with less aged characteristics of the particles of local origin.

2.3.2 Super- and subsaturated hygroscopicity

Figure 2.5f shows the temporal variations of the κ_{CCN} and κ_{GF}. Overall, the average κ_{CCN} (0.24 ± 0.16) observed in this study is similar to those reported for a suburban site in Paris

(κ_{CCN} = 0.08–0.24 at SS of 0.1–1.0%) [*Jurányi et al.*, 2013]. As expected from the GF values, the κ_{CCN} and κ_{GF} during P1 were significantly larger than those during P2 and P3 (also summerized in **Table 2.5**), exhibiting greater hygroscopicity during P1 under both

Table 2.5. κ values derived from the hygroscopic growth factor (κ_{GF}) and the CCN measurements (κ_{CCN}) for day, night, and the whole periods of P1, P2, and P3. κ_{GF} shown is the average of the sizes at 146 nm, 49.6 nm, and 24.1 nm. κ_{CCN} is the average value obtained at SS between 0.1% and 0.8%.

	P1			P2			P3		
	Day	Night	All	Day	Night	All	Day	Night	All
κ_{GF}	0.17 ± 0.07	0.21 ± 0.07	0.20 ± 0.08	0.12 ± 0.03	0.16 ± 0.04	0.14 ± 0.04	n/a*	n/a*	n/a*
κ_{CCN}	0.39 ± 0.16	0.46 ± 0.20	0.36 ± 0.16	0.14 ± 0.14	0.31 ± 0.13	0.15 ± 0.12	0.25 ± 0.11	0.27 ± 0.13	0.20 ± 0.11

* Data is not available.

supersaturated and subsaturated conditions. In order to examine the κ values derived from the CCNC and HTDMA measurements, **Figure 2.7** compares the average κ_{GF} (D_{dry} = 49, 146 nm) with κ_{CCN} values at similar D_{act} ranges (47.34–129.04 nm for P1; 69.81–189.54 nm for P2) obtained at SS of 0.1 and 0.3%. While the κ_{CCN} under all SS conditions correlated well with the corresponding κ_{GF} (R^2 = 0.82), the κ_{CCN} was generally larger than the κ_{GF} by 59% and 44% for P1 and P2, respectively. The degree of the difference in this study is similar to that (~37%) has been found for ambient aerosols at a mountainous site in central Germany [*Wu et al.*, 2013] and at an urban site in Japan [*Kawana et al.*, 2016].

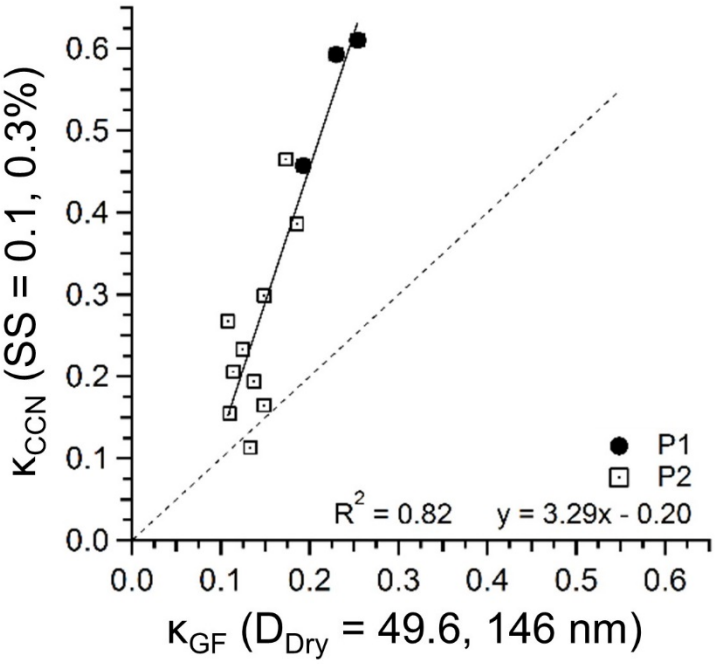

Figure 2.7 Scatterplot of κ_{CCN} versus κ_{GF}. The average κ_{GF} at D_{dry} of 49 and 146 nm are compared with the average κ_{CCN} at similar D_{act} under SS of 0.1% and 0.3%. The data obtained during P1 and P2 are indicated by solid circles and open squares, respectively.

Discrepancies between CCNC-derived and HTDMA-derived κ values have been reported in a number of previous studies, which have generally reported larger κ_{CCN} compared to κ_{GF} [*Roberts et al.*, 2010; *Cerully et al.*, 2011; *Hersey et al.*, 2013; *Hong et al.*, 2014; *Hansen et al.*, 2015]. Although *Carrico et al.* [2008] reported that κ_{CCN} and κ_{GF} (at RH = 90%) for laboratory-generated biomass burning particles agreed to within 20% and *Dusek et al.* [2011] also showed the agreement between κ_{CCN} and κ_{GF} (at RH = 85%) for particles with diamters of 100–150 nm, the difference between them increased with decreasing particles size. *Irwin et al.* [2010] found that the discrepancy between κ_{CCN} and κ_{GF} (at RH = 86%) increased with decreasing particle size for particles measured at a mountainous site in Germany. These discrepancies can be attributed to several factors: the differences in the size-dependence of chemical compositions, the effects of solutes on water activity under sub- and supersaturated conditions particularly in the presence of organic compounds, and particle mixing state [*Roberts et al.*, 2010; *Hersey et al.*, 2013; *Hong et al.*, 2014]. In general, surface active organic

compounds decrease the surface tension of particles and reduce the surface tension effect (Kelvin effect) [*Wex et al.*, 2008], which increases CCN activity [*Sorjamaa et al.*, 2004; *Wex et al.*, 2008; *Irwin et al.*, 2010; *Dusek et al.*, 2011]. The effect of the surface tension becomes more important for particles in the smaller size range (e.g., <~170 nm), because a certain amount of surfactant is more concentrated in a droplet of solution formed on smaller particles rather than larger ones [*Sorjamaa et al.*, 2004; *Wex et al.*, 2008; *Irwin et al.*, 2010; *Dusek et al.*, 2011]. On the other hand, the partitioning from bulk to surface of a particle decreases the concentration of the bulk solute with increasing the fraction of surfactants. This increases the water activity (Raoult effect) of the droplet and can compensate the reduction of the surface tension at the droplet-air interface, which reduces CCN activity [*Li et al.,* 1998*; Rood and Williams,* 2001*; Sorjamaa et al.,* 2004*; Wex et al.,* 2008*; Frosch et al.,* 2011*; Renbaum-Wolff et al.,* 2016]. Therefore, changes in the surface tension and the presence of organics can largely affect the particle hygroscopicity under supersaturated condition. In contrast, hygroscopic growth under subsaturated condition is insensitive towards changes in the surface tension [*Wex et al.*, 2008]. Consequently, the above effects can contribute to the discrepancy between κ_{CCN} and κ_{GF}.

With regard to the effect of the mixing state, for example, *Hersey et al.* [2013] suggested that a transition from externally mixed to internally mixed aerosols, as the aerosols evolved from west to east of the Los Angeles Basin, leads to an increased difference between κ_{CCN} and κ_{GF}. Photochemical aging of particles results in the conversion of externally mixed to internally mixed particles, which enhanced κ_{CCN} with increasing coating thickness on refractory black carbon in their case. In contrast, the aging resulted in the suppressed subsaturated water uptake (κ_{GF}) of the main hygroscopic mode, which is attributable to the formation of separate, organic layers that inhibit the water uptake during humidification under the conditions of the κ_{GF} measurement. These effects can also explain the increased discrepancy between κ_{GF} and κ_{CCN}

for aged aerosols. In this study, the reduced difference between κ_{CCN} and κ_{GF} during P2 (**Figure 2.5f**) indicates the dominance of externally mixed aerosols compared with the sulfate-rich, internally mixed aged aerosols observed during P1. Indeed, the GF distributions presented in **Figures 2.6a–2.6c** demonstrate that the observed particles show bimodal distributions during P2 and thus are indicative of the external mixture. On the other hand, the unimodal GF distribution during P1 supports the idea that most of the particles were internally mixed during this period.

2.3.3. Diurnal variations and size-dependence of particle hygroscopicity

Figure 2.8 shows diurnal profiles of the GF, N_{CCN}/N_{CN} ratio, and κ_{CCN}, in relation to the chemical compositions for each period. The bulk GF values at night (1.30 ± 0.08 for P1 and 1.24 ± 0.05 for P2) were larger than those in the daytime (1.24 ± 0.09 for P1 and 1.18 ± 0.03 for P2). A similar difference was also observed for κ_{CCN}, particularly during P2, when the κ_{CCN} in the daytime (0.14 ± 0.14) was substantially lower than that (0.31 ± 0.13) at night (**Table 2.5**). The larger hygroscopicity at 0:00–6:00 LT can be attributed to the increased concentrations of sulfate. **Figure 2.9** displays diurnal changes of the N_{CCN}/N_{CN} efficiency spectra as a function of D_{dry} at a SS of 0.1% and 0.3%, as representative profiles during each period. Indeed, the typical CCN spectra during the nighttime of P1 were similar to that of AS (**Figure 2.9a**), which is consistent with the chemical measurements exhibiting substantial mass fractions of sulfate (62.0 ± 43.5%) in the submicron particles. Even during P2, the CCN spectra at 00:00–01:30 were similar to those of AS (**Figure 2.9b**). This result supports the idea that the greater hygroscopicity at 0:00–6:00 LT can be attributed to the increased concentrations and mass fractions of sulfate.

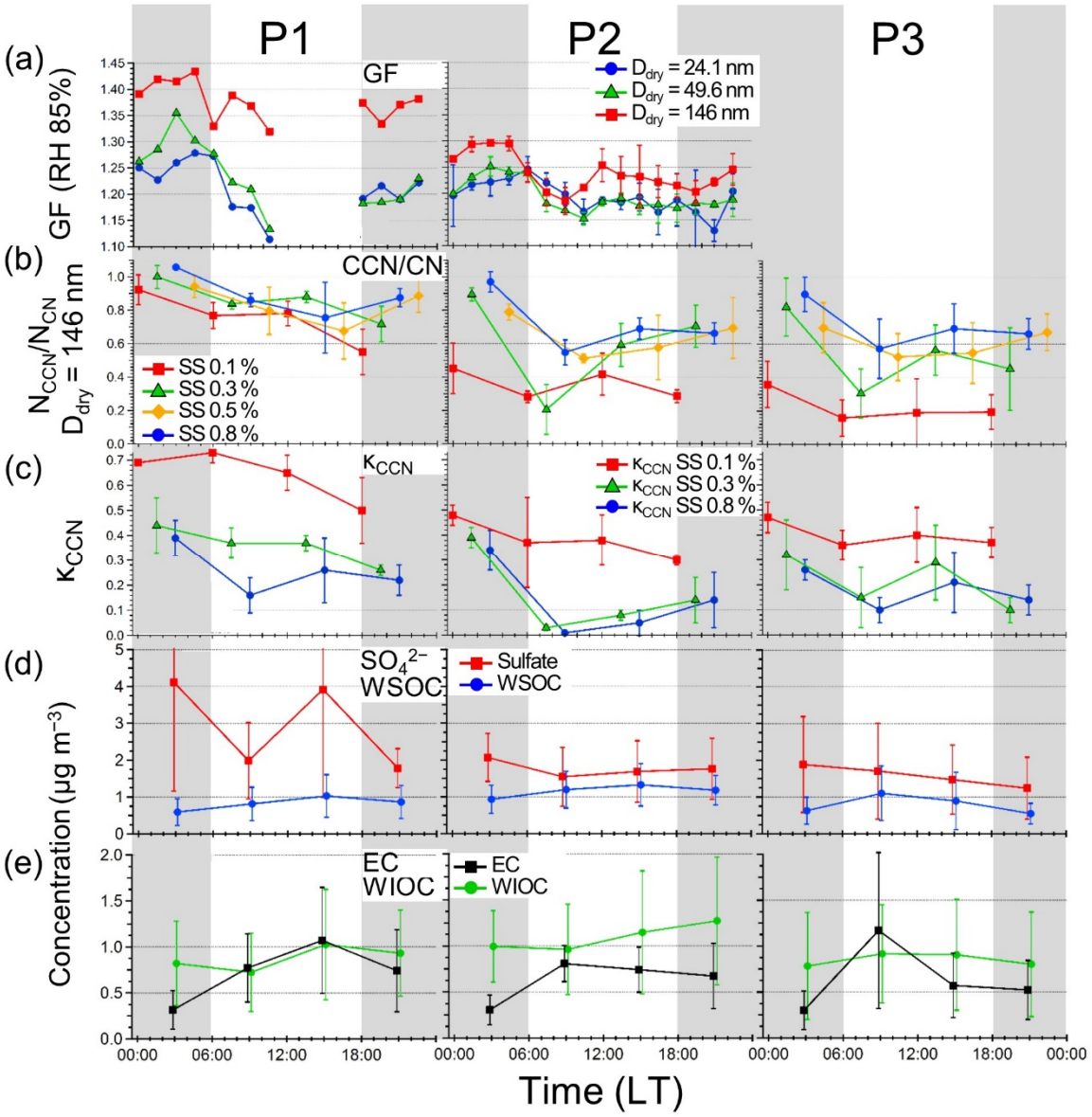

Figure 2.8 Diurnal profiles of (a) growth factors (GF) at RH of 85%, (b) N_{CCN}/N_{CN} ratios for particles with dry mobility diameter of 146 nm, (c) κ_{CCN} under SS of 0.1%, 0.3% and 0.8%, the mass concentrations of (d) sulfate and water-soluble organic carbon (WSOC), and (e) water-insoluble organic carbon (WIOC) and elemental carbon (EC). Bars indicate ± 1 σ (standard deviation) of each average value. Shaded area indicates the nighttime.

Particles with D_{dry} < 100 nm for 0.3% SS during P1 activated more readily than those during P2 and P3 (**Figure 2.9**). The CCN efficiency curves exhibit a much larger difference in the D_{act} between the ambient and AS particles during the daytime of P2 and P3. In general, the broad sigmoid of the CCN spectra is closely related to the heterogeneity of the aerosol chemical composition [*Moore et al.*, 2010; *Padró et al.*, 2012]. Combined with the bimodal GF

distribution during the daytime of P2 (**Figure 2.6**), the result indicates a larger degree of external mixture during these periods. This is particularly true for the particles at 0.3% SS, which emphasizes the increase of less-CCN active particles during the daytime. This can be explained by the increased concentrations of organics and EC during the day in P2 and P3 as shown in **Figures 2.8d** and **2.8e**. These observations indicate that increased organics and EC

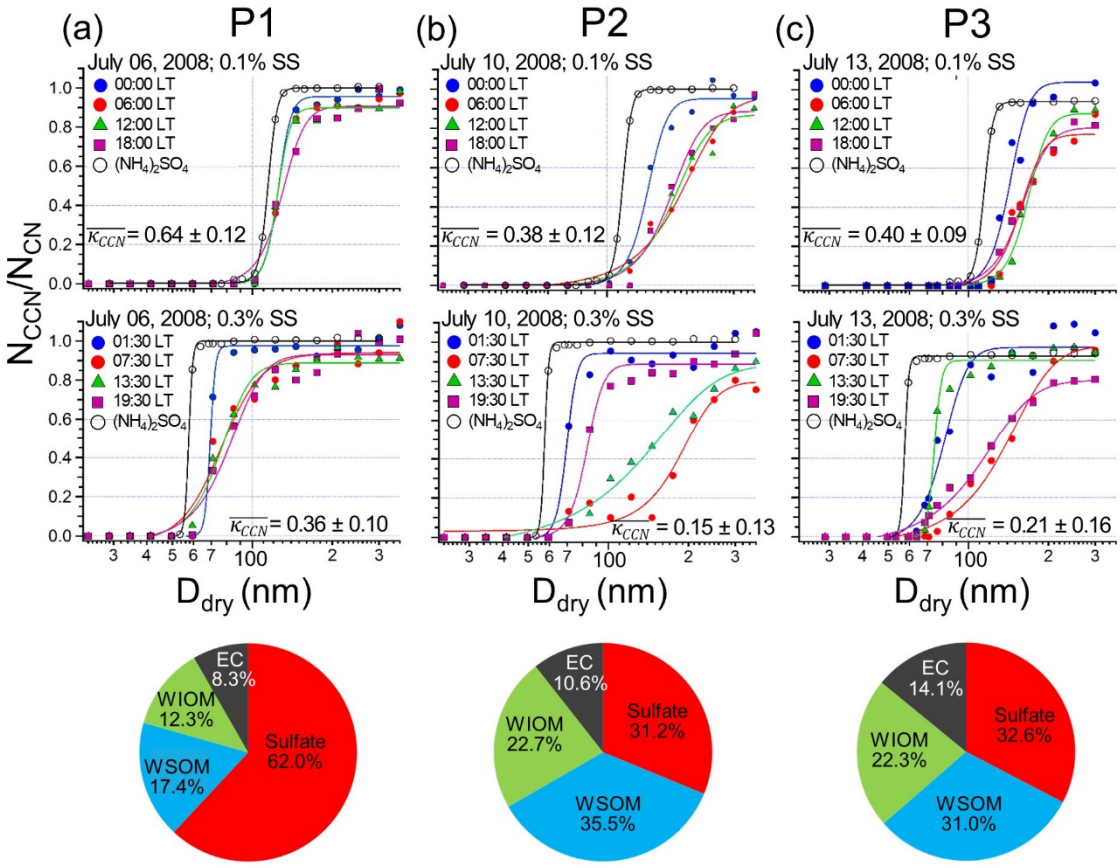

Figure 2.9 Diurnal changes in the N_{CCN}/N_{CN} efficiency spectra at SS of 0.1% and 0.3% on (a) July 6, (b) July 10, and (c) July 13, 2008, as representatives of periods P1, P2, and P3, respectively. The efficiency spectra was fitted using a cumulative distribution function given by *Rose et al.* [2008]. Pie chart shows the mass fractions of sulfate, WSOM, WIOM, and EC during each period.

concentrations suppressed the particle hygroscopicity during the day. The hygroscopicity of particles that activated at SS = 0.1% in the accumulation mode (**Figure 2.9**) is probably less affected by the diurnal changes in those emissions. This indicates that the suppression of κ_{CCN} in the smaller size ranges was attributable to these organics and EC. Similarly,

Crosbie et al. [2015] reported that the lowest hygroscopicity values correspond with the maximum concentrations of EC and OC, which they found in the early morning in Central Tucson. On the other hand, during nighttime, internally mixed aerosols dominated by sulfate increased the hygroscopicity of particles during P1 in this study (**Figure 2.8c**).

Many of the previous studies showed diurnal cycles of particle hygroscopicity, with peaks typically appearing in the afternoon in urban [*Crosbie et al.*, 2015], rural [*Cerully et al.*, 2015], marine [*Kalivitis et al.*, 2015], boreal forest, and grassland areas [*Paramonov et al.*, 2015]. This has been explained by atmospheric aging of aerosols through condensational growth of photochemically oxidized organics and sulfate. The diurnal pattern obtained in this study is rather similar to those reported for observational sites at higher altitudes in France, and in the central Himalayas [*Holmgren et al.*, 2014; *Dumka et al.*, 2015]. *Holmgren et al.* [2014] and *Dumka et al.* [2015] attributed the lower hygroscopicity during the daytime to the reduced influence of anthropogenic emissions on the observed aerosols due to the lifting of the planetary boundary layer.

To further investigate the GF mode, a distribution function was derived for each GF obtained every 90 min for each particle size (D_{dry} = 24.1 nm, 49.6 nm, and 146 nm) between July 6 and July 10. **Figure 2.10** presents a typical example of the observed bimodal GF distribution function for the particle size of 146 nm, measured during a specific time period (18:00–19:30) on July 6. The figure shows two peaks in the GF distribution, where one peak was observed at the GF of ~1.02 and the other one at the GF of ~1.40. The particle number

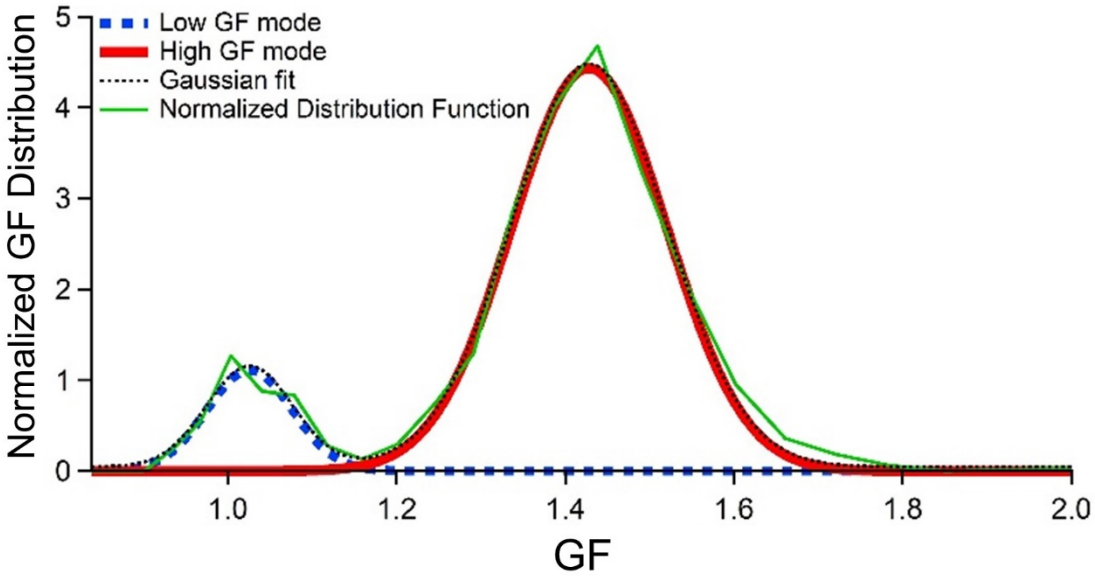

Figure 2.10 Example of a bimodal GF distribution. For the definition of high GF (N_{HGF}) and low GF (N_{LGF}) modes, see text. The GF distribution are calculated using a multiple Gaussian fit applied on the normalized distribution function. Separation of the modes was made by cluster analysis using the program IGOR Pro.

fractions of low and high GF modes are defined as N_{LGF} and N_{HGF}, respectively. The peaks for each size-segregated bimodal GF distribution are calculated using a multiple Gaussian fit. As introduced in Section 2.2.3, cluster analysis is applied to calculate the fraction of the particle number concentration of low and high GF modes; the peaks of the low and high GF modes were 1.02 and 1.35, respectively. **Figure 2.11a** shows the temporal variations of N_{LGF} and N_{HGF}, for particles at D_{dry} = 49.6 nm, whereas the N_{LGF} and N_{HGF} for particles at D_{dry} = 24.1 nm and 146 nm are shown in **Figures 2.12a** and **2.12b**, respectively. The temporal variation of N_{LGF} at D_{dry} = 49.6 nm followed that of the EC concentrations (**Figure 2.11b**). Although size-segregated EC data in the submicron range were not available in this study, the similar temporal trend indicates that the variation of the low GF in the small size particles is generally attributable to the contribution of EC.

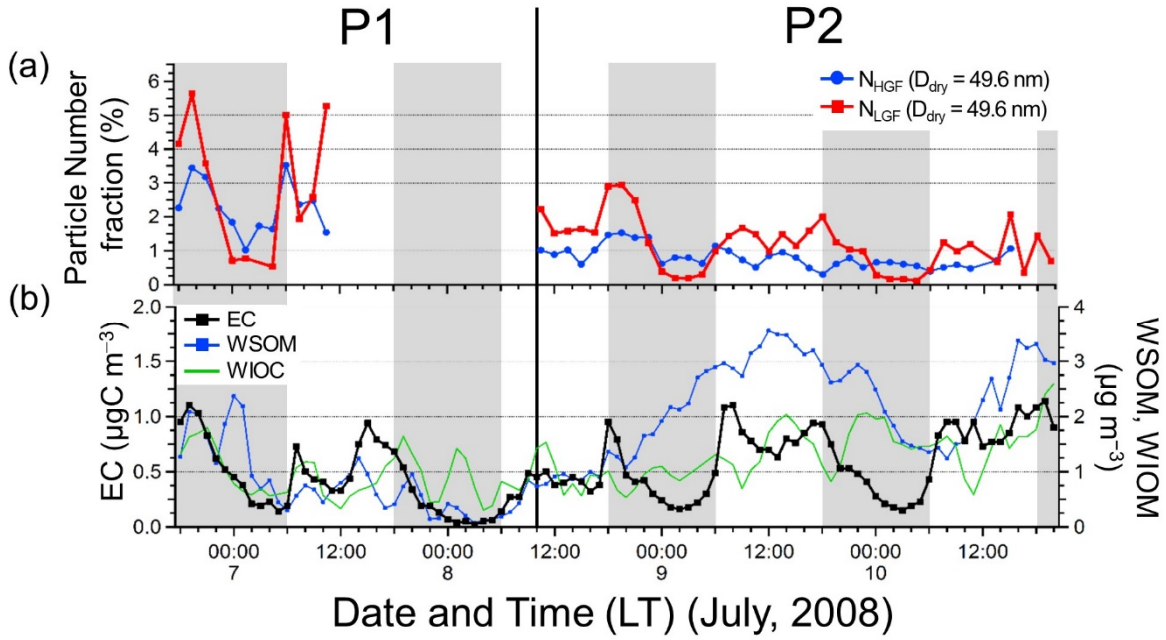

Figure 2.11 Temporal variations in (a) the particle number fraction for high GF mode (N_{HGF}) and low GF mode (N_{LGF}) particles at D_{dry} = 49.6 nm, and (b) the mass concentrations of EC, WSOM, and WIOM.

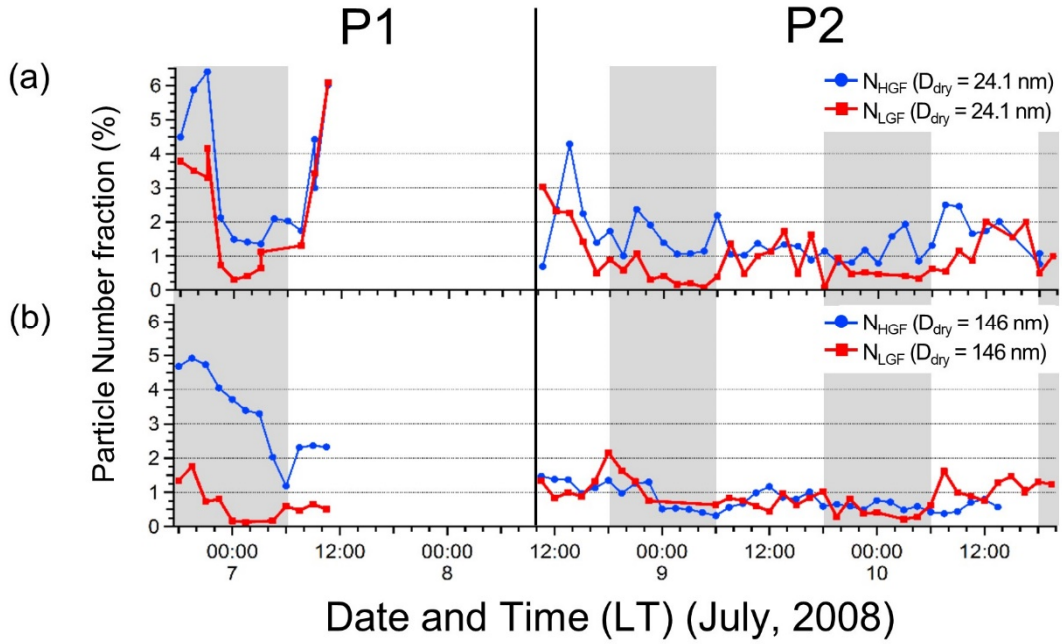

Figure 2.12 The number fractions of particles for high GF (N_{HGF}) and low GF modes (N_{LGF}) with the dry particle diameters of (a) 24.1 nm and (b) 146 nm. Shaded areas indicate night time.

Figure 2.13 shows the hygroscopic GF as a function of the WSOM-to-sulfate ratio at each D_{dry}. The hygroscopic GF values at D_{dry} = 146 nm tend to increase with decreasing

WSOM-to-sulfate ratios (**Figure 2.13a**), suggesting that the hygroscopicity in the accumulation size mode depends on the abundance of organic matter (OM) relative to sulfate. This can explain the fact that the GF of smaller size particles does not depend on the WSOM/sulfate ratios (**Figures 2.13b** and **2.13c**).

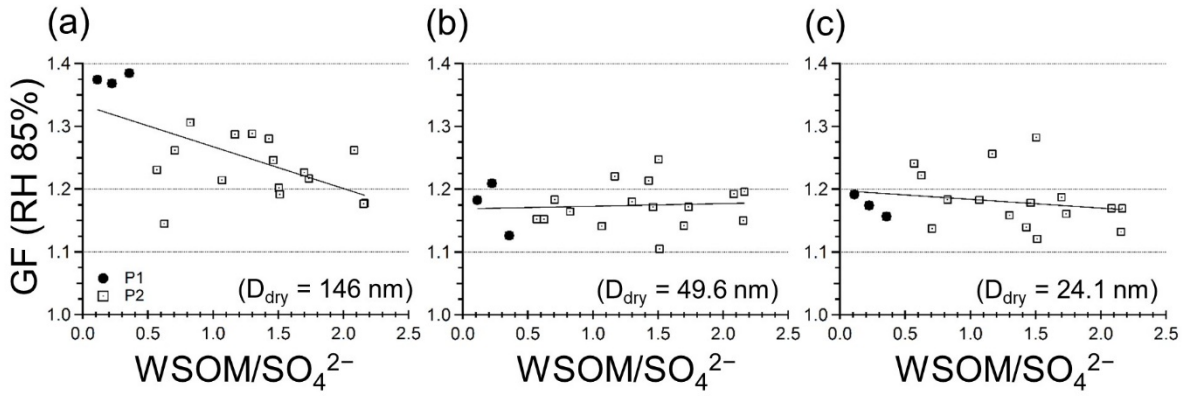

Figure 2.13 Scatter-plot of hygroscopic GF versus ratio of the WSOM to sulfate at D_{dry} of (a) 146 nm, (b) 49.6 nm, and (c) 24.1 nm. Data during P1 and P2 are indicated by solid circles and open squares, respectively.

Overall, the above result suggests that the particle hygroscopicity was suppressed during P2 due to increased external mixture of less aged particles containing organics, possibly from biogenic origins, and EC. In summary, the present study shows that the more-aged internally-mixed aerosol particles during P1 are of anthropogenic origin, and that their higher hygroscopic properties are due to the larger fraction of sulfate. On the other hand, less-aged, externally mixed, less hygroscopic particles during P2 and P3 are dominated by organic carbon of local biogenic origin. The results suggest that the abundance of OM relative to sulfate in the accumulation mode, and the absolute abundance of EC in the Aitken mode, are important factors controlling the hygroscopicity of submicron particles. This might be important for predicting cloud properties under the similar atmospheric conditions.

2.4 Conclusions

Continuous in situ measurements of size-segregated CCN spectra at four supersaturations (0.1%, 0.3%, 0.5% and 0.8%), and hygroscopic GF at 85% RH, were simultaneously conducted at a suburban site in northern Japan, in summer. Two distinct periods were observed in terms of differences in GF, D_{act}, and chemical compositions. The κ values derived from the CCN measurements were generally larger than those derived from the HTDMA measurements by 42%–56%. The GF (1.37 ± 0.04) with D_{dry} of 146 nm and bulk N_{CCN}/N_{CN} ratios (0.83 ± 0.12) showed higher values during the first period (P1). The data suggest the dominance of internally mixed sulfate aerosols in the accumulation size mode with relatively aged characterisitics.

On the other hand, the particles observed during the latter period (P2 and P3) showed external mixing dominated by organics, which was linked to low hygroscopicity and CCN activity. In particular, higher loading of WSOM, which accounted for ~60% of OM by mass, and increased WSOM/sulfate ratios, corresponded to low GF and N_{CCN}/N_{CN} ratios with larger D_{act} in the accumulation size range. This result suggests that WSOM, probably dominated by the influence of biogenic sources, is responsible for suppressing hygroscopicity and CCN activation in the accumulation size modes in this study.

Temporal variations in the number concentrations of low GF mode at D_{dry} = 49.6 nm were similar to those in the EC concentrations, suggesting that EC contributed to the reduction of the hygroscopicity in this smaller size range. These results suggest that the abundance of OM relative to sulfate in the accumulation mode and the absolute abundance of EC in the Aitken mode are important factors controlling hygroscopicity of submicron particles. The results demonstrate that chemical composition and particle mixing state are important factors to control hygroscopicity and CCN activation of the different size modes in the submicron particles during the study period. This chapter highlights the importance of the abundance of OM relative to sulfate in predicting cloud properties and their resultant climate effects in the

future.

References

Aggarwal, S. G., M. Mochida, Y. Kitamori, and K. Kawamura (2007), Chemical Closure Study on Hygroscopic Properties of Urban Aerosol Particles in Sapporo, Japan, Environ. Sci. Technol., 41(20), 6920–6925, doi:10.1021/es063092m.

Boreddy, S. K. R., K. Kawamura, and J. Jung (2014), Hygroscopic properties of particles nebulized from water extracts of aerosols collected at Chichijima Island in the western North Pacific: An outflow region of Asian dust, J. Geophys. Res. Atmos., 119(1), 167–178, doi:10.1002/2013JD020626.

Burkart, J., G. Steiner, G. Reischl, and R. Hitzenberger (2011), Long-term study of cloud condensation nuclei (CCN) activation of the atmospheric aerosol in Vienna, Atmos. Environ., 45(32), 5751–5759, doi:10.1016/j.atmosenv.2011.07.022.

Carrico, C. M., M. D. Petters, S. M. Kreidenweis, J. L. Collett, G. Engling, and W. C. Malm (2008), Aerosol hygroscopicity and cloud droplet activation of extracts of filters from biomass burning experiments, J. Geophys. Res., 113(D8), D08206, doi:10.1029/2007JD009274.

Cerully, K. M. et al. (2011), Aerosol hygroscopicity and CCN activation kinetics in a boreal forest environment during the 2007 EUCAARI campaign, Atmos. Chem. Phys., 11(23), 12369–12386, doi:10.5194/acp-11-12369-2011.

Cerully, K. M., A. Bougiatioti, J. R. Hite, H. Guo, L. Xu, N. L. Ng, R. Weber, and A. Nenes (2015), On the link between hygroscopicity, volatility, and oxidation state of ambient and water-soluble aerosols in the southeastern United States, Atmos. Chem. Phys., 15(15), 8679–8694, doi:10.5194/acp-15-8679-2015.

Chan, M. N., and C. K. Chan (2003), Hygroscopic Properties of Two Model Humic-like Substances and Their Mixtures with Inorganics of Atmospheric Importance, Environ. Sci. Technol., 37(22), 5109–5115, doi:10.1021/es034272o.

Chan, M. N., and C. K. Chan (2005), Mass transfer effects in hygroscopic measurements of aerosol particles, Atmos. Chem. Phys., 5(10), 2703–2712, doi:10.5194/acp-5-2703-2005.

Cocker, D. R., N. E. Whitlock, R. C. Flagan, and J. H. Seinfeld (2001), Hygroscopic Properties of Pasadena, California Aerosol, Aerosol Sci. Technol., 35(2), 637–647, doi:10.1080/02786820120653.

Crosbie, E., J.-S. Youn, B. Balch, A. Wonaschütz, T. Shingler, Z. Wang, W. C. Conant, E. a. Betterton, and A. Sorooshian (2015), On the competition among aerosol number, size and composition in predicting CCN variability: a multi-annual field study in an urbanized desert, Atmos. Chem. Phys., 15(12), 6943–6958, doi:10.5194/acp-15-6943-2015.

Dumka, U. C., D. Bhattu, S. N. Tripathi, D. G. Kaskaoutis, and B. L. Madhavan (2015), Seasonal inhomogeneity in cloud precursors over Gangetic Himalayan region during GVAX campaign, Atmos. Res., 155, 158–175, doi:10.1016/j.atmosres.2014.11.022.

Duplissy, J. et al. (2009), Intercomparison study of six HTDMAs: results and recommendations, Atmos. Meas. Tech., 2(2), 363–378, doi:10.5194/amt-2-363-2009.

Duplissy, J. et al. (2011), Relating hygroscopicity and composition of organic aerosol particulate matter, Atmos. Chem. Phys., 11(3), 1155–1165, doi:10.5194/acp-11-1155-2011.

Dusek, U. et al. (2006), Size matters more than chemistry for cloud-nucleating ability of aerosol particles., Science, 312(5778), 1375–8, doi:10.1126/science.1125261.

Dusek, U., G. P. Frank, A. Massling, K. Zeromskiene, Y. Iinuma, O. Schmid, G. Helas, T. Hennig, A. Wiedensohler, and M. O. Andreae (2011), Water uptake by biomass burning aerosol at sub- and supersaturated conditions: closure studies and implications for the role of organics, Atmos. Chem. Phys., 11(18), 9519–9532, doi:10.5194/acp-11-9519-2011.

Engelhart, G. J., A. Asa-Awuku, A. Nenes, and S. N. Pandis (2008), CCN activity and droplet growth kinetics of fresh and aged monoterpene secondary organic aerosol, Atmos. Chem. Phys., 8(14), 3937–3949, doi:10.5194/acp-8-3937-2008.

Engelhart, G. J., R. H. Moore, A. Nenes, and S. N. Pandis (2011), Cloud condensation nuclei activity of isoprene secondary organic aerosol, J. Geophys. Res., 116(D2), 1–11, doi:10.1029/2010JD014706.

Farmer, D. K., C. D. Cappa, and S. M. Kreidenweis (2015), Atmospheric Processes and Their Controlling Influence on Cloud Condensation Nuclei Activity, Chem. Rev., 115(10), 4199–4217, doi:10.1021/cr5006292.

Finessi, E. et al. (2012), Determination of the biogenic secondary organic aerosol fraction in the boreal forest by NMR spectroscopy, Atmos. Chem. Phys., 12(2), 941–959, doi:10.5194/acp-12-941-2012.

Fors, E. O., E. Swietlicki, B. Svenningsson, A. Kristensson, G. P. Frank, and M. Sporre (2011), Hygroscopic properties of the ambient aerosol in southern Sweden – a two year study, Atmos. Chem. Phys., 11(16), 8343–8361, doi:10.5194/acp-11-8343-2011.

Frosch, M., N. L. Prisle, M. Bilde, Z. Varga, and G. Kiss (2011), Joint effect of organic acids and inorganic salts on cloud droplet activation, Atmos. Chem. Phys., 11(8), 3895–3911, doi:10.5194/acp-11-3895-2011.

Gu, J. et al. (2011), Source apportionment of ambient particles: Comparison of positive matrix factorization analysis applied to particle size distribution and chemical composition data,

Atmos. Environ., 45(10), 1849–1857, doi:10.1016/j.atmosenv.2011.01.009.

Gysel, M., E. Weingartner, and U. Baltensperger (2002), Hygroscopicity of Aerosol Particles at Low Temperatures. 2. Theoretical and Experimental Hygroscopic Properties of Laboratory Generated Aerosols, Environ. Sci. Technol., 36(1), 63–68, doi:10.1021/es010055g.

Hansen, A. M. K., J. Hong, T. Raatikainen, K. Kristensen, A. Ylisirniö, A. Virtanen, T. Petäjä, M. Glasius, and N. L. Prisle (2015), Hygroscopic properties and cloud condensation nuclei activation of limonene-derived organosulfates and their mixtures with ammonium sulfate, Atmos. Chem. Phys., 15(12), 17317–17365, doi:10.5194/acpd-15-17317-2015.

Hersey, S. P. et al. (2013), Composition and hygroscopicity of the Los Angeles Aerosol: CalNex, J. Geophys. Res. Atmos., 118(7), 3016–3036, doi:10.1002/jgrd.50307.

Holmgren, H., K. Sellegri, M. Hervo, C. Rose, E. Freney, P. Villani, and P. Laj (2014), Hygroscopic properties and mixing state of aerosol measured at the high-altitude site Puy de Dôme (1465 m a.s.l.), France, Atmos. Chem. Phys., 14(18), 9537–9554, doi:10.5194/acp-14-9537-2014.

Hong, J. et al. (2014), Hygroscopicity, CCN and volatility properties of submicron atmospheric aerosol in a boreal forest environment during the summer of 2010, Atmos. Chem. Phys., 14(9), 4733–4748, doi:10.5194/acp-14-4733-2014.

Huff Hartz, K. E., J. E. Tischuk, M. N. Chan, C. K. Chan, N. M. Donahue, and S. N. Pandis (2006), Cloud condensation nuclei activation of limited solubility organic aerosol, Atmos. Environ., 40(4), 605–617, doi:10.1016/j.atmosenv.2005.09.076.

Hussein, T., A. Puustinen, P. P. Aalto, J. M. Mäkelä, K. Hämeri, and M. Kulmala (2004), Urban aerosol number size distributions, Atmos. Chem. Phys., 4(2), 391–411, doi:10.5194/acp-4-391-2004.

Intergovernmental Panel on Climate Change (2013), Climate Change 2013, The Physical Science Basis, in Contribution of Working Group I to the Fifth Assessment Report of the Intergovernmental Panel on Climate Change, edited by T.F. Stocker et al., 1535 pp., Cambridge Univ. Press, Cambridge, U. K. and New York.

Irwin, M., N. Good, J. Crosier, T. W. Choularton, and G. McFiggans (2010), Reconciliation of measurements of hygroscopic growth and critical supersaturation of aerosol particles in central Germany, Atmos. Chem. Phys., 10(23), 11737–11752, doi:10.5194/acp-10-11737-2010.

Jung, J., and K. Kawamura (2014), Hygroscopic properties of newly formed ultrafine particles at an urban site surrounded by deciduous forest (Sapporo, northern Japan) during the

summer of 2011, Atmos. Chem. Phys., 14(14), 7519–7531, doi:10.5194/acp-14-7519-2014.

Jung, J., Y. J. Kim, S. G. Aggarwal, and K. Kawamura (2011), Hygroscopic property of water-soluble organic-enriched aerosols in Ulaanbaatar, Mongolia during the cold winter of 2007, Atmos. Environ., 45(16), 2722–2729, doi:10.1016/j.atmosenv.2011.02.055.

Jung, J., Y. Miyazaki, and K. Kawamura (2013), Different characteristics of new particle formation between urban and deciduous forest sites in Northern Japan during the summers of 2010–2011, Atmos. Chem. Phys., 13(1), 51–68, doi:10.5194/acp-13-51-2013.

Jurányi, Z., M. Gysel, E. Weingartner, N. Bukowiecki, L. Kammermann, and U. Baltensperger (2011), A 17 month climatology of the cloud condensation nuclei number concentration at the high alpine site Jungfraujoch, J. Geophys. Res., 116(D10), D10204, doi:10.1029/2010JD015199.

Jurányi, Z., T. Tritscher, M. Gysel, M. Laborde, L. Gomes, G. Roberts, U. Baltensperger, and E. Weingartner (2013), Hygroscopic mixing state of urban aerosol derived from size-resolved cloud condensation nuclei measurements during the MEGAPOLI campaign in Paris, Atmos. Chem. Phys., 13(13), 6431–6446, doi:10.5194/acp-13-6431-2013.

Kalivitis, N., V.-M. Kerminen, G. Kouvarakis, I. Stavroulas, A. Bougiatioti, A. Nenes, H. E. Manninen, T. Petäjä, M. Kulmala, and N. Mihalopoulos (2015), Atmospheric new particle formation as a source of CCN in the eastern Mediterranean marine boundary layer, Atmos. Chem. Phys., 15(16), 9203–9215, doi:10.5194/acp-15-9203-2015.

Kawana, K., T. Nakayama, and M. Mochida (2016), Hygroscopicity and CCN activity of atmospheric aerosol particles and their relation to organics: Characteristics of urban aerosols in Nagoya, Japan, J. Geophys. Res. Atmos., 121(8), 4100–4121, doi:10.1002/2015JD023213.

King, S. M., T. Rosenoern, J. E. Shilling, Q. Chen, Z. Wang, G. Biskos, K. a. McKinney, U. Pöschl, and S. T. Martin (2010), Cloud droplet activation of mixed organic-sulfate particles produced by the photooxidation of isoprene, Atmos. Chem. Phys., 10(8), 3953–3964, doi:10.5194/acp-10-3953-2010.

Koehler, K. A., S. M. Kreidenweis, P. J. DeMott, A. J. Prenni, C. M. Carrico, B. Ervens, and G. Feingold (2006), Water activity and activation diameters from hygroscopicity data - Part II: Application to organic species, Atmos. Chem. Phys., 6(3), 795–809, doi:10.5194/acp-6-795-2006.

Laborde, M. et al. (2013), Black carbon physical properties and mixing state in the European megacity Paris, Atmos. Chem. Phys., 13(11), 5831–5856, doi:10.5194/acp-13-5831-2013.

Lee, S., Y. S. Ghim, S. W. Kim, and S. C. Yoon (2010), Effect of biomass burning and regional background aerosols on CCN activity derived from airborne in-situ measurements, Atmos. Environ., 44(39), 5227–5236, doi:10.1016/j.atmosenv.2010.08.044.

Li, Z., A. L. Williams, and M. J. Rood (1998), Influence of Soluble Surfactant Properties on the Activation of Aerosol Particles Containing Inorganic Solute, J. Atmos. Sci., 55(10), 1859–1866, doi:10.1175/1520-0469(1998)055<1859:IOSSPO>2.0.CO;2.

McFiggans, G. et al. (2006), The effect of physical and chemical aerosol properties on warm cloud droplet activation, Atmos. Chem. Phys., 6(9), 2593–2649, doi:10.5194/acp-6-2593-2006.

Miyazaki, Y., Y. Kondo, N. Takegawa, Y. Komazaki, M. Fukuda, K. Kawamura, M. Mochida, K. Okuzawa, and R. J. Weber (2006), Time-resolved measurements of water-soluble organic carbon in Tokyo, J. Geophys. Res. Atmos., 111(D23), doi:10.1029/2006JD007125.

Miyazaki, Y., S. G. Aggarwal, K. Singh, P. K. Gupta, and K. Kawamura (2009), Dicarboxylic acids and water-soluble organic carbon in aerosols in New Delhi, India, in winter: Characteristics and formation processes, J. Geophys. Res., 114(D19), D19206, doi:10.1029/2009JD011790.

Miyazaki, Y., J. Jung, P. Fu, Y. Mizoguchi, K. Yamanoi, and K. Kawamura (2012), Evidence of formation of submicrometer water-soluble organic aerosols at a deciduous forest site in northern Japan in summer, J. Geophys. Res. Atmos., 117(D19), doi:10.1029/2012JD018250.

Mochida, M., M. Kuwata, T. Miyakawa, N. Takegawa, K. Kawamura, and Y. Kondo (2006), Relationship between hygroscopicity and cloud condensation nuclei activity for urban aerosols in Tokyo, J. Geophys. Res. Atmos., 111(D23), doi:10.1029/2005JD006980.

Mochida, M., C. Nishita-Hara, Y. Kitamori, S. G. Aggarwal, K. Kawamura, K. Miura, and A. Takami (2010), Size-segregated measurements of cloud condensation nucleus activity and hygroscopic growth for aerosols at Cape Hedo, Japan, in spring 2008, J. Geophys. Res., 115(D21), D21207, doi:10.1029/2009JD013216.

Moore, R. H., A. Nenes, and J. Medina (2010), Scanning Mobility CCN Analysis—A Method for Fast Measurements of Size-Resolved CCN Distributions and Activation Kinetics, Aerosol Sci. Technol., 44(10), 861–871, doi:10.1080/02786826.2010.498715.

Orsini, D. A., Y. Ma, A. Sullivan, B. Sierau, K. Baumann, and R. J. Weber (2003), Refinements to the particle-into-liquid sampler (PILS) for ground and airborne measurements of water soluble aerosol composition, Atmos. Environ., 37(9–10), 1243–1259, doi:10.1016/S1352-2310(02)01015-4.

Padró, L. T., R. H. Moore, X. Zhang, N. Rastogi, R. J. Weber, and A. Nenes (2012), Mixing state and compositional effects on CCN activity and droplet growth kinetics of size-resolved CCN in an urban environment, Atmos. Chem. Phys., 12(21), 10239–10255, doi:10.5194/acp-12-10239-2012.

Paramonov, M., P. P. Aalto, a. Asmi, N. Prisle, V. M. Kerminen, M. Kulmala, and T. Petäjä (2013), The analysis of size-segregated cloud condensation nuclei counter (CCNC) data and its implications for cloud droplet activation, Atmos. Chem. Phys., 13(20), 10285–10301, doi:10.5194/acp-13-10285-2013.

Paramonov, M. et al. (2015), A synthesis of cloud condensation nuclei counter (CCNC) measurements within the EUCAARI network, Atmos. Chem. Phys., 15(21), 12211–12229, doi:10.5194/acp-15-12211-2015.

Pavuluri, C. M., K. Kawamura, M. Uchida, M. Kondo, and P. Fu (2013), Enhanced modern carbon and biogenic organic tracers in Northeast Asian aerosols during spring/summer, J. Geophys. Res. Atmos., 118(5), 2362–2371, doi:10.1002/jgrd.50244.

Peng, C., M. N. Chan, and C. K. Chan (2001), The Hygroscopic Properties of Dicarboxylic and Multifunctional Acids: Measurements and UNIFAC Predictions, Environ. Sci. Technol., 35(22), 4495–4501, doi:10.1021/es0107531.

Petters, M. D., and S. M. Kreidenweis (2007), A single parameter representation of hygroscopic growth and cloud condensation nucleus activity, Atmos. Chem. Phys., 7(8), 1961–1971, doi:10.5194/acp-7-1961-2007.

Pöschl, U. et al. (2010), Rainforest Aerosols as Biogenic Nuclei of Clouds and Precipitation in the Amazon, Science (80-.)., 329(5998), 1513–1516, doi:10.1126/science.1191056.

Prenni, A. (2003), Water uptake of internally mixed particles containing ammonium sulfate and dicarboxylic acids, Atmos. Environ., 37(30), 4243–4251, doi:10.1016/S1352-2310(03)00559-4.

Prenni, A. J., M. D. Petters, S. M. Kreidenweis, P. J. DeMott, and P. J. Ziemann (2007), Cloud droplet activation of secondary organic aerosol, J. Geophys. Res., 112(D10), D10223, doi:10.1029/2006JD007963.

Renbaum-Wolff, L., M. Song, C. Marcolli, Y. Zhang, P. F. Liu, J. W. Grayson, F. M. Geiger, S. T. Martin, and A. K. Bertram (2016), Observations and implications of liquid–liquid phase separation at high relative humidities in secondary organic material produced by α-pinene ozonolysis without inorganic salts, Atmos. Chem. Phys., 16(12), 7969–7979, doi:10.5194/acp-16-7969-2016.

Roberts, G. C., and A. Nenes (2005), A Continuous-Flow Streamwise Thermal-Gradient CCN

Chamber for Atmospheric Measurements, Aerosol Sci. Technol., 39(3), 206–221, doi:10.1080/027868290913988.

Roberts, G. C., D. a. Day, L. M. Russell, E. J. Dunlea, J. L. Jimenez, J. M. Tomlinson, D. R. Collins, Y. Shinozuka, and a. D. Clarke (2010), Characterization of particle cloud droplet activity and composition in the free troposphere and the boundary layer during INTEX-B, Atmos. Chem. Phys., 10(14), 6627–6644, doi:10.5194/acp-10-6627-2010.

Rood, M. J., and A. L. Williams (2001), Reply, J. Atmos. Sci., 58(11), 1468–1473, doi:10.1175/1520-0469(2001)058<1468:R>2.0.CO;2.

Rose, D., S. S. Gunthe, E. Mikhailov, G. P. Frank, U. Dusek, M. O. Andreae, and U. Pöschl (2008), Calibration and measurement uncertainties of a continuous-flow cloud condensation nuclei counter (DMT-CCNC): CCN activation of ammonium sulfate and sodium chloride aerosol particles in theory and experiment, Atmos. Chem. Phys., 8(5), 1153–1179, doi:10.5194/acp-8-1153-2008.

Saathoff, H., K.-H. Naumann, M. Schnaiter, W. Schöck, O. Möhler, U. Schurath, E. Weingartner, M. Gysel, and U. Baltensperger (2003), Coating of soot and (NH4)2SO4 particles by ozonolysis products of α-pinene, J. Aerosol Sci., 34(10), 1297–1321, doi:10.1016/S0021-8502(03)00364-1.

Seinfeld, J. H., and S. N. Pandis (2006), Atmospheric chemistry and physics: from air pollution to climate change, 2nd ed., Wiley, Inc., New York, USA.

Sihto, S.-L. et al. (2011), Seasonal variation of CCN concentrations and aerosol activation properties in boreal forest, Atmos. Chem. Phys., 11(24), 13269–13285, doi:10.5194/acp-11-13269-2011.

Silvergren, S., U. Wideqvist, J. Ström, S. Sjogren, and B. Svenningsson (2014), Hygroscopic growth and cloud forming potential of Arctic aerosol based on observed chemical and physical characteristics (a 1 year study 2007-2008), J. Geophys. Res. Atmos., 119(24), 14,080-14,097, doi:10.1002/2014JD021657.

Sorjamaa, R., B. Svenningsson, T. Raatikainen, S. Henning, M. Bilde, and A. Laaksonen (2004), The role of surfactants in Köhler theory reconsidered, Atmos. Chem. Phys., 4(8), 2107–2117, doi:10.5194/acp-4-2107-2004.

Suda, S. R., M. D. Petters, A. Matsunaga, R. C. Sullivan, P. J. Ziemann, and S. M. Kreidenweis (2012), Hygroscopicity frequency distributions of secondary organic aerosols, J. Geophys. Res. Atmos., 117(D4), doi:10.1029/2011JD016823.

Sun, J., and P. Ariya (2006), Atmospheric organic and bio-aerosols as cloud condensation nuclei (CCN): A review, Atmos. Environ., 40(5), 795–820,

doi:10.1016/j.atmosenv.2005.05.052.

Swietlicki, E. et al. (2008), Hygroscopic properties of submicrometer atmospheric aerosol particles measured with H-TDMA instruments in various environments—a review, Tellus B, 38, doi:10.1111/j.1600-0889.2008.00350.x.

Varutbangkul, V., F. J. Brechtel, R. Bahreini, N. L. Ng, M. D. Keywood, J. H. Kroll, R. C. Flagan, J. H. Seinfeld, A. Lee, and a. H. Goldstein (2006), Hygroscopicity of secondary organic aerosols formed by oxidation of cycloalkenes, monoterpenes, sesquiterpenes, and related compounds, Atmos. Chem. Phys., 6(9), 2367–2388, doi:10.5194/acp-6-2367-2006.

Virkkula, A., R. Van Dingenen, F. Raes, and J. Hjorth (1999), Hygroscopic properties of aerosol formed by oxidation of limonene, α-pinene, and β-pinene, J. Geophys. Res. Atmos., 104(D3), 3569–3579, doi:10.1029/1998JD100017.

Vlasenko, a., S. Sjögren, E. Weingartner, H. W. Gäggeler, and M. Ammann (2005), Generation of Submicron Arizona Test Dust Aerosol: Chemical and Hygroscopic Properties, Aerosol Sci. Technol., 39(5), 452–460, doi:10.1080/027868290959870.

Wang, H., K. Kawamura, and D. Shooter (2005), Carbonaceous and ionic components in wintertime atmospheric aerosols from two New Zealand cities: Implications for solid fuel combustion, Atmos. Environ., 39(32), 5865–5875, doi:10.1016/j.atmosenv.2005.06.031.

Weingartner, E., H. Burtscher, and U. Baltensperger (1997), Hygroscopic properties of carbon and diesel soot particles, Atmos. Environ., 31(15), 2311–2327, doi:10.1016/S1352-2310(97)00023-X.

Wex, H., F. Stratmann, D. Topping, and G. McFiggans (2008), The Kelvin versus the Raoult Term in the Köhler Equation, J. Atmos. Sci., 65(12), 4004–4016, doi:10.1175/2008JAS2720.1.

Whitehead, J. D. et al. (2016), Biogenic cloud nuclei in the central Amazon during the transition from wet to dry season, Atmos. Chem. Phys., 16(15), 9727–9743, doi:10.5194/acp-16-9727-2016.

Wise, M. E., J. D. Surratt, D. B. Curtis, J. E. Shilling, and M. A. Tolbert (2003), Hygroscopic growth of ammonium sulfate/dicarboxylic acids, J. Geophys. Res., 108(D20), 4638, doi:10.1029/2003JD003775.

Wu, Z. J. et al. (2013), Relating particle hygroscopicity and CCN activity to chemical composition during the HCCT-2010 field campaign, Atmos. Chem. Phys., 13(16), 7983–7996, doi:10.5194/acp-13-7983-2013.

Yttri, K. E. et al. (2007), Elemental and organic carbon in PM_{10}: a one year measurement campaign within the European Monitoring and Evaluation Programme EMEP, Atmos.

Chem. Phys., 7(22), 5711–5725, doi:10.5194/acp-7-5711-2007.

Chapter 3. Evidence of a Reduction in Cloud Condensation Nuclei Activity of Water-Soluble Aerosols Caused by Biogenic Emissions in a Cool-Temperate Forest

3.1 Introduction

In forested regions with strong influence of biogenic sources, organic matter (OM) accounts for substantial fractions of the submicron particle mass. A majority of biogenic OM in submicron particles consists of biogenic secondary organic aerosol (BSOA) derived from biogenic volatile organic compounds (BVOCs) including isoprene and monoterpenes, whereas primary biological aerosol particles (PBAPs) can also be a significant source of organic aerosol (OA). Previous field studies conducted in areas dominated by biogenic OA, such as the Amazon [*Gunthe et al.*, 2009; *Pöschl et al.*, 2010], boreal forests [*Cerully et al.*, 2011; *Sihto et al.*, 2011; *Paramonov et al.*, 2013] or mountainous forests [*Levin et al.*, 2012, 2014], have reported values of hygrosopicity parameter (κ) below 0.3. Some studies have reported higher hygroscopicity for particles with larger diameters between 0.1 and 2.5 μm, which can be explained by the enrichment of sulfate in those particle size ranges [*Pöschl et al.*, 2010; *Levin et al.*, 2014; *Whitehead et al.*, 2016]. Meanwhile, lower κ values for particles with diameters between 10 and 100 nm have been attributed to a larger fraction of organic mass [*Pöschl et al.*, 2010; *Levin et al.*, 2014; *Whitehead et al.*, 2016]. Because most of the κ measurements were made by intensive field campaigns for periods of a few weeks, it is worth investigating how κ changes relative to changes in biogenic emissions throughout the year. Seasonal variability in cloud condensation nuclei (CCN) concentrations and aerosol hygroscopicity has been

previously investigated in forested areas [*Fors et al.*, 2011; *Sihto et al.*, 2011; *Levin et al.*, 2012; *Paramonov et al.*, 2013; *Holmgren et al.*, 2014], although limited chemical data is available to fully interpret them. Several field studies have shown lower hygroscopicity for particles in the accumulation mode in summer, which has been attributed to a large fraction of organic mass, likely of biogenic origin [*Levin et al.*, 2012; *Paramonov et al.*, 2013].

The objective of this chapter is to elucidate the impact of seasonal changes in the types and relative amounts of BSOA and PBAPs on the cloud forming potential of aerosols in forest environments. Submicron aerosol samples were collected in the Tomakomai Experimental Forest (TOEF) in northern Japan, which is a cool-temperate mixed forest. In this chapter, the impact of seasonal changes in the water-soluble OM (WSOM) composition on the cloud forming potential of submicron aerosols is discussed by using molecular tracers with positive matrix factorization (PMF) analysis [*Paatero and Tapper*, 1994]. Moreover, this chapter presents evidence for modification of the aerosol hygroscopicity by specific types of biogenic emissions and discuss their implications for climate.

3.2 Methods

3.2.1 Location and submicron aerosol sampling

Ambient submicron aerosol samples were collected in Hokkaido University's 2715 ha Tomakomai Experimental Forest (TOEF) (42°43'N, 141°36'E) located in the southwestern part of Hokkaido, northern Japan in the cool-temperate zone. The southern boundary of the forest site faces Tomakomai city and its industrial port area towards the Pacific Ocean. The mixed cool temperate forest consists of mature and secondary deciduous forest, and manmade coniferous forest with various types of forest floor covers. Tree species include Mongolian oak (*Quercus crispula*), mono maple (*Acer mono*), Korean mountain ash (*Sorbus alnifolia*),

Japanese linden (*Tilia japonica*) and the planted species Japanese larch (*Larix leptolepsis*), sakhalin fir (*Abies sachalinensis*), and sakhalin spruce (*Picea glehnii*) [*Hiura*, 2005]. The soil consists of volcanogenic regosols, which are shallow and less weathered [*Shibata et al.*, 1998]. The meteorological data for the sampling site was obtained from the Japan Meteorological Agency (available at http://www.jma.go.jp/jma/index.html). The predominant local wind direction in autumn and winter was from the north, corresponding to the forested area (**Figure 3.1**). In contrast, fractions of air transported from the south (coastal urban area) were dominant in summer. The monthly averaged temperature ranged from -1.9 ± 2.9°C (winter) to 18.2 ± 3.1°C (summer) for the years 2013 and 2015.

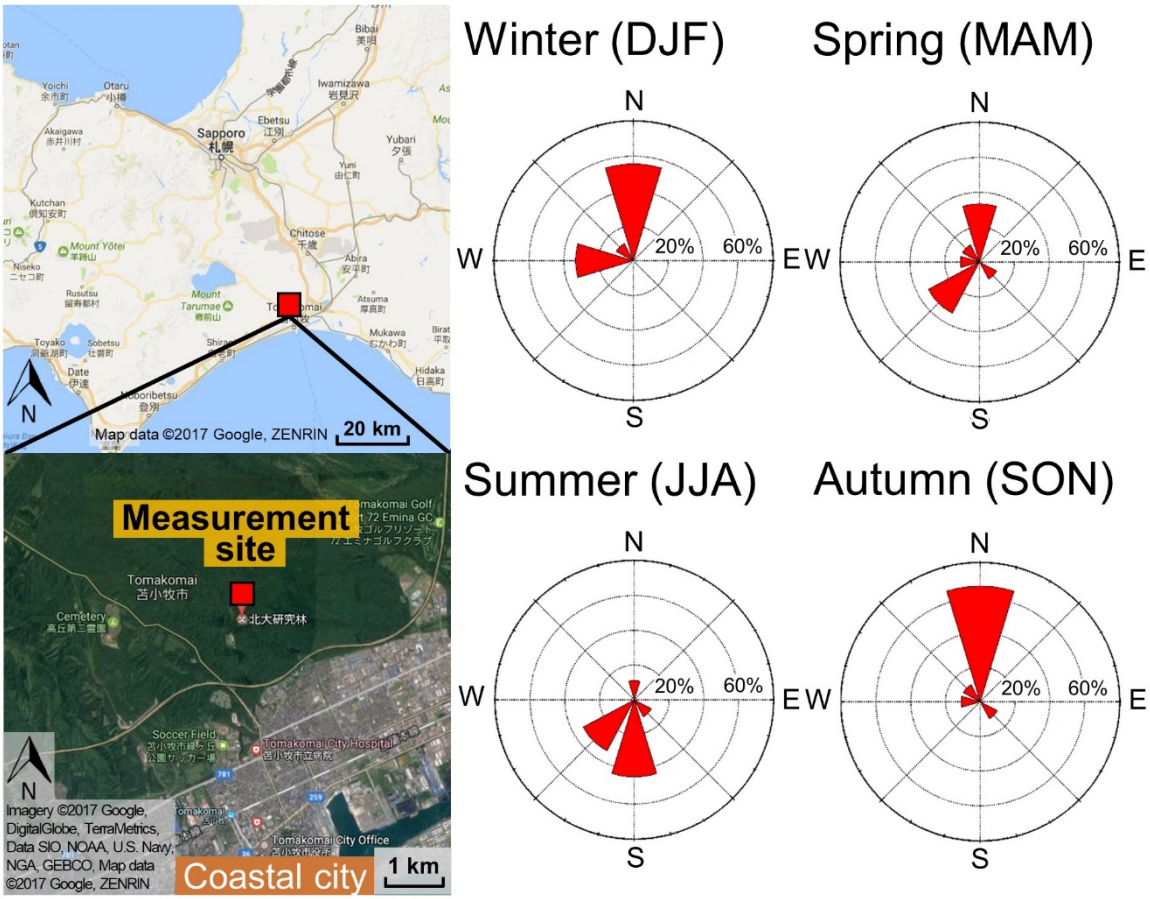

Figure 3.1 Location of the sampling site (Tomakomai Experimental Forest, TOEF) and the observed frequencies of local wind directions with wind speed >2 m s^{-1} for the year 2013. Map data ©2017 Google, ZENRIN; Imagery ©2017 Google, DigitalGlobe, TerraMetrics, Data SIO, NOAA, U.S. Navy, NGA, GEBCO (https://maps.google.com/). Maps are modified with Microsoft PowerPoint 2013.

Submicron aerosol samples were collected continuously using a high-volume air sampler (HVAS; Model 120SL, Kimoto Electric, Osaka, Japan) at an altitude of ~18 m above the forest floor at the research site. A cascade impactor (CI; Model TE-234, Tisch Environmental, Cleves, OH, USA) attached to the HVAS was used to collect size-segregated particles [*Miyazaki et al.*, 2012] with a flow rate of 1130 L min^{-1}. In this chapter, analytical results obtained from the bottom stage of the impactor are only used, which collected particles with aerodynamic diameter smaller than 0.95 μm. The sampling duration of each aerosol sample was approximately 1 week. The samples were collected on quartz fiber filters (25 cm × 20 cm) from January to December in 2013, and from February to December in 2015. Quartz fiber filters were pre-combusted at 410°C for 6 hours to remove any contaminants. Collected filters were individually stored in glass jars with a Teflon-lined screwed cap at −20°C to limit chemical reactions on the filter and losses of volatile compounds. In total, 37 samples for 2013 and 15 samples for 2015 have been analyzed, with the focus on 2013 presented in this chapter.

3.2.2 Hygroscopicity measurement and determination of κ_{CCN}

To measure the hygroscopic parameters of submicron water-soluble aerosols, a filter cut of 0.79 cm^2 was extracted with 7 mL ultrapure water using an ultrasonic bath (5 min × 3 times). The extracts were filtered through a 0.22 μm pore syringe filter (Millex-GV, 0.22 μm, Millipore) to remove any insoluble particles with diameters larger than 0.22 μm. Polydisperse aerosols were generated by first atomizing the filter extracts and then drying them with two diffusion dryers (silica gel and molecular sieve) in series. After passing the impactor and bipolar charger of the electrostatic classifier (TSI Model 3080), particles with a specific dry mobility diameter (D_{dry}) were selected by a differential mobility analyzer (DMA, TSI Model 3081). The classified flow was then split into two parallel streams: one went into the

condensation particle counter (CPC, TSI Model 3775) to measure the total concentration of condensation nuclei (N_{CN}), whereas the other stream was channeled into a continuous-flow thermal-gradient diffusion chamber (CCN-100, Droplet Measurement Technologies) to measure the number concentration of CCN (N_{CCN}) [*Roberts and Nenes*, 2005]. The flow rate into the CCN counter was 0.5 L min^{-1} with a sheath-to-sample flow ratio of 10.

In order to measure size-resolved CCN activity and growth kinetics, Scanning Mobility CCN Analysis (SMCA) was performed [*Moore et al.*, 2010]. In short, the method involves scanning a dynamic mobility diameter ranging from 10.4 to 220.7 nm with the DMA over a time period of 255 s. The specific supersaturation (SS, 0.25% to 1.0%) in the CCN counter was kept constant during the scan. The CCN activity of the particles generated was characterized by the activation diameter (D_{act}) at the corresponding SS, where the D_{act} of CCN is defined as the D_{dry} at which N_{CCN} reaches 50% of the total N_{CN} at a certain SS [*Rose et al.*, 2008]. D_{act} can be determined by expressing the ratio of N_{CCN} to N_{CN} with respect to D_{dry} and fitting the data to a sigmoid curve [*Rose et al.*, 2008]. A multiple-charge correction was applied to the N_{CCN} and N_{CN} using the algorithm provided in *Moore et al.* [2010]. The algorithm re-bins misclassified multiply charged particles into their actual size bins based on an equilibrium charge distribution.

The hygroscopicity parameter, κ_{CCN}, can be calculated for particles with D_{dry} at a certain SS as follows [*Petters and Kreidenweis*, 2007]:

$$\kappa(SS, D_{dry}) \approx \frac{4\,A^3}{27\,D_{dry}^3 \ln^2 SS_c} \qquad \textbf{(3.1)}$$

$$A = \frac{4\,\sigma_{s/a}\,M_w}{R\,T\,\rho_w} \qquad \textbf{(3.2)}$$

where SS_c represents the critical supersaturation for activation, ρ_W is the density of water, M_W is the molar mass of water, $\sigma_{s/a}$ is the surface tension of the pure water–air interface ($\sigma_{s/a} = 0.072$ J m^{-2}), R is the universal gas constant, and T is the absolute temperature (T = 298 K). Calibration was performed with ammonium sulfate before and after the measurements.

3.2.3 Chemical analysis of water-soluble aerosols

The term water-soluble aerosols in the present study is technically defined as particles sampled on the filter and extracted with ultrapure water followed by being filtered through the syringe filter [*Miyazaki et al.*, 2012, 2014]. To determine the WSOC concentration of the $PM_{1.0}$ filter samples, another filter cut of 3.14 cm^2 was extracted with 20 mL ultrapure water using an ultrasonic bath for 15 min. The extracts were filtered through the same type of 0.22 μm pore syringe filter as described above, before being injected into a total organic carbon analyzer (Model TOC-L_{CHP}, Shimadzu). The mass concentrations of WSOC were converted to those of water-soluble organic matter (WSOM) using a conversion factor of 1.8 [*Yttri et al.*, 2007; *Finessi et al.*, 2012].

Another portion of the filter (3.80 cm^2) was extracted with dichloromethane/methanol to measure biogenic molecular tracers: 2-methyltetrols (the sum of 2-methylerythritol and 2-methylthreitol) [*Claeys*, 2004], pinic acid, 3-methyl-1,2,3-butanetricarboxylic acid (3-MBTCA) [*Yu et al.*, 1999; *Claeys et al.*, 2007; *Szmigielski et al.*, 2007], trehalose, arabitol, mannitol, and sucrose [*Simoneit et al.*, 2004; *Elbert et al.*, 2007]. The –COOH and –OH functional groups in the extracts were reacted with N,O-bis-(trimethylsilyl) trifluoroacetamide (BSTFA) to form trimethylsilyl (TMS) esters and TMS ethers, respectively. The TMS derivatives were then analyzed for the compounds listed above using a capillary gas

chromatograph (GC7890, Agilent) coupled to a mass spectrometer (MSD5975C, Agilent). Additionally, another cut of the filter (3.14 cm^2) was extracted with 10 mL of ultrapure water under ultrasonication to determine the concentration of major inorganic ions (NO_3^-, SO_4^{2-}, Na^+, NH_4^+, K^+). The same syringe filter type as described above was used, before the extract was injected into the ion chromatograph (Model 761 compact IC; Metrohm) [*Miyazaki et al.*, 2009].

3.2.4 Positive matrix factorization (PMF)

Positive matrix factorization (PMF) [*Paatero and Tapper*, 1994] is a multivariate factor analysis technique used to resolve the identities and contributions of unknown mixtures to the observed components. Observed species are expressed as the sum of contributions from a number of time-invariant source profiles (factors) and residuals that cannot be modeled. By minimizing the residual term, the solution that best reproduces the observations can be determined. Further details of the PMF model and its application can be found elsewhere [*Paatero and Tapper*, 1994; *Norris et al.*, 2014].

Thirteen chemical components in thirty-seven sample sets were used as input data in the PMF model for the year 2013 (**Figure 3.2**). The analytical measurement uncertainties of each component were taken into account for the calculation. The calculation was performed with 100 runs. To maximize the amount of data, missing values were replaced with the median values of the species [*Reff et al.*, 2007]. The data from species with a signal-to-noise (S/N) ratio equal to or less than 0.5 were excluded from the analysis. Moreover, the data of species with an S/N ratio equal to or less than 1.0 were labeled as “weak”. Based on the scaled residual analysis with ± 3 standard deviations, NO_3^- and NH_4^+ were additionally labeled as “weak”. Uncertainties for these weak species are tripled [*Paatero and Hopke*, 2003]. To determine the

best solution, three to seven factor solutions were calculated, which resulted in the selection of five factors as the best solutions.

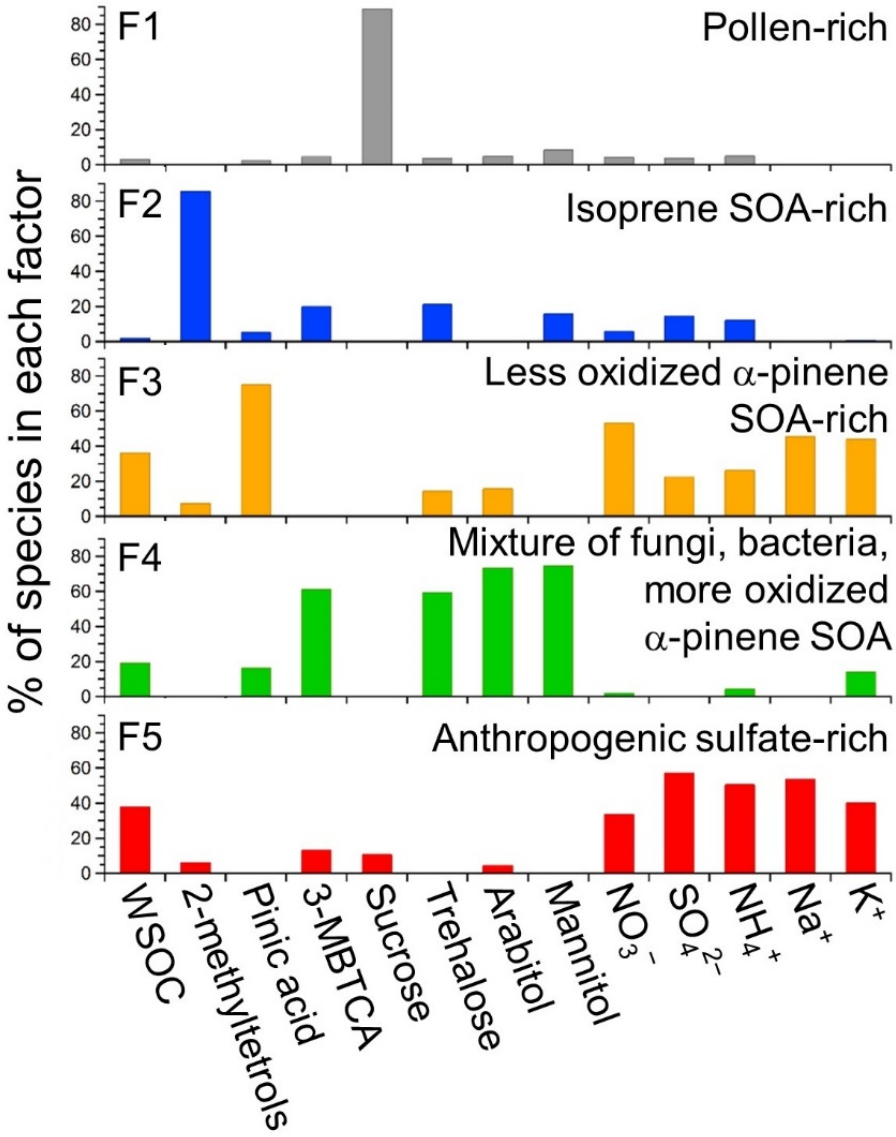

Figure 3.2 Five factor profiles derived from the PMF solution. The percentage of chemical species in each factor is shown.

The uncertainty of the PMF solution is estimated by displacement (DISP) analysis and bootstrapping (BS) analysis [*Paatero et al.*, 2014]. With DISP, each fitted element of the factor profile in the solution is "displaced" by predetermined error levels to determine changes, or swaps, in the factor profiles. No swaps occurred at the lowest level. With BS, multiple PMF solutions are generated by using a series of data sets that are resampled versions of the original

data set. By comparing the factor contributions, each BS factor is mapped to a base factor of the original PMF solution. The threshold of the minimum correlation for mapping was 0.6, and 100 bootstrapping runs were carried out. All BS factors could be mapped, and only BS Factor 4 showed mapping to the base Factor below 100% (94%) (**Table 3.1**). In this case, four of the BS runs were mapped to F1 instead of F4, likely due to the fact that both factors contain contributions of PBAP tracers.

Table 3.1. Results of the analysis for the uncertainty in the five-factor solution in the PMF calculation. Q is a goodness-of-fit parameter, Q_{robust} indicates Q excluding points which did not fit. $Q_{expected}$ is the calculated Q, whereas %dQ indicates percent change in Q when swaps occur.

Diagnostic	5 Factors
$Q_{robust}/Q_{expected}$	4.56
DISP %dQ:	<0.05%
Number of DISP swaps	0
Factors with BS (100 runs) < 100%	Factor 4 (96%)
BS unmapped	0

3.2.5 Estimation of the predicted κ values

The predicted hygroscopicity parameter (κ_{mix}) was calculated by applying a mixing rule [*Petters and Kreidenweis*, 2007] to the aerosol chemical composition as follows:

$$\kappa_{mix} = \varepsilon_{AS}\kappa_{AS} + \varepsilon_{org}\kappa_{org} \quad \textbf{(3.3)}$$

where κ_{AS} and κ_{org} are typical κ values for ammonium sulfate (~0.6) [*Petters and Kreidenweis*, 2007; *Gunthe et al.*, 2009] and biogenic secondary organic aerosols (~0.1) [*Gunthe et al.*, 2009; *Dusek et al.*, 2010], respectively. The ε_{AS} and ε_{org} values are the volume fractions of ammonium sulfate and organics, respectively, which were calculated from the mass concentrations using the density of ammonium sulfate (ρ_{AS} = 1.77 g cm^{-3}) and the assumed density of organics (ρ_{org} = 1.4 g cm^{-3}) [*Cerully et al.*, 2011].

3.3 Results and Discussion

3.3.1 Seasonal variations in aerosol hygroscopicity

Figure 3.3 shows the seasonal variations in the monthly-averaged κ_{CCN} values of the submicron water-soluble aerosols in 2013 and 2015. The κ_{CCN} values ranged between 0.26 and 0.56 with an overall average of 0.44 ± 0.07. These κ_{CCN} values are generally larger than those for ambient particles obtained by in-situ measurements in other forest environments (typically below 0.3) [*Gunthe et al.*, 2009; *Pöschl et al.*, 2010; *Cerully et al.*, 2011; *Fors et al.*, 2011; *Sihto et al.*, 2011; *Levin et al.*, 2012, 2014; *Paramonov et al.*, 2013; *Whitehead et al.*, 2016]. This is expected, given that the aerosol from filter extracts is completely water-soluble, as well as because the observed aerosols at this study site were not purely organics, as discussed below.

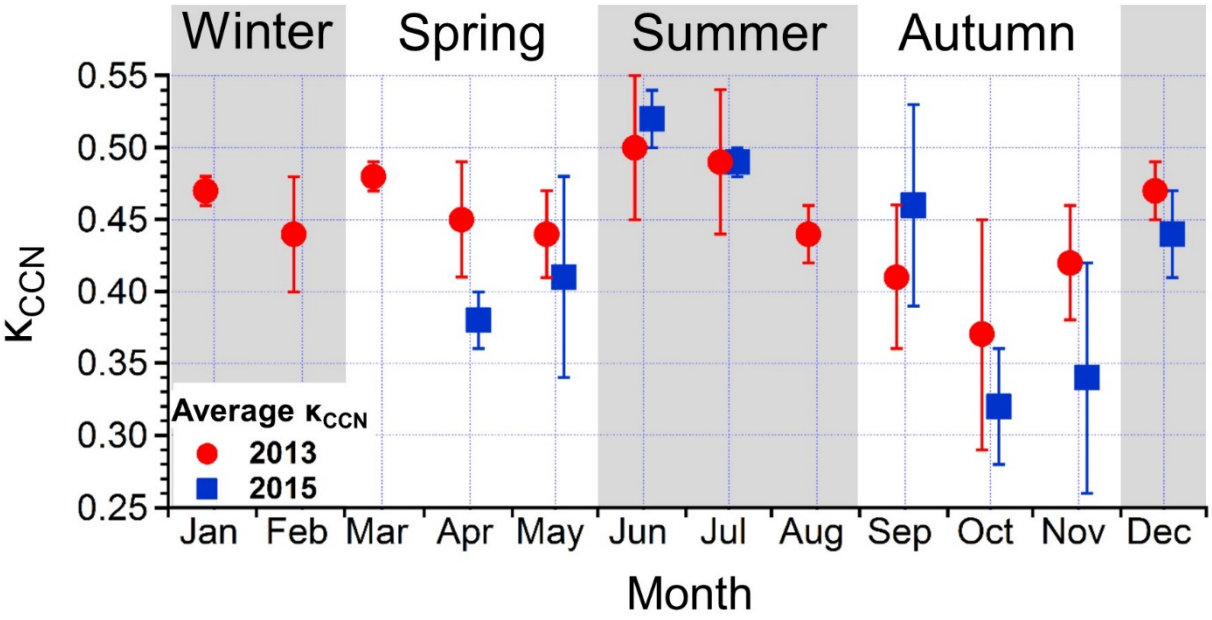

Figure 3.3 Time series of κ_{CCN} of the submicron water-soluble aerosol for the year 2013 (red circles) and 2015 (blue squares). Each season is categorized by shaded areas.

The κ_{CCN} values exhibited maxima in summer (June–August) and minima in autumn (September–November). This seasonal trend in κ_{CCN} was observed in both 2013 and 2015. The κ_{CCN} values in summer (0.50–0.52) are close to typical values of hygroscopic sulfate aerosols

(~0.6). In contrast, the lower values observed in autumn (0.32–0.37) are similar to those for particles dominated by organics in forest environments, which typically range from 0.1 to 0.4 [*Gunthe et al.*, 2009; *Pöschl et al.*, 2010; *Cerully et al.*, 2011; *Fors et al.*, 2011; *Sihto et al.*, 2011; *Levin et al.*, 2012, 2014; *Paramonov et al.*, 2013; *Whitehead et al.*, 2016].

While the seasonal pattern of κ is highly dependent on the location, *Sihto et al.* [2011] reported the lowest hygroscopicity in boreal forest in November, which they explained to be the result of a change in the chemical composition of aerosols. *Paramonov et al.* [2013] showed a seasonal variation in κ_{CCN} with a minimum (~0.2) in July and a maximum (0.74) in February with in-situ ambient measurements during a 29-month period in a boreal forest in southern Finland. *Levin et al.* [2012] also observed minimum κ_{CCN} values of 0.16 in July and September, and a maximum of 0.3 in April. Those previous studies suggested that the low hygroscopicity in summer was due to a larger organic mass fraction, which is likely attributed to increased emissions of BVOCs and subsequent formation of SOA. However, they have limited chemical measurements available to confirm this, although they mentioned that a change in the chemical composition of aerosols potentially affects κ. Because κ_{CCN} is closely linked to the chemical characteristics of aerosol [*Petters and Kreidenweis*, 2007], the observations together with the previous studies in the forested areas suggest that a seasonal difference in the chemical composition could control the seasonal variation in κ_{CCN}.

3.3.2 Seasonal trends of water-soluble organics and sulfate in submicron aerosols

In order to investigate the chemical composition of the observed submicron particles, **Figures 3.4a–b** present seasonal changes in the mass fractions of water-extracted aerosols together with the mass concentrations of water-soluble organic carbon (WSOC) and sulfate in 2013. On average, sulfate was the dominant component in summer, accounting for ~59% of

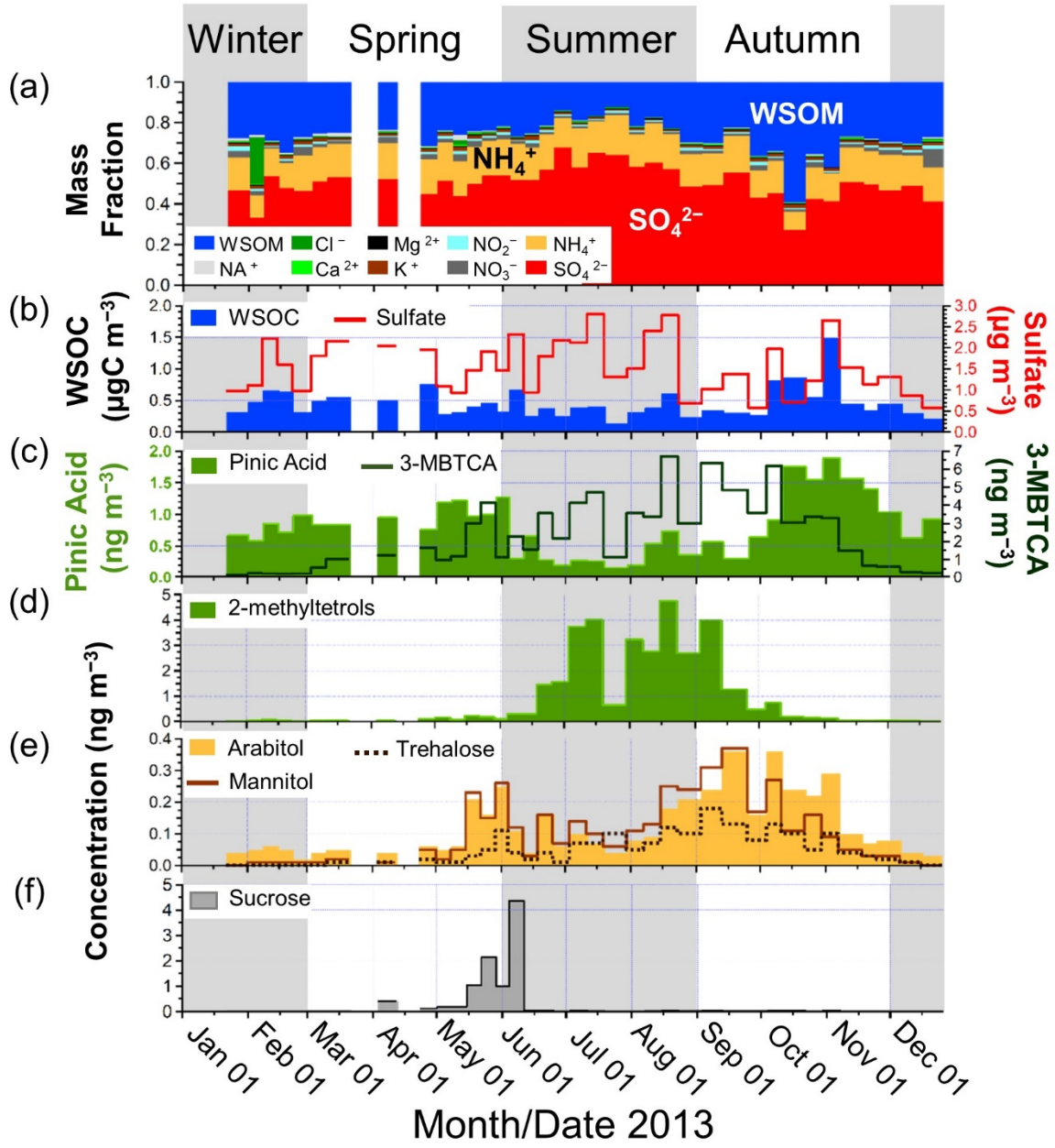

Figure 3.4 Time series of (a) the mass fraction of the chemical components in water-soluble aerosols, the mass concentrations of (b) WSOC and sulfate, (c) pinic acid and 3-methyl-1,2,3-butanetricarboxylic acid (3-MBTCA), (d) 2-methyltetrols, (e) arabitol, trehalose, and mannitol, and (f) sucrose for the year 2013. Each season is categorized by shaded areas.

the submicron water-soluble aerosols. In contrast, the mass fractions (~35%) and concentrations of WSOM (WSOC) showed maxima in autumn (**Table 3.2**). These seasonal patterns were also observed in the year 2015 (**Table 3.3**). **Figure 3.5** displays the relationship between κ_{CCN} and the WSOM-to-sulfate ratios. Throughout the entire period of 2013, the κ_{CCN}

value is negatively correlated with the WSOM/sulfate ratios (R^2 = 0.60 and 0.66 for all the individual data and monthly average data, respectively). The R^2 values were also as large as 0.79 (all data) and 0.76 (monthly averages) for the data obtained in 2015. This suggests that the fraction of organics relative to sulfate is an important factor that controls the CCN activity of the submicron water-soluble aerosols at the study site.

Table 3.2. Average κ_{CCN} and mass concentrations of WSOM, inorganic species, and biogenic molecular tracers, together with the ambient temperature in each season for the year 2013. Individual seasonal category is defined as each three months period: Spring (March–May), Summer (June–August), Autumn (September–November), and Winter (December–February).

	Spring	Summer	Autumn	Winter
κ_{CCN}	0.46±0.03	0.47±0.05	0.40±0.06	0.45±0.03
WSOM (μg m^{-3})	0.82±0.26	0.66±0.27	1.07±0.64	0.76±0.30
NO_3^- (μg m^{-3})	0.07±0.03	0.03±0.01	0.05±0.02	0.07±0.03
SO_4^{2-} (μg m^{-3})	1.65±0.41	1.89±0.68	1.35±0.57	1.19±0.51
Na^+ (μg m^{-3})	0.03±0.02	0.01±0.00	0.02±0.00	0.02±0.01
NH_4^+ (μg m^{-3})	0.57±0.12	0.56±0.20	0.45±0.19	0.36±0.10
K^+ (μg m^{-3})	0.04±0.01	0.02±0.01	0.04±0.02	0.04±0.01
2-methyltetrols (ng m^{-3})	0.12±0.06	2.32±1.49	0.72±1.16	0.04±0.02
Pinic acid (ng m^{-3})	1.01±0.17	0.36±0.19	1.16±0.52	0.77±0.14
3-MBTCA (ng m^{-3})	1.66±1.09	3.29±1.50	3.34±1.94	0.23±0.05
Sucrose (ng m^{-3})	0.57±0.67	0.42±1.25	0.02±0.01	0.00±0.00
Trehalose (ng m^{-3})	0.03±0.03	0.06±0.03	0.09±0.05	0.00±0.00
Arabitol (ng m^{-3})	0.10±0.08	0.10±0.05	0.21±0.10	0.04±0.01
Mannitol (ng m^{-3})	0.09±0.09	0.13±0.07	0.16±0.11	0.01±0.00
Temperature (ºC)	4.5±3.8	18.2±3.2	12.2±5.4	−3.1±3.2

Table 3.3. Average κ_{CCN} and mass concentrations of WSOM and inorganic species, together with the ambient temperature in each season in 2015. Individual seasonal category is defined as each three months period: Spring (March–May), Summer (June–August), Autumn (September–November), and Winter (December–February).

	Spring	Summer	Autumn	Winter
κ_{CCN}	0.40±0.06	0.51±0.02	0.37±0.09	0.44±0.03
WSOM (μg m^{-3})	1.60±0.23	0.83±0.48	2.21±2.27	0.72±0.00
NO_3^- (μg m^{-3})	0.09±0.04	0.01±0.01	0.06±0.10	0.01±0.00
SO_4^{2-} (μg m^{-3})	1.69±0.44	1.87±1.16	0.98±0.47	1.01±0.00
Na^+ (μg m^{-3})	0.06±0.01	0.01±0.01	0.01±0.01	0.01±0.00
NH_4^+ (μg m^{-3})	0.52±0.19	0.59±0.35	0.32±0.17	0.32±0.00
K^+ (μg m^{-3})	0.02±0.01	0.00±0.00	0.06±0.09	0.00±0.00
Temperature (ºC)	6.6±3.8	18.0±3.0	10.9±5.6	−0.8±2.0

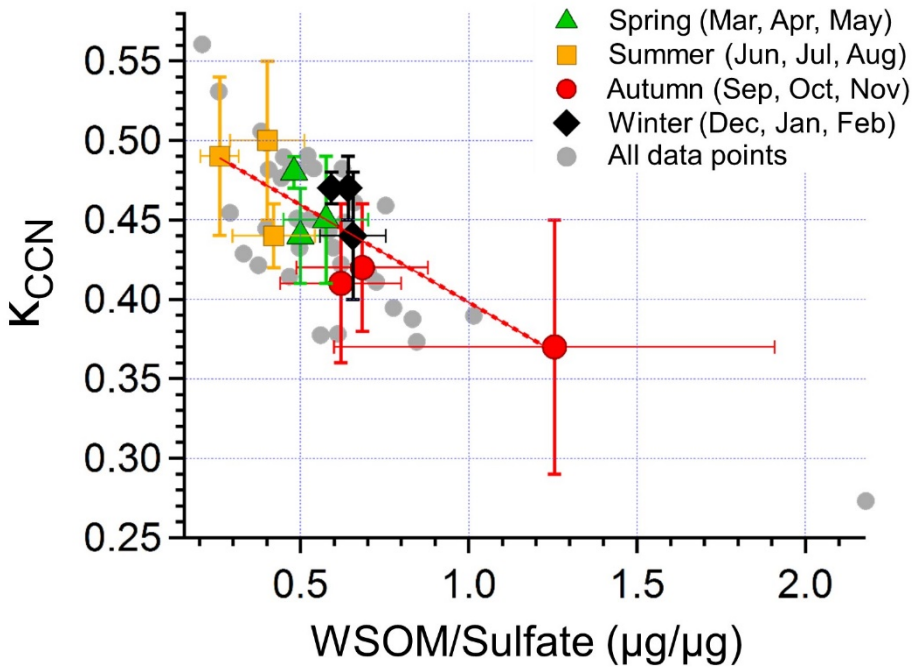

Figure 3.5 Scatter plot of monthly average κ_{CCN} and the WSOM-to-sulfate ratios with their standard deviations in spring (green triangles), summer (yellow squares), autumn (red circles), and winter (black diamonds) for the year 2013. Individual data are also shown in grey solid circles obtained for each sampling duration of approximately one week.

It should be noted that even during periods with similar WSOM-to-sulfate mass ratios of 0.62–0.64, κ_{CCN} differed between autumn (0.41–0.42) and winter (0.44–0.47) (**Figure 3.5**), which indicates that the difference in the chemical composition of WSOM can modify κ_{CCN}.

Specifically, it is suggested that WSOM in autumn contains less hygroscopic compounds than during the winter period. To explore the possible sources of WSOM and the resulting chemical compositions, **Figures 3.4c– f** present the seasonal variations in the concentrations of representative tracers for BSOA and PBAPs. It is apparent that the concentrations of pinic acid, which is a first-generation oxidation product of α-pinene and is typically used as a tracer for α-pinene derived SOA [*Yu et al.*, 1999; *Claeys et al.*, 2007], reach a maximum in autumn (**Figure 3.4c**). Moreover, the concentrations of arabitol, trehalose, and mannitol also exhibited maxima during the same season (**Figure 3.4e**), although the appearance of their peaks is slightly different from that of pinic acid. These sugar compounds are used as tracers of biological materials, including fungi and bacteria [*Simoneit et al.*, 2004; *Elbert et al.*, 2007]. In particular, trehalose is known to be a fungal metabolite as well as a stress protectant for the soil microbial community, and has been proposed as a molecular marker for fugitive dust from biologically active surface soils [*Rogge et al.*, 2007]. The seasonal profiles indicate that the increase of WSOM during the autumn period can be associated with increased concentrations of both α-pinene derived SOA and PBAPs.

Previous studies have suggested that α-pinene has been found to originate from roots, litter, and soil microbial activity [*Aaltonen et al.*, 2011; *Faiola et al.*, 2014; *Peñuelas et al.*, 2014] in combination with high nitrification rates [*Kirikae et al.*, 2001]. Local wind speeds were relatively low of average 3.2 ± 0.5 m s^{-1} with a prevailing northerly wind (**Figure 3.1**) from the forested area in autumn. This supports the hypothesis of a significant influence of local emissions and subsequent vertical transport of α-pinene and its oxidation products within the canopy. Moreover, the enhanced concentrations of pinic acid together with these sugar compounds in autumn indicate that most of the observed pinic acid, and thus its precursor (α-pinene), in this season originated from the forest floor rather than from the leaves. Indeed, previous studies estimated that the emissions of monoterpene, dominated by α-pinene, from

the forest floor (~300 μg m^{-2} h^{-1} at 30 °C), were larger than those from the canopy by ~35% in the Idaho Experimental Forest, northwestern USA in autumn [*Aaltonen et al.*, 2011, 2013; *Faiola et al.*, 2014].

The concentrations of 2-methyltetrols, which is used as a tracer for isoprene-derived SOA [*Claeys*, 2004], showed a maximum in summer when the sulfate fraction dominated as described above. The seasonal trend of 2-methyltetrols (**Figure 3.4d**) closely followed that of the ambient temperature (**Table 3.2**). The increased sulfate concentration is likely due to the higher influence of anthropogenic emissions originating from the industrial area of the Tomakomai city located in the south of the forest site. This is supported by the predominant southerly wind direction in summer (**Figure 3.1**).

3.3.3 Source apportionment of WSOC by positive matrix factorization (PMF) analysis

A PMF analysis was performed to apportion sources of the measured WSOC, which is closely linked to κ_{CCN}. The PMF resolved five interpretable factors, which were characterized by the enrichment of each tracer compound (**Figure 3.2**). Factor 1 (F1) was dominated by the contribution of sucrose (89%), which is a primary saccharide of pollen grains. Consequently, it is referred to here as "pollen-rich". Factor 2 (F2) is characterized by 2-methyltetrols (86%), whereas Factor 3 (F3) was dominated by pinic acid (75%). On the basis of the characteristics of each source profile, F2 and F3 are referred to here as "isoprene-SOA-rich" and "less oxidized α-pinene-SOA-rich", respectively. Factor 4 (F4) is characterized by large contributions of mannitol (75%), arabitol (74%), trehalose (60%), and 3-methyl-1,2,3-butanetricarboxylic acid (3-MBTCA) (61%). It has been recognized that 3-MBTCA is a highly oxidized compound of α-pinene [*Szmigielski et al.*, 2007]. Although F4 was difficult to convincingly attribute to a specific source, given the possibility that these tracers for PBAP are associated with re-

suspended soil and associated biota and that 3-MBTCA is a highly oxidized product of α-pinene, F4 was labeled here as "mixtures of fungi, bacteria, and more oxidized α-pinene SOA". On the other hand, Factor 5 (F5) is dominated by sulfate (57%), sodium (54%), and ammonium (51%). The observed sulfate is suggested to originate from anthropogenic activity rather than from sea salt, because of the negligible fraction of sea-salt sulfate (< 2%) calculated from the concentrations of sodium (**Table 3.2**). Consequently, F5 is referred to here as "anthropogenic sulfate-rich" as a possible source category of WSOC.

Figure 3.6 displays seasonal differences in the contribution of each source factor to the WSOC mass resolved by the PMF. The results show that 98% of the measured WSOC mass concentration in 2013 was successfully reproduced by the PMF model. In autumn, 75% of the WSOC mass was attributable to the sum of F3 and F4, both of which are dominated by the contribution of α-pinene derived SOA and fungi/bacteria derived WSOC. The significant contribution of α-pinene derived SOA was also apparent in spring, when the sum of F3 and F4 accounted for 57% of WSOC mass on average. The pollen-rich factor (F1) contributed only a

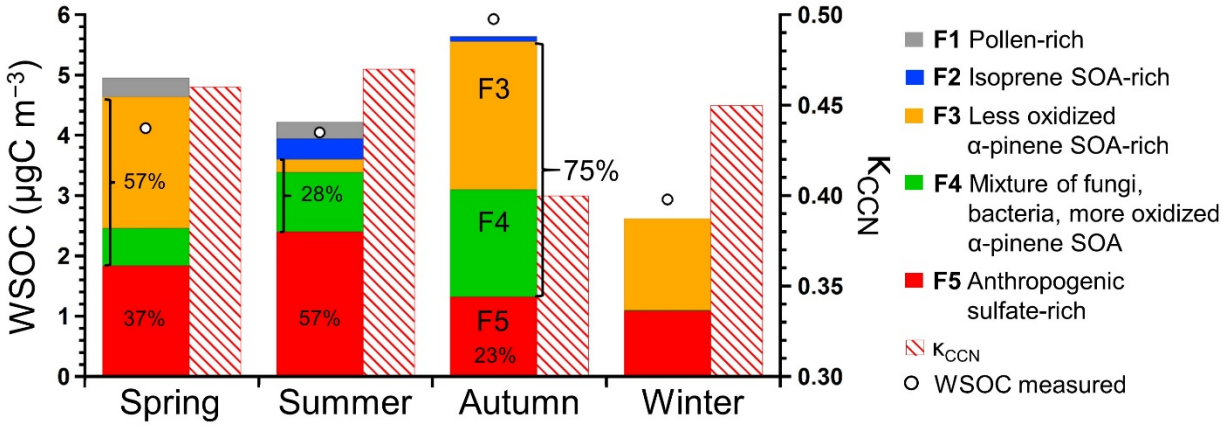

Figure 3.6 Contribution of each PMF-derived factor to the WSOC mass concentration and the average κ_{CCN} in each season. Open circles indicate the average mass concentrations of the measured WSOC.

minor fraction of the submicron WSOC, even in spring and summer (<7%). In summer, the anthropogenic sulfate-rich factor (F5) contributed significantly to WSOC mass (~57%), whereas the contribution of α-pinene derived SOA and fungi/bacteria derived organics to the WSOC was smaller (~28%). The increased concentrations of sulfate can also facilitate the formation of highly oxidized, hydrophilic OA, which implies that the formation of highly oxidized organics could have been a major component of observed WSOC in summer. In contrast, the WSOC in winter was attributed to less oxidized α-pinene SOA and anthropogenic sulfate-rich factors, with the lowest average concentration through the year. The present result indicates that the relative abundance and contributions of different sources to the WSOC mass are important for controlling the variation of the CCN activity.

3.3.4 Factors controlling the hygroscopicity parameter at the forest site

The modification of κ_{CCN} associated with the increased contributions of α-pinene SOA is supported by previous studies. Oxidation products of α-pinene are known to be surfactants and as such, when mixed with inorganic salts, they have been found to affect the surface tension of the solution [*Sorjamaa et al.*, 2004; *Padró et al.*, 2010; *Frosch et al.*, 2011]. In general, depression in the surface tension caused by surfactants lowers the Kelvin (surface tension) effects [*Wex et al.*, 2008], which leads to increasing CCN activity [*Sorjamaa et al.*, 2004; *Wex et al.*, 2008; *Dusek et al.*, 2011]. On the other hand, surfactants also affect the Raoult (water activity) effects, which can compensate the Kelvin effects [*Li et al.*, 1998; *Sorjamaa et al.*, 2004; *Frosch et al.*, 2011] (**Figure 1.3**). In mixed particles, κ can be modelled as the volume weighted average of the constituent' κ values, which is estimated based on volume-mixing rules [*Petters and Kreidenweis*, 2007]. The estimated κ (κ_{mix}) is defined as $\kappa_{mix} = \sum \varepsilon_i \kappa_i$, where ε_i and κ_i are the volume fraction and the κ value of each constituent, respectively. When κ_{mix} is

simply determined for two-component mixtures of WSOM and ammonium sulfate (**Table 3.2** and also see the method section), the observed κ_{CCN} and predicted κ_{mix} values agreed to within 17%, which is consistent with previous studies [*Gunthe et al.*, 2009, 2011; *Padró et al.*, 2010; *Cerully et al.*, 2011]. It is noted that the κ_{CCN} shown here is the apparent κ, which is sensitive to the assumption used in the calculations (**equations (3.1)** and **(3.2)**) and is different from intrinsic κ [*Sullivan et al.*, 2009]. *Padró et al.* [2010] evaluated κ for water-extracted aerosols in Mexico City by assuming the surface tension of water and 15% suface tension from the contributions of organics. They demonstrated that when κ_{CCN} is calculated allowing for a 15% surface tension depression, surfactant characteristics of the water-soluble aerosol can result in a reduction in organic hygroscopicity.

The reduction in hygroscopicity can be explained with an increased fraction of surface active organic compounds [*Li et al.*, 1998; *Sorjamaa et al.*, 2004; *Frosch et al.*, 2011]. While surfactants generally reduce the surface tension effect (Kelvin effect) of the droplet, which leads to increased CCN activity [*Wex et al.*, 2008; *Dusek et al.*, 2011], subsequent phase partitioning and/or organic coating lead to an organic-rich phase on the surface of the droplet and inner aqueous phase. This process can compensate for the surface tension effect if the fraction of surfactants is large. The surfactants lower the Raoult (water activity) effects [*Li et al.*, 1998; *Sorjamaa et al.*, 2004], which may result in a reduction in CCN activity [*Li et al.*, 1998; *Sorjamaa et al.*, 2004; *Frosch et al.*, 2011]. In recent laboratory experiments, *Renbaum-Wolff et al.* [2016] demonstrated that internally mixed sulfate and SOA, enriched with the oxidation products of α-pinene, results in a particle with a liquid-liquid phase separation. Furthermore, they showed that phase partitioning occurs with a phase enriched with α-pinene secondary OM on the surface of the particle and the water-rich inner phase above 95% RH. This surface organic-rich phase can prevent particles from activating as CCN.

By laboratory experiments, *Ma et al.* [2013] showed that when the particle mass fraction of organics exceeded 70%, coating by α-pinene derived SOA with 10–15 nm thickness on pre-existing particles occurs within a reaction time of 30 min. They found that the coating thickness is sufficient enough to lead to a noticeable change in the CCN activity of pre-exiting particles. In the current study, the large mass fraction of α-pinene derived SOA (75%) was observed only in autumn which was larger by 47% than that in summer. In general, α-pinene derived SOA contain compounds with molecular weights higher than those in isoprene derived SOA [*Khalizov et al.*, 2013; *Ma et al.*, 2013]. Oxidation products with high-molecular weight have been found to be related to low hygroscopicity [*Varutbangkul et al.*, 2006]. Consequently, the possible coating in autumn can prevent or delay the water uptake and activation of the particles to form cloud droplets. These mechanisms can partly explain the reduction of κ_{CCN} in autumn when the mass fraction of WSOM, dominated by α-pinene derived SOA, was large relative to that of sulfate.

It is interesting to note that F3 has a significant contribution of nitrate (53%; **Figure 3.2**). In fact, the concentration of nitrate showed a positive correlation with that of pinic acid ($R^2 = 0.26$) in autumn, whereas there was an insignificant correlation with benzoic acid ($R^2 = 0.04$), which is measured as a tracer of anthropogenic origin. These results, together with low local wind speeds and prevailing wind direction from the forest area (**Figure 3.1**), indicate that a substantial fraction of the NO_x originated from soil [*Kirikae et al.*, 2001] in the forest rather than from anthropogenic sources, to form aerosol nitrate. Nitrate radicals in the atmosphere are known to have a high reactivity to α-pinene and can subsequently form α-pinene nitrates [*Ma et al.*, 2011]. Recently, chamber experimental and modelling studies have shown that the addition of nitrate functional groups inhibit CCN activation by reducing its miscibility with water [*Suda et al.*, 2014; *Petters et al.*, 2016], which also supports the observed reduction in CCN activity for particles in the vicinity of a biogenic source area.

3.3.5 Possible impact of α-pinene derived SOA on the CCN number concentrations on the regional scale

In this subsection, to what extent these organic aerosols can affect the CCN number concentrations on a regional scale, is roughly estimated. The spatial distributions of α-pinene derived SOA is mainly controlled by the residence time in the atmosphere, which depends on particle losses due to chemical reactions, coagulation, dry deposition, and impaction or scavenging through clouds or precipitation. The chemical lifetime of α-pinene SOA ranges from 10 hours to 4 days estimated by photochemical chamber experiments in a laboratory [*Wang et al.*, 2011]. On the other hand, the physical lifetime of submicron particles varies from ~1 to ~3 days depending on meteorological conditions in the boundary layer [*Williams et al.*, 2002]. Assuming an average local wind speed of 3 m s^{-1} obtained at the measurement site and the maximum residence time of ~3 days, α-pinene SOA can impact the regional scale within approximately 800 km.

This has important implications for the number concentrations of CCN. In autumn, 35% of the total soluble mass (TSM, **Figure 3.4a**) is composed of WSOM, 75% of which is attributable to α-pinene derived SOA (26% of TSM**, Figure 3.6**). In order to estimate the reduction of the activated CCN number due to α-pinene SOA: (1) If α-pinene SOA is absent, all particles are activated as CCN, and (2) the bulk mass fraction of TSM is proportional to the mass and number fractions of particles. Two extreme cases are considered here: For the first case, when α-pinene SOA coated 100% of the surface of each single particle, the reduction of the CCN number was estimated to be ~26% which is reflected by the mass fraction of α-pinene derived SOA to TSM. The second case assumes that activation of each single particle can be suppressed even when the mass fraction of organics exceeds 70% [*Ma et al.*, 2013] (Chapter 3.3.4). This estimate resulted in the reduction of activated CCN by ~37%. Overall, the reduction of the CCN number was estimated to be ~32% as the average of the two cases.

Considering the CCN number concentration of ~200 cm^{-3} in typical boreal forest atmospheres [*Spracklen et al.*, 2008; *Tunved et al.*, 2008], coating of pre-existing hygroscopic particles with α-pinene SOA leads to a reduction of the CCN number concentration to 136 cm^{-3}. The reduced number concentrations of CCN can reduce a negative radiative effect and precipitation, which may also affect the biogeochemical cycles.

3.4 Conclusions

The two year-long measurements of water-soluble aerosols conducted at the cool-temperate forest site revealed a recurring seasonal trend of the hygroscopicity κ_{CCN} with a maximum in summer and a 15% lower minimum in autumn. Chemical analysis showed that the reduction of κ_{CCN} was linked to higher WSOM/sulfate ratios due to increased WSOM mass. Positive matrix factorization analysis (PMF) indicated that α-pinene-derived secondary organic aerosol (SOA) contributed with ~75% to the WSOM mass in autumn, which was larger by 47% than in summer. The majority of these α-pinene-derived SOA was attributable to emissions from litter/soil microbial activity near the forest floor. It is thus suggested that the formation of α-pinene-derived SOA associated with soil/litter mostly found near the forest floor, can significantly contribute to reducing the cloud forming potential of submicron particles.

The reduction of the hygroscopicity can be explained by organic coatings on pre-existing hygroscopic particles, and/or phase partitioning of these organics in the droplets. Coating and phase partitioning can prevent or delay the water uptake and therefore the CCN activation. It is estimated that the coating of particles by α-pinene derived organics in autumn can reduce the number of activated CCN particles by roughly ~32%. Considering the atmospheric lifetime of these SOA of ~3 days at maximum, the result has important implications for the regional climate as the corresponding particles can be distributed over the spatial scale of ~800 km. If

sulfate-rich aerosols are coated with α-pinene derived organics, the negative effect of radiative forcing can be reduced by the changes in the cloud properties particularly in the lower troposphere.

Additional field studies are needed to investigate the mechanism for organics from the forest floor reducing the CCN activity. Future work should include more sample sets from the other forest environment and provide comprehensive in-situ measurements of size distribution, chemical compositions, and CCN concentrations to evaluate the relationships of these physicochemical characteristics. The present study demonstrates that the aerosol hygroscopicity is controlled by different types of biogenic sources, which is important for predicting regional climate effects of organic aerosols due to changes in types and amounts of biogenic emissions particularly in cool-temperate/boreal forests in the future.

References

Aaltonen, H., J. Pumpanen, M. Pihlatie, H. Hakola, H. Hellén, L. Kulmala, T. Vesala, and J. Bäck (2011), Boreal pine forest floor biogenic volatile organic compound emissions peak in early summer and autumn, Agric. For. Meteorol., 151(6), 682–691, doi:10.1016/j.agrformet.2010.12.010.

Aaltonen, H., J. Aalto, P. Kolari, M. Pihlatie, J. Pumpanen, M. Kulmala, E. Nikinmaa, T. Vesala, and J. Bäck (2013), Continuous VOC flux measurements on boreal forest floor, Plant Soil, 369(1–2), 241–256, doi:10.1007/s11104-012-1553-4.

Cerully, K. M. et al. (2011), Aerosol hygroscopicity and CCN activation kinetics in a boreal forest environment during the 2007 EUCAARI campaign, Atmos. Chem. Phys., 11(23), 12369–12386, doi:10.5194/acp-11-12369-2011.

Claeys, M. (2004), Formation of Secondary Organic Aerosols Through Photooxidation of Isoprene, Science (80-.)., 303(5661), 1173–1176, doi:10.1126/science.1092805.

Claeys, M. et al. (2007), Hydroxydicarboxylic Acids: Markers for Secondary Organic Aerosol from the Photooxidation of α-Pinene, Environ. Sci. Technol., 41(5), 1628–1634, doi:10.1021/es0620181.

Dusek, U., G. P. Frank, J. Curtius, F. Drewnick, J. Schneider, A. K?rten, D. Rose, M. O. Andreae, S. Borrmann, and U. P?schl (2010), Enhanced organic mass fraction and decreased hygroscopicity of cloud condensation nuclei (CCN) during new particle formation events, Geophys. Res. Lett., 37(3), L03804, doi:10.1029/2009GL040930.

Dusek, U., G. P. Frank, A. Massling, K. Zeromskiene, Y. Iinuma, O. Schmid, G. Helas, T. Hennig, A. Wiedensohler, and M. O. Andreae (2011), Water uptake by biomass burning aerosol at sub- and supersaturated conditions: closure studies and implications for the role of organics, Atmos. Chem. Phys., 11(18), 9519–9532, doi:10.5194/acp-11-9519-2011.

Elbert, W., P. E. Taylor, M. O. Andreae, and U. Pöschl (2007), Contribution of fungi to primary biogenic aerosols in the atmosphere: wet and dry discharged spores, carbohydrates, and inorganic ions, Atmos. Chem. Phys., 7(17), 4569–4588, doi:10.5194/acp-7-4569-2007.

Faiola, C. L., G. S. VanderSchelden, M. Wen, F. C. Elloy, D. R. Cobos, R. J. Watts, B. T. Jobson, and T. M. VanReken (2014), SOA Formation Potential of Emissions from Soil and Leaf Litter, Environ. Sci. Technol., 48(2), 938–946, doi:10.1021/es4040045.

Finessi, E. et al. (2012), Determination of the biogenic secondary organic aerosol fraction in the boreal forest by NMR spectroscopy, Atmos. Chem. Phys., 12(2), 941–959, doi:10.5194/acp-12-941-2012.

Fors, E. O., E. Swietlicki, B. Svenningsson, A. Kristensson, G. P. Frank, and M. Sporre (2011),

Hygroscopic properties of the ambient aerosol in southern Sweden – a two year study, Atmos. Chem. Phys., 11(16), 8343–8361, doi:10.5194/acp-11-8343-2011.

Frosch, M., N. L. Prisle, M. Bilde, Z. Varga, and G. Kiss (2011), Joint effect of organic acids and inorganic salts on cloud droplet activation, Atmos. Chem. Phys., 11(8), 3895–3911, doi:10.5194/acp-11-3895-2011.

Gunthe, S. S. et al. (2009), Cloud condensation nuclei in pristine tropical rainforest air of Amazonia: size-resolved measurements and modeling of atmospheric aerosol composition and CCN activity, Atmos. Chem. Phys., 9(19), 7551–7575, doi:10.5194/acp-9-7551-2009.

Gunthe, S. S. et al. (2011), Cloud condensation nuclei (CCN) from fresh and aged air pollution in the megacity region of Beijing, Atmos. Chem. Phys., 11(21), 11023–11039, doi:10.5194/acp-11-11023-2011.

Hiura, T. (2005), Estimation of aboveground biomass and net biomass increment in a cool temperate forest on a landscape scale, Ecol. Res., 20(3), 271–277, doi:10.1007/s11284-005-0042-0.

Holmgren, H., K. Sellegri, M. Hervo, C. Rose, E. Freney, P. Villani, and P. Laj (2014), Hygroscopic properties and mixing state of aerosol measured at the high-altitude site Puy de Dôme (1465 m a.s.l.), France, Atmos. Chem. Phys., 14(18), 9537–9554, doi:10.5194/acp-14-9537-2014.

Khalizov, A. F., Y. Lin, C. Qiu, S. Guo, D. Collins, and R. Zhang (2013), Role of OH-Initiated Oxidation of Isoprene in Aging of Combustion Soot, Environ. Sci. Technol., 47(5), 2254–2263, doi:10.1021/es3045339.

Kirikae, M., H. Shibata, Y. Tanaka, T. Sakuma, and R. Hatano (2001), Significance of nitrification and vegetation uptake in proton budgets in forest surface soil, Soil Sci. Plant Nutr., 47(2), 253–264, doi:10.1080/00380768.2001.10408389.

Levin, E., a Prenni, M. Petters, S. Kreidenweis, R. Sullivan, S. Atwood, J. Ortega, P. Demott, and J. Smith (2012), An annual cycle of size-resolved aerosol hygroscopicity at a forested site in Colorado, J. Geophys. Res., 117(D6), D06201, doi:10.1029/2011JD016854.

Levin, E. J. T., a. J. Prenni, B. B. Palm, D. a. Day, P. Campuzano-Jost, P. M. Winkler, S. M. Kreidenweis, P. J. DeMott, J. L. Jimenez, and J. N. Smith (2014), Size-resolved aerosol composition and its link to hygroscopicity at a forested site in Colorado, Atmos. Chem. Phys., 14(5), 2657–2667, doi:10.5194/acp-14-2657-2014.

Li, Z., A. L. Williams, and M. J. Rood (1998), Influence of Soluble Surfactant Properties on the Activation of Aerosol Particles Containing Inorganic Solute, J. Atmos. Sci., 55(10),

1859–1866, doi:10.1175/1520-0469(1998)055<1859:IOSSPO>2.0.CO;2.

Ma, S. X., J. D. Rindelaub, K. M. McAvey, P. D. Gagare, B. A. Nault, P. V. Ramachandran, and P. B. Shepson (2011), α-Pinene nitrates: synthesis, yields and atmospheric chemistry, Atmos. Chem. Phys., 11(13), 6337–6347, doi:10.5194/acp-11-6337-2011.

Ma, Y., S. D. Brooks, G. Vidaurre, A. F. Khalizov, L. Wang, and R. Zhang (2013), Rapid modification of cloud-nucleating ability of aerosols by biogenic emissions, Geophys. Res. Lett., 40(23), 6293–6297, doi:10.1002/2013GL057895.

Miyazaki, Y., S. G. Aggarwal, K. Singh, P. K. Gupta, and K. Kawamura (2009), Dicarboxylic acids and water-soluble organic carbon in aerosols in New Delhi, India, in winter: Characteristics and formation processes, J. Geophys. Res., 114(D19), D19206, doi:10.1029/2009JD011790.

Miyazaki, Y., J. Jung, P. Fu, Y. Mizoguchi, K. Yamanoi, and K. Kawamura (2012), Evidence of formation of submicrometer water-soluble organic aerosols at a deciduous forest site in northern Japan in summer, J. Geophys. Res. Atmos., 117(D19), doi:10.1029/2012JD018250.

Miyazaki, Y., P. Fu2, K. Ono, E. Tachibana, K. Kawamura, P. Fu, K. Ono, E. Tachibana, and K. Kawamura (2014), Seasonal cycles of water-soluble organic nitrogen aerosols in a deciduous broadleaf forest in northern Japan, J. Geophys. Res. Atmos., 119(3), 1440–1454, doi:10.1002/2013JD020713.

Moore, R. H., A. Nenes, and J. Medina (2010), Scanning Mobility CCN Analysis—A Method for Fast Measurements of Size-Resolved CCN Distributions and Activation Kinetics, Aerosol Sci. Technol., 44(10), 861–871, doi:10.1080/02786826.2010.498715.

Norris, G., R. Duvall, S. Brown, and S. Bai (2014), EPA Positive Matrix Factorization (PMF) 5.0 Fundamentals and User Guide, edited by U.S. Environmental Protection Agency, Washington, DC.

Paatero, P., and P. K. Hopke (2003), Discarding or downweighting high-noise variables in factor analytic models, Anal. Chim. Acta, 490(1–2), 277–289, doi:10.1016/S0003-2670(02)01643-4.

Paatero, P., and U. Tapper (1994), Positive matrix factorization: A non-negative factor model with optimal utilization of error estimates of data values, Environmetrics, 5(2), 111–126, doi:10.1002/env.3170050203.

Paatero, P., S. Eberly, S. G. Brown, and G. A. Norris (2014), Methods for estimating uncertainty in factor analytic solutions, Atmos. Meas. Tech., 7(3), 781–797, doi:10.5194/amt-7-781-2014.

Padró, L. T., D. Tkacik, T. Lathem, C. J. Hennigan, A. P. Sullivan, R. J. Weber, L. G. Huey, and A. Nenes (2010), Investigation of cloud condensation nuclei properties and droplet growth kinetics of the water-soluble aerosol fraction in Mexico City, J. Geophys. Res., 115(D9), D09204, doi:10.1029/2009JD013195.

Paramonov, M., P. P. Aalto, a. Asmi, N. Prisle, V. M. Kerminen, M. Kulmala, and T. Petäjä (2013), The analysis of size-segregated cloud condensation nuclei counter (CCNC) data and its implications for cloud droplet activation, Atmos. Chem. Phys., 13(20), 10285–10301, doi:10.5194/acp-13-10285-2013.

Peñuelas, J., D. Asensio, D. Tholl, K. Wenke, M. Rosenkranz, B. Piechulla, and J. P. Schnitzler (2014), Biogenic volatile emissions from the soil, Plant. Cell Environ., 37(8), 1866–1891, doi:10.1111/pce.12340.

Petters, M. D., and S. M. Kreidenweis (2007), A single parameter representation of hygroscopic growth and cloud condensation nucleus activity, Atmos. Chem. Phys., 7(8), 1961–1971, doi:10.5194/acp-7-1961-2007.

Petters, M. D., S. M. Kreidenweis, and P. J. Ziemann (2016), Prediction of cloud condensation nuclei activity for organic compounds using functional group contribution methods, Geosci. Model Dev., 9(1), 111–124, doi:10.5194/gmd-9-111-2016.

Pöschl, U. et al. (2010), Rainforest Aerosols as Biogenic Nuclei of Clouds and Precipitation in the Amazon, Science (80-.)., 329(5998), 1513–1516, doi:10.1126/science.1191056.

Reff, A., S. I. Eberly, and P. V Bhave (2007), Receptor modeling of ambient particulate matter data using positive matrix factorization: review of existing methods., J. Air Waste Manag. Assoc., 57(2), 146–154, doi:10.1080/10473289.2007.10465319.

Renbaum-Wolff, L., M. Song, C. Marcolli, Y. Zhang, P. F. Liu, J. W. Grayson, F. M. Geiger, S. T. Martin, and A. K. Bertram (2016), Observations and implications of liquid–liquid phase separation at high relative humidities in secondary organic material produced by α-pinene ozonolysis without inorganic salts, Atmos. Chem. Phys., 16(12), 7969–7979, doi:10.5194/acp-16-7969-2016.

Roberts, G. C., and A. Nenes (2005), A Continuous-Flow Streamwise Thermal-Gradient CCN Chamber for Atmospheric Measurements, Aerosol Sci. Technol., 39(3), 206–221, doi:10.1080/027868290913988.

Rogge, W. F., P. M. Medeiros, and B. R. T. Simoneit (2007), Organic marker compounds in surface soils of crop fields from the San Joaquin Valley fugitive dust characterization study, Atmos. Environ., 41(37), 8183–8204, doi:10.1016/j.atmosenv.2007.06.030.

Rose, D., S. S. Gunthe, E. Mikhailov, G. P. Frank, U. Dusek, M. O. Andreae, and U. Pöschl

(2008), Calibration and measurement uncertainties of a continuous-flow cloud condensation nuclei counter (DMT-CCNC): CCN activation of ammonium sulfate and sodium chloride aerosol particles in theory and experiment, Atmos. Chem. Phys., 8(5), 1153–1179, doi:10.5194/acp-8-1153-2008.

Shibata, H., M. Kirikae, Y. Tanaka, T. Sakuma, and R. Hatano (1998), Proton Budgets of Forest Ecosystems on Volcanogenous Regosols in Hokkaido, Northern Japan, Water. Air. Soil Pollut., 105(1/2), 63–72, doi:10.1023/A:1005086400473.

Sihto, S.-L. et al. (2011), Seasonal variation of CCN concentrations and aerosol activation properties in boreal forest, Atmos. Chem. Phys., 11(24), 13269–13285, doi:10.5194/acp-11-13269-2011.

Simoneit, B. R. T., V. O. Elias, M. Kobayashi, K. Kawamura, A. I. Rushdi, P. M. Medeiros, W. F. Rogge, and B. M. Didyk (2004), Sugars - Dominant Water-Soluble Organic Compounds in Soils and Characterization as Tracers in Atmospheric Particulate Matter, Environ. Sci. Technol., 38(22), 5939–5949, doi:10.1021/es0403099.

Sorjamaa, R., B. Svenningsson, T. Raatikainen, S. Henning, M. Bilde, and A. Laaksonen (2004), The role of surfactants in Köhler theory reconsidered, Atmos. Chem. Phys., 4(8), 2107–2117, doi:10.5194/acp-4-2107-2004.

Spracklen, D. V, B. Bonn, and K. S. Carslaw (2008), Boreal forests, aerosols and the impacts on clouds and climate, Philos. Trans. R. Soc. A Math. Phys. Eng. Sci., 366(1885), 4613–4626, doi:10.1098/rsta.2008.0201.

Suda, S. R. et al. (2014), Influence of Functional Groups on Organic Aerosol Cloud Condensation Nucleus Activity, Environ. Sci. Technol., 48(17), 10182–10190, doi:10.1021/es502147y.

Sullivan, R. C., M. J. K. Moore, M. D. Petters, S. M. Kreidenweis, G. C. Roberts, and K. a. Prather (2009), Effect of chemical mixing state on the hygroscopicity and cloud nucleation properties of calcium mineral dust particles, Atmos. Chem. Phys., 9(10), 3303–3316, doi:10.5194/acp-9-3303-2009.

Szmigielski, R. et al. (2007), 3-methyl-1,2,3-butanetricarboxylic acid: An atmospheric tracer for terpene secondary organic aerosol, Geophys. Res. Lett., 34(24), L24811, doi:10.1029/2007GL031338.

Tunved, P., J. Ströom, M. Kulmala, V.-M. Kerminen, M. Dal Maso, B. Svenningson, C. Lunder, and H.-C. Hansson (2008), The natural aerosol over Northern Europe and its relation to anthropogenic emissions—implications of important climate feedbacks, Tellus B Chem. Phys. Meteorol., 60(4), 473–484, doi:10.1111/j.1600-0889.2008.00363.x.

Varutbangkul, V., F. J. Brechtel, R. Bahreini, N. L. Ng, M. D. Keywood, J. H. Kroll, R. C. Flagan, J. H. Seinfeld, A. Lee, and a. H. Goldstein (2006), Hygroscopicity of secondary organic aerosols formed by oxidation of cycloalkenes, monoterpenes, sesquiterpenes, and related compounds, Atmos. Chem. Phys., 6(9), 2367–2388, doi:10.5194/acp-6-2367-2006.

Wang, J., J. F. Doussin, S. Perrier, E. Perraudin, Y. Katrib, E. Pangui, and B. Picquet-Varrault (2011), Design of a new multi-phase experimental simulation chamber for atmospheric photosmog, aerosol and cloud chemistry research, Atmos. Meas. Tech., 4(11), 2465–2494, doi:10.5194/amt-4-2465-2011.

Wex, H., F. Stratmann, D. Topping, and G. McFiggans (2008), The Kelvin versus the Raoult Term in the Köhler Equation, J. Atmos. Sci., 65(12), 4004–4016, doi:10.1175/2008JAS2720.1.

Whitehead, J. D. et al. (2016), Biogenic cloud nuclei in the central Amazon during the transition from wet to dry season, Atmos. Chem. Phys., 16(15), 9727–9743, doi:10.5194/acp-16-9727-2016.

Williams, J., M. de Reus, R. Krejci, H. Fischer, and J. Ström (2002), Application of the variability-size relationship to atmospheric aerosol studies: estimating aerosol lifetimes and ages, Atmos. Chem. Phys., 2(2), 133–145, doi:10.5194/acp-2-133-2002.

Yttri, K. E. et al. (2007), Elemental and organic carbon in PM10: a one year measurement campaign within the European Monitoring and Evaluation Programme EMEP, Atmos. Chem. Phys., 7(22), 5711–5725, doi:10.5194/acp-7-5711-2007.

Yu, J., D. R. Cocker III, R. J. Griffin, R. C. Flagan, and J. H. Seinfeld (1999), Gas-Phase Ozone Oxidation of Monoterpenes: Gaseous and Particulate Products, J. Atmos. Chem., 34(2), 207–258, doi:10.1023/A:1006254930583.

Chapter 4. Impact of Biogenic Organic Aerosols on Aerosol Optical Properties

4.1 Introduction

4.1.1 Biogenic aerosols and their direct effect on the climate

In addition to the impact on cloud formation as discussed in the previous chapter, atmospheric aerosols with a size range from 10 nm to 1 μm in diameter play a key role in regulating the direct radiative effect (DRE) as described in Chapter 1.1. The impact of aerosols on the DRE depends on their abundance and distribution within the atmospheric column, their hygroscopicity, and on their optical properties [*Moise et al.*, 2015]. Because the incoming solar radiation peaks at wavelength between 380 nm and 750 nm, biogenic organic aerosols especially in that size range are important to constrain the impact on the DRE [*Scott et al.*, 2014]. *Scott et al.* [2014] estimated that the global annual mean DRE by biogenic secondary organic aerosol (BSOA) ranged between −0.08 Wm^{-2} and −0.78 Wm^{-2}, while *Lihavainen et al.* [2009] estimated that a regional DRE over boreal forest in summer ranged between −0.37 Wm^{-2} and −0.74 Wm^{-2}. These studies emphasize that there still remains large uncertainties in the impact of BSOA on the DRE.

The abundance and chemical composition of BSOA and their interaction with pre-existing particles can affect the aerosol extinction characteristics. Furthermore, uncertainties in the absorbing and scattering characteristics of those aerosols make it difficult to understand whether the radiative forcing by biogenic aerosols is negative or positive on regional scales [*Andrews et al.*, 2017]. In this chapter, the effects of biogenic emissions of organics on the aerosol optical properties are investigated.

4.1.2 Objective

In Chapter 3, it was suggested that BSOA, formed via BVOCs most likely emitted from the forest floor, can reduce the cloud forming potential of pre-existing sulfate particles [*Müller et al.*, 2017]. The interaction between organic emissions and pre-existing particles might not be constrained to the canopy height and can also impact the DRE by affecting the scattering and absorption characteristics. The objective of this chapter is to investigate the impact of biogenic organic emissions from the forest on aerosol optical properties on a regional scale. Ground-based remote sensing measurements were continuously made to obtain the extinction as well as scattering/absorption characteristics of atmospheric aerosols. These retrievals are compared with the chemical data obtained from the filter-based aerosol measurements as shown in Chapter 3.

4.2 Methods

One of the important parameters to represent the optical properties of aerosols can be measured by sun photometry using sun-photometers. A sun-photometer measures atmospheric extinction or optical depth in the total atmospheric column of the direct radiation from the sun. With the total extinction, the spectral extinction of the solar irradiance at each wavelength by aerosols can be derived. This parameter is generally defined as aerosol optical depth (AOD), which provides information about the aerosol loading in the atmospheric column. The AOD values below 0.2 typically indicate a clear atmosphere, whereas the values > 0.4 are associated with high aerosol loadings such as those from polluted sources [e.g., *Salinas et al.*, 2013]. According to the Beer–Lambert–Bourger law [*Bouguer*, 1729; *Beer*, 1852], the solar irradiance at a wavelength λ (I (λ)), which reaches the instrument, is defined as:

$$I(\lambda) = I_0(\lambda) \times e^{-\tau_t(\lambda)\, m(\xi)} \quad \textbf{(4.1)}$$

where I_0 is the irradiance at the top of the atmosphere; τ_t corresponds to the total atmospheric optical depth. m (ξ) is the optical air mass, which is defined as a path length of the radiation passing through the atmosphere to the sea level and depends on the solar zenith angle ξ. The τ_t is composed of the optical depth due to molecular scattering (Rayleigh scattering), molecular absorption, and AOD. Applying the Ångström formula [*Ångström*, 1929], the AOD τ_a can be expressed as:

$$\tau_a(\lambda) = \tau_{a0}(\lambda) \times \lambda^{-\alpha} \quad \textbf{(4.2)}$$

where α is the Ångström exponent (AE), and τ_{a0} is the AOD at a reference wavelength (usually around 1 µm). The Ångström exponent describes the dependency of AOD on the wavelength. It is a measure for the aerosol size, which typically classifies the particle size into coarse mode (with radii $r > 0.5$ µm for $AE < 1$) and fine mode (with $r < 0.5$ µm for $AE > 1$) [*Salinas et al.*, 2009]. Based on the relationship between AOD and AE, the retrieved aerosols can be classified according to their characteristics of extinction and size of particles [*Toledano et al.*, 2007; *Salinas et al.*, 2009; *Tan et al.*, 2015].

Another important parameter derived from solar almucantar retrievals of the sun-photometer measurements is the single scattering albedo ω (SSA) which is the ratio of scattering to extinction (absorption + scattering):

$$\omega = \frac{\sigma_{sca}}{\sigma_{abs} + \sigma_{sca}} \quad \textbf{(4.3)}$$

where σ_{abs} and σ_{sca} represent the optical absorption and scattering cross sections, respectively [*Moise et al.*, 2015]. The SSA primarily shows whether aerosol particles have a warming or

cooling radiative effect [e.g., *Hansen et al.*, 1997]. SSA > 0.95 generally indicates scattering/reflective aerosols, whereas SSA < 0.90 represents more absorbing aerosols. The mixture of absorbing and scattering aerosols have SSA values typically between 0.90 and 0.95.

For the measurements of these parameters, a sky radiometer (POM-01; Prede Co., Ltd., Tokyo, Japan) was deployed by the University of Toyama for the Skynet project (http://skyrad.sci.u-toyama.ac.jp/skyrad_web/index.html) at the Tomakomai experimental forest (42.676 N, 141.600 E) at 30 m height. The sky radiometer measures the direct solar irradiance and diffuse solar radiance at five wavelengths (0.4, 0.5, 0.675, 0.87, 1.02 μm). Measurements were made every ~10 minutes. Quality-assured data for AOD, AE and SSA were computed using the SKYRAD.pack Version 4.2. [*Nakajima et al.*, 1996]. The chemical data for the submicron particles obtained within the canopy is the same as that shown and discussed in Chapter 3.

4.3 Results and Discussion

4.3.1 Seasonal variations in aerosol optical depth

Figure 4.1a shows the temporal variation of AOD at a wavelength of 500 nm from June to December 2015 in comparison with the total soluble mass (TSM) in the submicron particles measured within the forest canopy. The AOD values ranged from 0.03 to 0.72 with an average of 0.17 ± 0.13. *Eck et al.* [2009] reported that monthly averaged AOD at the wavelength of 500 nm was less than 0.1 for background aerosol levels in the boreal region in Central Alaska. During periods with large influence of biomass burning, they observed AOD values above 0.4. In this study, the observed AOD values less than 0.1 correspond to the atmospheric condition with small numbers of particles, whereas the values larger than 0.4 can be interpreted to conditions with larger particle number concentrations.

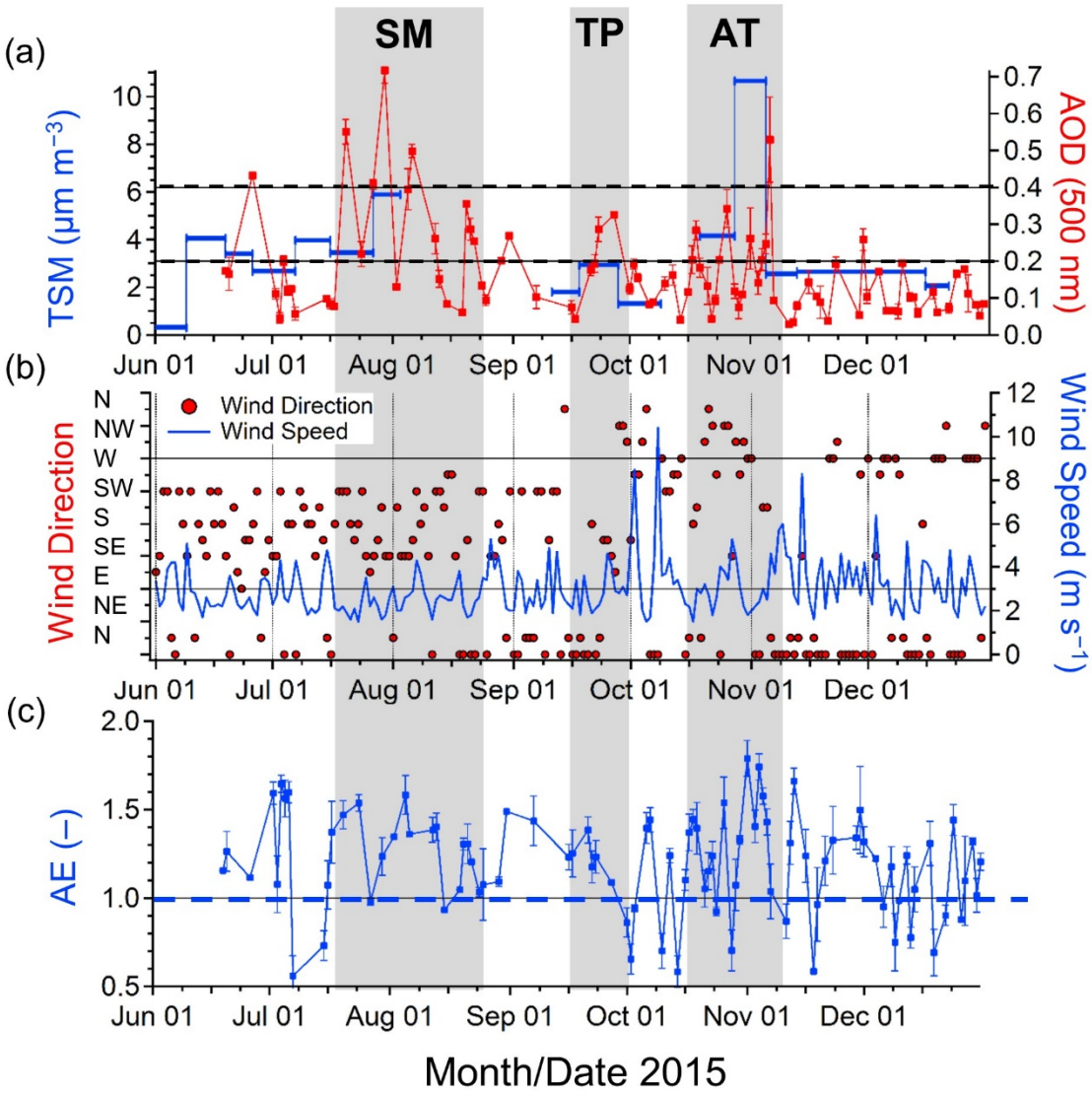

Figure 4.1 Time series of (a) the total soluble mass (TSM) in the submicron particles collected on the filters and the aerosol optical depth (AOD) at a wavelength of 500 nm, (b) local wind direction and wind speeds, and (c) the Angström Exponent (AE) from June to December, 2015. AE > 1 represents fine mode aerosols with radii < 0.5 μm; AE < 1 coarse mode aerosols with radii > 0.5 μm. Shaded areas divide three periods summer (SM), transition period (TP), and autumn (AT).

Based on the characteristics of the optical properties (**Figure 4.1a**) and the local wind direction and speeds (**Figure 4.1b**), three periods can be defined in terms of the increased AOD during the measurement period. During the period from the end of July to the middle of August, defined here as the summer period (SM), the wind direction was mainly southerly. The AOD values were generally larger than 0.40 during SM. During the period from October to November, defined as autumn period (AT), the dominant wind direction was northerly, when

the AOD values were 0.17 ± 0.12 with a peak > 0.4. The period of September corresponded to the transition period (defined as TP), when the average AOD was 0.25 ± 0.06. The average values of the data in each period are given in **Table 1**.

Table 1. Average optical properties and chemical data for the three periods summer (SM), transition period (TP), and autumn (AT). Aerosol optical depth (AOD) at 500 nm, Angström Exponent (AE), single scattering albedo (SSA) at 500 nm, sulfate (SO_4^{2-}), water-soluble organic matter (WSOM), and total soluble mass (TSM).

	Summer (SM)	Transition (TP)	Autumn (AT)
AOD (500 nm)	0.40 ± 0.18	0.25 ± 0.06	0.17 ± 0.12
AE	1.36 ± 0.18	1.22 ± 0.11	1.27 ± 0.28
SSA (500 nm)	0.98 ± 0.01	0.95 ± 0.02	0.93 ± 0.04
SO_4^{2-} (μg m^{-3})	2.78 ± 0.63	1.67 ± 0.00	1.04 ± 0.50
WSOM (μg m^{-3})	0.98 ± 0.39	0.74 ± 0.00	4.02 ± 2.51
TSM (μg m^{-3})	4.67 ± 1.22	2.93 ± 0.00	5.79 ± 3.50

4.3.2 Comparison of the aerosol optical depth with the chemical measurement

To understand the impact of the aerosol mass on the aerosol extinction properties, **Figure 4.1a** also shows the temporal variations of TSM, which ranged from 0.31 μg m^{-3} to 10.65 μg m^{-3} with an average of 4.46 μg m^{-3} ± 2.31 μg m^{-3}. The temporal trend of TSM was similar to that of AOD in SM, TP, and AT. Previously, the dependence of satellite-derived AOD on particulate matter (PM) has been studied in rural background and metropolitan sites around Helsinki, and urban and rural sites in the United States [*Natunen et al.*, 2010; *Toth et al.*, 2014]. Moreover, ground- and satellite-based AOD were investigated at urban and suburban sites in Singapore [*Chew et al.*, 2016]. In those studies, increased AOD values correlated with increased $PM_{2.5}$ in the presence of an aerosol layer near the surface or a well-mixed planetary boundary layer [*Natunen et al.*, 2010; *Toth et al.*, 2014; *Chew et al.*, 2016]. In this study, the low local horizontal wind speeds (3.0 ± 1.2 m s^{-1}) (**Figure 4.1b**) indicate that

the increase of the AOD was largely influenced by the increased TSM by the vertical transport from the forest canopy.

Figure 4.1c shows the temporal variation of the AE. The average AE value was 1.19 ± 0.28, whereas it often exceeded 1.00 during the period SM, TP, and AT (**Table 1**). This temporal trend of AE indicates that aerosols residing in the fine mode fraction are responsible for the increased AOD. Although the TSM represents the water-soluble fraction of the submicron particle mass, the significant correlation between TSM and AOD (R^2 = 0.60) with the dominance of fine-mode size for AOD suggests that the most of the increase in AOD was likely associated with the increase in TSM. This allows the comparison of the chemical properties measured in the canopy with the optical properties of the total atmospheric column. In order to investigate the relation between the increased AOD and chemical properties of the TSM, **Figure 4.2a** shows the temporal variation of the chemical mass fraction of the TSM in the submicron particles obtained from the filter sampling. As already discussed in Chapter 3, sulfate was the major mass fraction (~60%) of the TSM during SM and TP. On the other hand, the mass fraction was dominated by the water-soluble organic matter (WSOM) (~70%) in AT (**Table 1**). The result indicates that the AOD is mainly controlled by sulfate-dominated particles in SM and TP. In contrast, the increased WSOM can be responsible for the increased AOD values in AT.

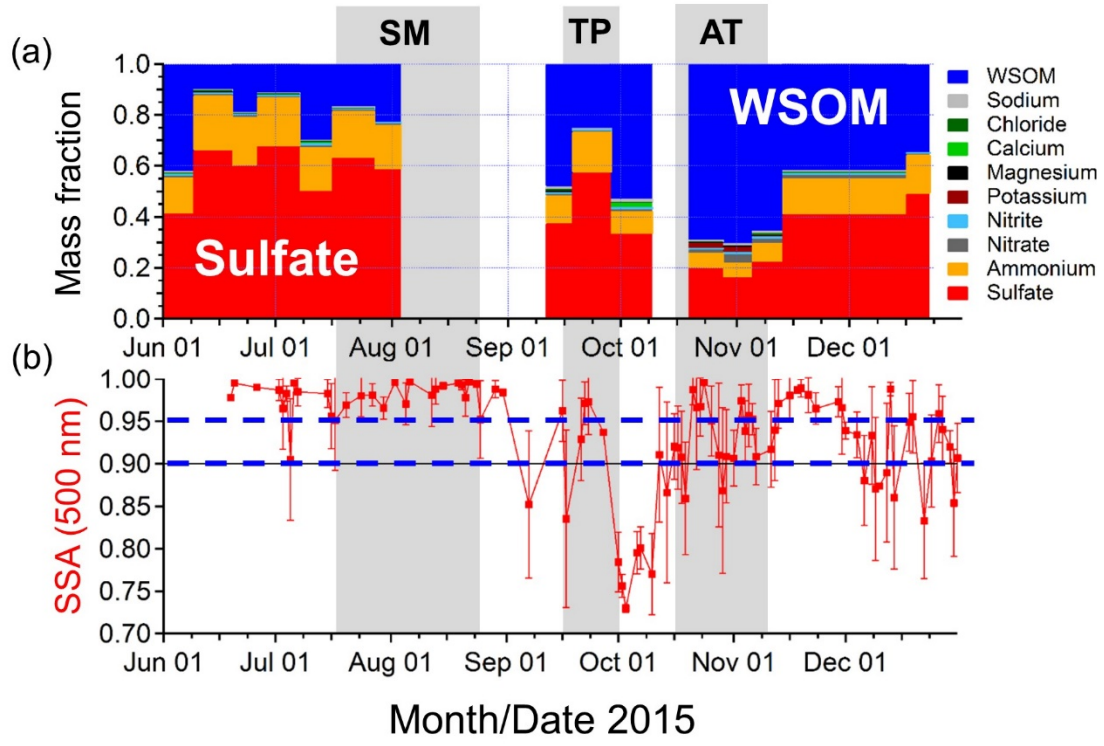

Figure 4.2 Time series of (a) the chemical mass fraction of submicron water-soluble aerosols from the filter-based measurement, and (b) the single scattering albedo (SSA) at 500 nm from June to December, 2015. SSA > 0.95 represents scattering aerosols; SSA < 0.90 absorbing aerosols, and 0.90 < SSA < 0.95 those of a mixture of absorbing and scattering characteristics. Shaded areas divide three periods summer (SM), transition period (TP), and autumn (AT).

4.3.3 Possible impact of the biogenic organic species on light scattering/absorbing characteristics of aerosols

In Chapter 3, it was discussed that the increased fraction and concentration of sulfate in summer were mainly due to the inflow of anthropogenic aerosols near the forest. The large concentration of hygroscopic sulfate particles have been related to increased AOD [e.g., *Nguyen et al.*, 2016]. The current study suggests that the increased AOD in summer is likely related to the increased influence of sulfate particles. On the other hand, recent studies also reported that increased solar extinction in summer was associated with increased BVOC emissions [*Goldstein et al.*, 2009] and/or large aerosol water content [*Nguyen et al.*, 2016] in southeastern USA. In order to investigate the effect of the chemical composition on the

scattering and absorption characteristics of particles, **Figure 4.2b** shows the temporal variation of the single scattering albedo (SSA) at a wavelength of 500 nm. In general, the values of SSA in SM were larger than 0.95 (0.98 ± 0.01), indicating that the observed aerosols had mainly scattering characteristics. In contrast, most of the SSA values in AT were in the range of 0.90–0.95 (0.93 ± 0.04) which were generally lower than those in SM and TP by 5% and 2%, respectively (**Table 1**). This suggests that contributions of aerosols with more absorbing characteristics were more important in AT.

In general, with regard to absorbing characteristics of aerosol particles, black carbon (BC) containing particles like soot are highly absorptive [*Eck et al.*, 2009; *Russell et al.*, 2010; *Giles et al.*, 2012]. Humic substance from soils, plant debris, and biogenic aerosols may be a source of light absorbing organic particulate matter, which is referred to as brown carbon (BrC) [*Moise et al.*, 2015]. Some portion of BrC can be produced as light-absorbing secondary organic aerosol (SOA) in the atmosphere, which is often linked to water-soluble organic carbon (WSOC) [*Moise et al.*, 2015]. Changes of relative humidity is suggested to promote BrC production under conditions like in agricultural and forested areas. The produced BrC can become a dominant contributor to aerosol absorption [*Moise et al.*, 2015], which leads to lowering SSA. The study in Chapter 3 indicated that the pre-existing hygroscopic particles such as sulfate were possibly coated with biogenic organics, namely oxidation products of α-pinene, at the same forest site in AT. Indeed, the absorbing characteristics of α-pinene SOA have been reported by laboratory experiments [*Zhong and Jang*, 2011; *Lambe et al.*, 2013]. The current study indicates that organic coatings of particles reduced the SSA. This reduction was estimated to be about 5% from SM to AT (**Table 1**).

To summarize, the comparative study in this chapter indicates that biogenic organic aerosols observed in the canopy at the forest site can affect the optical characteristics of pre-existing particles on a regional scale. Specifically, it was indicated that hygroscopic sulfate

particles coated by biogenic organics, as discussed in Chapter 3, can reduce the SSA by ~5% and consequently, increase the light absorption by aerosol particles. This might have important implications for the prediction of the radiative effect of aerosols on a regional scale in future.

4.4 Conclusions

The filter-based aerosol measurements were compared with aerosol optical properties retrieved from a sky radiometer at the Tomakomai forest site. The data of these ground-based remote sensing measurements contain aerosol characteristics of extinction and scattering/absorption from June to December 2015. The comparison showed that the temporal trend of the mass concentrations of total soluble mass (TSM) were generally similar to aerosol optical depth (AOD), which was typically greater than 0.2 in summer and autumn. The result indicates that the increase in AOD was likely linked to the increased TSM. In summer, the mass of TSM is dominated by sulfate which was linked to aerosols with a single scattering albedo (SSA) generally larger than 0.95, indicating that most of the observed aerosols had scattering characteristics in that season. In contrast, the increased mass fraction of water-soluble organic matter (WSOM) in autumn was likely associated with more absorbing aerosols with SSA mostly ranging between 0.90 and 0.95. The result indicates that the coating of pre-existing hygroscopic particles with biogenic organics can reduce the scattering efficiency of sulfate particles in autumn. Specifically, the observations indicate that biogenic organic aerosols at the forest site can reduce the SSA by ~5% which leads to an increase in the aerosol absorption. This result has important implications for the prediction of the effect of biogenic organic aerosols on the regional radiative forcing in future. Additional comprehensive field and laboratory studies are required to confirm the results and to investigate the mechanism of how biogenic secondary organic aerosol (BSOA) affect the optical properties.

References

Andrews, E., J. A. Ogren, S. Kinne, and B. Samset (2017), Comparison of AOD, AAOD and column single scattering albedo from AERONET retrievals and in situ profiling measurements, Atmos. Chem. Phys., 17(9), 6041–6072, doi:10.5194/acp-17-6041-2017.

Ångström, A. (1929), On the Atmospheric Transmission of Sun Radiation and on Dust in the Air, Geogr. Ann., 11, 156–166, doi:10.2307/519399.

Beer (1852), Bestimmung der Absorption des rothen Lichts in farbigen Flüssigkeiten, Ann. der Phys. und Chemie, 162(5), 78–88, doi:10.1002/andp.18521620505.

Bouguer, P. (1729), Essai D'Optique, Sur La Gradation de La Lumiere, edited by C. J. (Paris).

Chew, B. N., J. R. Campbell, E. J. Hyer, S. V. Salinas, J. S. Reid, E. J. Welton, B. N. Holben, and S. C. Liew (2016), Relationship between aerosol optical depth and particulate matter over Singapore: Effects of aerosol vertical distributions, Aerosol Air Qual. Res., 16(11), 2818–2830, doi:10.4209/aaqr.2015.07.0457.

Eck, T. F. et al. (2009), Optical properties of boreal region biomass burning aerosols in central Alaska and seasonal variation of aerosol optical depth at an Arctic coastal site, J. Geophys. Res., 114(D11), D11201, doi:10.1029/2008JD010870.

Giles, D. M., B. N. Holben, T. F. Eck, A. Sinyuk, A. Smirnov, I. Slutsker, R. R. Dickerson, a. M. Thompson, and J. S. Schafer (2012), An analysis of AERONET aerosol absorption properties and classifications representative of aerosol source regions, J. Geophys. Res. Atmos., 117(D17), doi:10.1029/2012JD018127.

Goldstein, A. H., C. D. Koven, C. L. Heald, and I. Y. Fung (2009), Biogenic carbon and anthropogenic pollutants combine to form a cooling haze over the southeastern United States, Proc. Natl. Acad. Sci., 106(22), 8835–8840, doi:10.1073/pnas.0904128106.

Hansen, J., M. Sato, and R. Ruedy (1997), Radiative forcing and climate response, J. Geophys. Res. Atmos., 102(D6), 6831–6864, doi:10.1029/96JD03436.

Lambe, A. T. et al. (2013), Relationship between oxidation level and optical properties of secondary organic aerosol, Environ. Sci. Technol., 47(12), 6349–6357, doi:10.1021/es401043j.

Lihavainen, H., V.-M. Kerminen, P. Tunved, V. Aaltonen, A. Arola, J. Hatakka, A. Hyv?rinen, and Y. Viisanen (2009), Observational signature of the direct radiative effect by natural boreal forest aerosols and its relation to the corresponding first indirect effect, J. Geophys. Res., 114(D20), D20206, doi:10.1029/2009JD012078.

Moise, T., J. M. Flores, and Y. Rudich (2015), Optical Properties of Secondary Organic Aerosols and Their Changes by Chemical Processes, Chem. Rev., 115(10), 4400–4439,

doi:10.1021/cr5005259.

Müller, A., Y. Miyazaki, E. Tachibana, K. Kawamura, and T. Hiura (2017), Evidence of a reduction in cloud condensation nuclei activity of water-soluble aerosols caused by biogenic emissions in a cool-temperate forest, Sci. Rep., 7(1), 8452, doi:10.1038/s41598-017-08112-9.

Nakajima, T., G. Tonna, R. Rao, P. Boi, Y. Kaufman, and B. Holben (1996), Use of sky brightness measurements from ground for remote sensing of particulate polydispersions, Appl. Opt., 35(15), 2672, doi:10.1364/AO.35.002672.

Natunen, A., A. Arola, T. Mielonen, J. Huttunen, M. Komppula, and K. E. J. Lehtinen (2010), A multi-year comparison of PM2.5 and AOD for the helsinki region, Boreal Environ. Res., 15(6), 544–552.

Nguyen, T. K. V, V. P. Ghate, and A. G. Carlton (2016), Reconciling satellite aerosol optical thickness and surface fine particle mass through aerosol liquid water, Geophys. Res. Lett., 1–10, doi:10.1002/2016GL070994.

Russell, P. B., R. W. Bergstrom, Y. Shinozuka, A. D. Clarke, P. F. DeCarlo, J. L. Jimenez, J. M. Livingston, J. Redemann, O. Dubovik, and A. Strawa (2010), Absorption Angstrom Exponent in AERONET and related data as an indicator of aerosol composition, Atmos. Chem. Phys., 10(3), 1155–1169, doi:10.5194/acp-10-1155-2010.

Salinas, S. V, B. N. Chew, and S. C. Liew (2009), Retrievals of aerosol optical depth and Angström exponent from ground-based Sun-photometer data of Singapore., Appl. Opt., 48(8), 1473–84.

Salinas, S. V., B. N. Chew, M. Mohamad, M. Mahmud, and S. C. Liew (2013), First measurements of aerosol optical depth and Angstrom exponent number from AERONET's Kuching site, Atmos. Environ., 78, 231–241, doi:10.1016/j.atmosenv.2013.02.016.

Scott, C. E. et al. (2014), The direct and indirect radiative effects of biogenic secondary organic aerosol, Atmos. Chem. Phys., 14(1), 447–470, doi:10.5194/acp-14-447-2014.

Tan, F., H. San Lim, K. Abdullah, T. L. Yoon, and B. Holben (2015), AERONET data–based determination of aerosol types, Atmos. Pollut. Res., 6(4), 682–695, doi:10.5094/APR.2015.077.

Toledano, C., V. E. Cachorro, A. Berjon, A. M. De Frutos, M. Sorribas, B. A. De Morena, and P. Goloub (2007), Aerosol optical depth and Angstr ¨ om exponent climatology at El Arenosillo AERONET site (Huelva , Spain), Q. J. R. Meteorol. Soc., 133, 795–807, doi:10.1002/qj.

Toth, T. D., J. Zhang, J. R. Campbell, E. J. Hyer, J. S. Reid, Y. Shi, and D. L. Westphal (2014), Impact of data quality and surface-to-column representativeness on the PM2.5 / satellite AOD relationship for the contiguous United States, Atmos. Chem. Phys., 14(12), 6049–6062, doi:10.5194/acp-14-6049-2014.

Zhong, M., and M. Jang (2011), Light absorption coefficient measurement of SOA using a UV-Visible spectrometer connected with an integrating sphere, Atmos. Environ., 45(25), 4263–4271, doi:10.1016/j.atmosenv.2011.04.082.

Chapter 5. General Conclusions

In order to elucidate the effects of terrestrial biogenic emissions of organics on the cloud forming potential of atmospheric aerosols, two field experiments were conducted at a suburban site in Sapporo and a cool-temperate forest site in Tomakomai. At both observational sites, the chemical composition, the particle hygroscopicity, and the cloud condensation nuclei (CCN) activity of submicron particles were simultaneously measured by using on-line and off-line techniques.

The time-resolved online measurements of submicron aerosols at the suburban site in summer suggest that chemical composition and mixing state of particles are important factors to control hygroscopicity (κ) and CCN activity of aerosols. Specifically, the observed particles with external mixing dominated by organics were linked to low hygroscopicity and CCN activity. On average, water-soluble organic matter (WSOM) accounted for ~60% of organic matter (OM) by mass. The increase in the WSOM mass with increased WSOM/sulfate ratios corresponded to a low hygroscopicity. The result suggests that WSOM at the observational site, likely dominated by the influence of biogenic sources, can suppress the hygrosocopicity and activation of particles as CCN.

To investigate the effects of types and amounts of terrestrial biogenic emissions of organics on the CCN activity, two year-long offline measurements of water-soluble aerosols were conducted at the cool-temperate forest in Tomakomai. The measurement showed that κ derived from CCN measurements (κ_{CCN}) exhibited a distinct seasonal trend with a maximum in summer and a minimum in autumn. The chemical analysis revealed that the reduction of the hygroscopicity from summer to autumn by 15% was linked to an increase in the WSOM/sulfate

ratios due to the increase in the WSOM mass, which supports the result of the time-resolved online measurements. Positive matrix factorization analysis (PMF) indicated that α-pinene derived secondary organic aerosols (SOA) contributed to ~75% of the WSOM mass in autumn, which was larger by 47% than in summer. The majority of these α-pinene derived SOA in autumn was attributable to emissions from litter/soil microbial activity near the forest floor. These findings suggest that WSOM, most likely α-pinene SOA originated from the forest floor, can significantly suppress the aerosol CCN activity in cool-temperate forests, which was suggested for the first time.

The reduction of the hygroscopicity can be explained by organic coatings on pre-existing hygroscopic particles such as sulfate, and/or phase partitioning of these organics in the droplets. It was estimated that particles coated with α-pinene derived SOA can reduce the number of activated CCN particles by roughly~32% in autumn. Considering the lifetime of α-pinene SOA (~10 hours to ~3 days) with the observed local wind speeds, the SOA can affect the distribution of CCN within ~800 km. This estimate implies that hygroscopic particles coated with α-pinene SOA can reduce the cloud forming potential of aerosols, which leads to modification of the negative indirect effect of radiative forcing on a regional scale.

Comparison of the filter-based aerosol measurements with aerosol optical properties retrieved from a sky radiometer at the Tomakomai forest site showed that the increased aerosol mass in the forest canopy corresponded to increase in the aerosol optical depth of submicron particles in autumn. The increased mass fraction of sulfate in summer (60%) was linked to the enhanced properties of aerosol scattering (single scattering albedo, SSA > 0.95). On the other hand, the increase in the mass fraction of WSOM in autumn (70%) was found to be mainly associated with more absorbing characteristics of aerosols (SSA 0.90–0.95). This suggests that the biogenic organic aerosols at the forest site can modify the aerosol optical properties on a regional scale.

This study provides important implications for reducing the large uncertainties of the aerosol radiative effect in cool-temperate and boreal forest environments. The study suggests the importance of the forest floor as a source of biogenic secondary organic aerosol (BSOA) and the subsequent impact on reducing CCN and the scattering characteristics of aerosols. Specifically, the negative aerosol radiative effect is expected to be reduced on a regional scale. The effects of BSOA on radiative forcing suggested by this study should be taken into account in aerosol-climate models for predicting the impact of aerosols on the climate in future, especially when possible changes in the emissions of BSOA due to land-use changes are considered. Additional field studies at other forest sites and comprehensive in-situ measurements are needed to elucidate the mechanism of the reduction of the CCN activity by biogenic organic aerosols and their impact on optical properties on both regional and global scale.